UNITED TECHNOLOGIES

UNITED TECHNOLOGIES RESEARCH CENTER

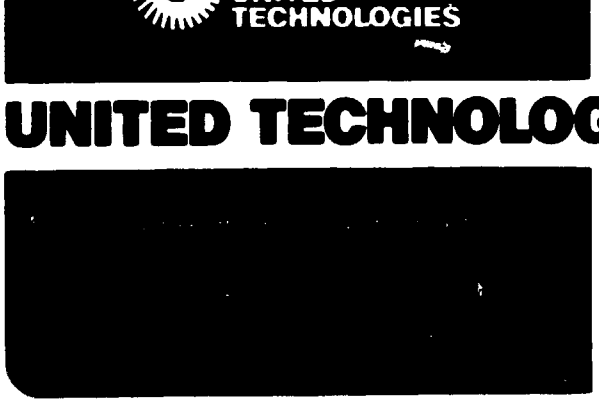

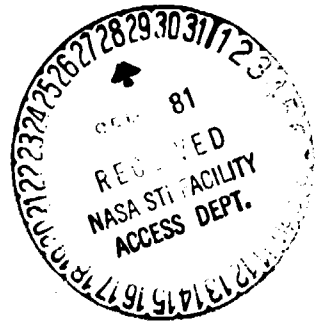

NASA CR-165464

R81-915215-4

Study of the Effects of Gaseous Environment on the Hot Corrosion of Superalloy Materials

Final Report

Work Performed for
NASA-Lewis Research Center
Contract No. NAS3-22488

Reported by 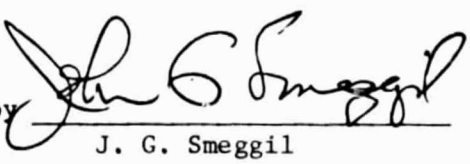
J. G. Smeggil

Approved by 
N. S. Bornstein

Date July 1981

Study of the Effects of Gaseous Environment on the Hot Corrosion of Superalloy Materials

TABLE OF CONTENTS

I. INTRODUCTION

The accelerated degradation of gas turbine materials due to the presence of condensed salts is commonly called hot corrosion. The hot corrosion problem has been intensively studied for more than a decade, and it is realized that its solution requires a basic understanding of the responsible mechanisms so that appropriate corrective action can be taken. It is important to also realize that, based upon current knowledge, the hot corrosion problem currently encountered will be a major problem for machines using coal-derived synthetic fuel oils and gases because corrodents are formed from naturally occurring impurities in the coal (Ref. 1). Furthermore, these impurities are not readily removed by current processing techniques. Among the compounds that are likely to be found in the hot section of turbines operating in marine and industrial environments is NaCl (e.g. Ref. 2-4).

Indeed, based upon equilibrium calculations, the environment within gas turbine engines operating under conditions conducive to hot corrosion will be relatively rich in the gaseous species NaCl (Refs. 3, 4). Moreover, it has been previously shown in this study that gas phase sodium chloride reacts with the normally protective scales that form on NiAl, Ni-Cr alloys and the nickel base superalloy B-1900 (Refs. 5, 6).

With respect to the simple alumina formers, the gas reacts at the metal-oxide interface, transporting aluminum to the free surface where it oxidizes to form Al_2O_3 whiskers. The depletion of aluminum at the oxide-metal interface results in the formation of voids, which after prolonged exposure, grow and eventually contribute to isothermal scale cracking of sufficient magnitude to be readily detected by thermogravimetric techniques (Ref. 5).

It was also shown that NaCl(g) reacts with chromia, and the chromium content of oxide scales can be significantly reduced by gaseous sodium chloride such that oxidation rates are significantly increased (Refs. 5, 6). Furthermore, the presence of NaCl vapors in oxidizing atmospheres leads to "S"-shaped thermogravimetric curves characteristic of breakaway oxidation kinetics.

It is well established that in the presence of condensed sodium sulfate the rate of oxidation of many nickel-base superalloys are increased orders of magnitude. In laboratory tests, it was shown that, after prolonged exposure, the rate of oxidation of salt-coated B-1900 coupons eventually deceased (Ref. 5). However, as shown in that study, when the same alloy was exposed at 900°C in the presence of low levels of NaCl vapors, oxidation rates were increased by orders of magnitude (Ref. 5). In fact, at the end of 100 hour tests, thermogravimetric curves for specimens exposed to NaCl(g) at 900°C exhibited highly positive slopes, which indicated that the rapid rates of oxidation would continue until the alloy was totally consumed.

Examination of selected specimens exposed for varying durations to air containing NaCl vapors revealed the presence of alumina whiskers. The formation of the whiskers and the subsequent enrichment of molybdenum at the scale-alloy interface are believed to be contributing factors to the accelerated oxidation of the alloy.

It was also shown that, during thermal transients, metallurgical transformations can occur in CoCrAlY coatings. In the presence of gaseous NaCl, severe alloy depletion effects and internal precipitation of aluminum oxide and chromium oxide are observed. Such a microstructure has been reported for a gas turbine operating under cyclic conditions in a marine environment. When carbon and Na_2SO_4 are present and the alloy is aged at lower temperatures, accelerated corrosion is observed producing a characteristic microstructure whose features agree with that reported for low power operation of Navy gas turbine engines (Refs. 7, 8, 9).

The objective of the study reported herein was to determine the role of gaseous chlorides in the accelerated oxidation phenomena called hot corrosion. The work described herein was divided into two tasks. In the first task experiments were conducted to determine the effect of the gaseous environment on the hot corrosion of superalloy materials. The role of silicon in alloys exposed to oxidation in the presence of gaseous sodium chloride was examined. Lastly, the possibility of minor alloying additions such as yttrium and hafnium serving to attenuate the deleterious effects of gaseous corrodents was investigated. In the second task, the role played by carbon and gaseous NaCl in low power hot corrosion was examined.

This work was supported by the NASA-Lewis Research Center under Contract No. NAS3-22488, Mr. Carl Stearns, NASA Project Manager.

II. BACKGROUND

All structural alloys are, with respect to high temperature oxidizing environments, thermodynamically unstable and react to form surface layers or scales. The composition and the adherence of such scales depends in part upon substrate and environmental compositions as well as the parameters of time and temperature.

Oxidation is the general term used to describe the formation and growth of the surface oxide layer(s) that develops on structural materials. Hot corrosion is the phrase used to describe the accelerated oxidation associated with the presence of molten salts. The principle constituents of such salts found on hot gas path turbine component surfaces are the alkali sulfates. Moreover, discrete sulfide particles are commonly observed near surfaces of materials which have undergone hot corrosion effects resulting from sodium sulfate deposits. Thusly, the terms "hot corrosion" and "sulfidation" are frequently used interchangeably. Moreover, because sea salt crystals are ever present in the air and inadvertently present in liquid fuels, hot corrosion (or sulfidation) is a major concern to both users and producers of gas turbine engines.

In investigating sulfidation corrosion, researchers have studied both the chemical reactions that occur between fused alkali salts and metallic substrates and the mechanisms by which salts deposit onto turbomachinery. It is generally agreed that the source of the corrosive alkali is sea salt crystals and that the condensed salt always associated with sulfidation corrosion is primarily sodium sulfate. Many mechanisms have been proposed to account for the deposition of salts onto turbomachinery. However, in addition to condensed salt deposits, gas turbine components will also be exposed to atmospheres containing low partial pressures of chloride-bearing species. Stearns et al. (Ref. 3) and Kohl et al. (Ref. 4) have reported that gaseous NaCl is expected to be the major sodium-bearing species in the hot section of the gas turbine.

In previously reported studies aimed at defining the role of gaseous corrodents, the United Technologies Research Center undertook to examine the effects of gaseous environments on the sulfidation attack of superalloys (Refs. 5, 6). The results of those studies are succinctly summarized thusly:

1. Gaseous NaCl and HCl interact with and modify the oxide scale that forms on the intermetallic compound NiAl. Specifically, it was shown that, during isothermal oxidation in the presence of such gaseous halides, the oxide scale was covered with numerous alumina

whiskers. The size and density of such whiskers are NaCl(g) concentration dependent. It was also shown that increasing the concentration of NaCl(g) increases the number of whiskers while the individual whisker size is decreased.

2. Experiments were conducted to determine if the Al_2O_3 whiskers were formed by rearrangement of the surface Al_2O_3 or if they originated from aluminum at the metal-oxide interface. Neither impure nor high purity dense alumina developed Al_2O_3 whiskers on exposure to NaCl(g)-bearing atmospheres. Thus, it was concluded that the aluminum source for the Al_2O_3 whisker formation is not at the surface, i.e., the gas-scale interface. It was proposed that a halogen-containing species reacts with the alloy substrates to form an "Al-NaCl" vapor moiety which diffuses through the alumina scale and reacts with oxygen at the free surface to form alumina whiskers. The precise nature of this "Al-NaCl" species is as yet unknown. Such a transport mechanism is consistent with the observation of isothermal rupture, spallation, and reformation of alumina scales.

3. At the 10 ppm level, the concentration of NaCl is sufficient to rupture protective alumina scales. It has been found that the NaCl concentration in a laboratory box furnace atmosphere was about 20 ppm.

4. In the presence of sodium sulfate deposits and with NaCl vapors in test atmospheres, alumina whiskers are produced. At 1050°C in the presence of NaCl vapors, incubation periods associated with sulfidation are prolonged. To account for this observation, it was proposed that the "Al-NaCl" species removes oxygen from Na_2SO_4 to form alumina whiskers. Furthermore, the newly formed alumina reacts with sodium oxide present in the condensed salt to further delay the sulfidation-initiation process.

5. In air environments alone, B-1900 exhibited excellent oxidation resistance. However, in the presence of low levels of NaCl vapors, oxidation rates were increased by orders of magnitude. In fact, at the end of 100 hour tests, thermogravimetric curves for specimens exposed to NaCl(g) at 900°C indicated highly positive slopes. On the other hand, sodium sulfate-coated specimens exposed at 900°C to air without NaCl(g) indicated flat or even decreasing oxidation rates, indicative of protective scale formation. Moreover, for B-1900 specimens oxidized in air with NaCl vapors, alumina whiskers similar to those found for the simple alumina formers were evident on oxide scales. The attendant isothermal cracking of the protective scale and the enrichment of molybdenum at the scale-alloy interface are contributing

factors to the accelerated oxidation of this alloy. As was shown in that study, the deleterious effect of NaCl(g) is also observed when the alloy is coated with molten sodium sulfate.

6. NaCl vapors were also shown to interact with chromia-rich scales. At 900°C NaCl(g) was shown to react with chromia-rich scales to produce "S" shaped curves. An "S" shaped curve is indicative of "breakaway" oxidation where the rate of oxygen pickup is noticeably increased as a result of scale rupture. Based upon metallographic and x-ray diffraction studies, the oxide scale formed in the presence of NaCl(g) is composed of both the spinel, $NiCr_2O_4$, and Cr_2O_3. Moreover, areas are observed where chromia depletion is markedly evident. The formation of the spinel and the loss of chromium is consistent with the formation of volatile chromium-containing species. Stearns et al. and Fryburg et al. have shown that the vapor species responsible for the loss of chromium from the alloys primarily are $(NaCl)_xCrO_3(g)$, x = 1, 2, 3, and $(NaOH)_xCrO_3(g)$, x = 1, 2 (Refs. 10, 11). When Ni-25Cr and chromium specimens are coated with Na_2SO_4 and subsequently exposed to air and gaseous NaCl, "S" shaped oxidation curves are not observed. It appeared as if Na_2SO_4 mitigates the deleterious effect of NaCl(g) although the mechanism by which this occurs was not known.

7. The role of reducing agents was examined and it was found that finely divided carbon co-deposited with Na_2SO_4 onto NiAl decreased the rate of corrosion at 900°C, but exhibited no effect at 1050°C. For the chromia-forming Ni-25Cr alloy, the data suggested that carbon influenced isothermal scale breakage, but the cause was not known.

8. Accelerated corrosion has been observed to occur in some Navy gas turbine engines that operate predominantly at reduced power (Ref. 12). Because low power operation implies reduced air flows, burner temperatures, and metal temperatures, the concentration of NaCl(g) in the environment and rate of deposition of salts and combustion products are changed. Amplifying briefly on this, the anticipated effects of low power engine operation include carbon formation during initial engine ignition and shutdown. Furthermore unlike operation at normal power levels, carbon-enriched atmospheres and the production of fuel chars have been reported for Naval gas turbines during operation at reduced power levels (Ref. 2). Thus, for a gas turbine operated in a cyclic mode, frequent opportunities exist for either unburnt fuel or fuel chars to impact turbine hardware and locally burn. Moreover such carbon, unlike the quickly burning powders used in the prior study (Ref. 6), can exist for prolonged durations at elevated temperatures. Burn-off rates for carbon have been previously

reported to strongly depend on the form in which it is present (Ref. 13). Although the effect of strictly reducing atmospheres on corrosion processes has been reported (Ref. 14), the effect of alternating oxidizing/reducing conditions on Na_2SO_4/NaCl(g)-induced hot corrosion has been largely overlooked.

The objective of the study reported herein is to determine the role of gaseous chlorides in the accelerated oxidation phenomena called hot corrosion. The work described herein is divided into two tasks. In the first task experiments are conducted to determine the effect of the gaseous environment on the hot corrosion of superalloy materials. In this task selected alloys are exposed at elevated temperatures to varying concentrations of gaseous sodium chloride. The role of silicon in alloys exposed to oxidation in the presence of gaseous sodium chloride is examined. Lastly, the possibility of minor alloying additions such as yttrium and hafnium serving to attenuate the deleterious effects of gaseous corrodents is investigated. In the second task, the role played by carbon and gaseous NaCl in low power hot corrosion is to be determined.

III. EXPERIMENTAL APPROACH

A. Materials

The air used in these experiments is taken from the laboratory service strip. The water content of this air is brought to a constant level by passage over anhydrous calcium sulfate. The gas flow for all experiments is 300 scc/min, and the flow velocity is 0.18 cm/sec. The NaCl used is an "ultrapure" grade.

The alloys, along with their nominal composition, used in Task 1 of this study are listed in Table I. Task 2 coating compositions were evaluated both as castings and protective coatings on appropriate superalloy substrates.

The NiAl and CoCrAl compositions were prepared by arc melting buttons under an argon atmosphere then annealing at 1300°C (2370°F) for 24 hours in flowing hydrogen. The Ni-Si, Ni40Cr-Si and CoCrAlY-Si specimens were prepared by melting the metals in an alumina crucible for 20 minutes under an argon atmosphere after which time the specimens were annealed for 24 hours at 1100°C in argon. The γ/γ'-α eutectic was directionally solidified at 50 cm per hour. The other alloys were similarily prepared by melting in an alumina crucible under an argon atmosphere.

All specimens were machined to approximately 1.3 cm x 1.3 cm x 0.2 cm (4.4 sq cm surface area) and ground to 600 grit. Specimens were suspended either from a hole drilled into the sample or from a platinum wire wrapped around the sample. Prior to insertion into the experimental apparatus, test specimens were washed and degreased; the final rinse was with absolute ethanol.

B. Procedures

All oxidation experiments were conducted using Ainsworth type RV-AU-1 balances, which are readable to 0.01 milligrams and reproducible to $\pm$ 0.02 milligrams. The specimens were introduced into a quartz tube (2.5" OD) which was heated by a three zone Marshall furnace maintained at $\pm$ 5°C of the set temperature by a Leeds and Northrup proportional controller series 60.

The sodium chloride vapors were generated from the fused salt held in a platinum crucible on a movable pedestal within the quartz tube. The temperature of the crucible was measured by a thermocouple lying immediately adjacent to the pedestal. The concentration of sodium chloride gas was determined from the differences in weights of the platinum crucible before and after each experiment and the mass flow of air.

IV. RESULTS AND DISCUSSION

Task I - Effect of Gaseous Environments on Hot Corrosion of Superalloy Materials

A. Complex Alloy Substrates

As noted, it was previously demonstrated that the response of alloys to gaseous mixtures of air and a few parts per million NaCl differ substantially depending on the composition of the substrate. Whereas 10ppm NaCl(g) significantly increased the oxidation rate of NiAl, the alloy B-1900 underwent catastrophic corrosion (Refs. 5, 6). The observation that the nickel base superalloy developed regions enriched in molybdenum at the base of the corrosion front infers that the enrichment in molybdenum at the scale-alloy interface as well as the isothermal rupturing of protective alumina scales by the NaCl(g) are contributing factors to the accelerated oxidation of this alloy.

In order to study the relationship between refractory metal content, oxide morphology and sodium chloride concentrations, the alloys listed in Table I were chosen for this study. The choice of alloys encompasses the complex nickel base superalloys B-1900, IN792, and the gamma-gamma prime alloys containing various amounts of either alpha molybdenum or molybdenum-rich precipitates, as well as the alloy Hastelloy X, in which molybdenum is present primarily as a solid solution strengthener. The nickel base alloys NX-188 and IN792 have been included to examine the effect of smaller quantitives of discrete refractory metal precipitated phases. It is further noted that the nickel base superalloys B-1900 and gamma-gamma prime alloys including NX-188 will tend to form aluminum-enriched scales whereas Hastelloy X and MAR M-509 tend to form chromia-rich scales. MAR M-509 is included to separately study the role of tungsten.

1. Thermogravimetric Studies-Air Alone

In order to establish base lines, all of the alloys have been isothermally oxidized at 900 and 1050°C in flowing air, cf. Figs. 1-6. A more detailed study of the tungsten-modified NX-188 was conducted in the temperature range 600-1200°C. It is realized that accelerated oxidation of iron alloys containing various amounts of molybdenum has been reported when the alloys were exposed in stagnant air (Ref. 15). In order to determine if the same effects occur in the Ni-Mo-Al system, all of the Ni-Mo-Al alloys, including IN-792 were exposed in stagnant air at 900°C for durations up to 260 hours. No meaningful differences were noted in the oxidation rates of the alloys when exposed to flowing or stagnant air, eg. Fig. 6.

For the compositions tested here, the kinetic data suggests two categories of alloys. In the first class MAR-M509, IN-792 and Hastelloy X, as well as B-1900, reported previously (cf. Fig. 18 in Ref. 5), exhibit comparatively low oxidation rates at both 900 and 1050°C, Figs. 3-5. On the other hand, at 900°C the alloys γ/γ'-α, NX-188 and W-modified NX-188 exhibit comparatively higher oxidation rates, Figs. 1, 2, 6.

In the case of the model tungsten-containing NX-188 alloy, when the data shown in Fig. 6 are plotted on logarithmic coordinates, the slopes of the curves are between 0.5 and 0.33. The negative deviations from parabolic behavior could be due to both volatilization effects as well as the eventual growth of slower developing suboxide scales. If such deviations are ignored, and parabolic behavior assumed, then the calculated activation energy for the oxidation process is about 30 kcal/mole.

Needle-like crystals were deposited onto colder sections of the quartz tubes, most notable for experiments conducted at or above 800°C. Examination of these crystals by energy dispersive x-ray (EDAX) techniques revealed the presence of both Mo and W and the complete absence of Ni and Al. It is presumed that these deposits are mixtures of MoO_3 and WO_3.

However, metallographic studies, as will be discussed, show the localized formation of protective alumina scales. Since the rate of growth of alumina is slower than NiO, negative deviations from parabolic oxidation kinetics described in terms of NiO scale formation are expected.

The steady-state kinetic rates were observed to increase monotonically from 600°C approximately 1050°C. The inversion in the kinetic rate that was observed at 1100°C could be associated with both volatilization effects and the local formation of alumina scales. It was also determined that the same oxidation kinetics were observed for specimens oxidized at 900°C in flowing and stagnant air.

2. Metallographic Studies-Air Alone

Thin protective scales form on the alloys when exposed to air alone. In greater detail, for the model tungsten-modified NX-188 alloy, the oxides identified by x-ray diffraction for specimens exposed at or above 900°C are:

1. an outer layer of NiO
2. a middle layer of $NiMoO_4$, $NiWO_4$ and $NiAl_2O_4$; and
3. the isostructural phases MoO_2 and WO_2 at the scale-metal interface.

As the exposure temperature increased from 800°C to 1200°C, the relative amount of $NiAl_2O_4$ in the middle oxide layer was qualitatively observed to increase relative to the $NiMoO_4$ and $NiWO_4$ phases. Scales on specimens oxidized at 600°C and 700°C exhibited outer NiO layers in addition to faint unidentified lines in an underlying thin oxide layer. Al_2O_3 was not identified in the oxide scales.

The oxidized specimens were examined by metallographic, microprobe and scanning electron microscopy techniques. The outermost oxide layer for all specimens was NiO. For specimens cooled to room temperature from exposure at 900°C or greater, exfoliation of the outer NiO layer was generally associated with microcracking and fragmentation in the middle $NiMoO_4$, $NiWO_4$, $NiAl_2O_4$ layer. Hence, it is unknown if this layer is protective at test temperature. Microcracking is assumed to be associated with volume changes caused by crystallographic transformation as reported for $NiMoO_4$ (Refs. 15, 16, 17). However, metallographic and SEM analyses of the outer NiO oxide layer indicates that this scale formed on the model alloy is porous. Moreover, two kinds of porosity occur.

In the temperature range of 600-800°C, isolated pin hole porosity is frequently observed, Fig. 7. In cross-section, a protective NiO layer does not form across apparently protected α-Mo(W) grains which appear at the gas metal interface, Fig. 8. At present the oxide scale formed on the surface of the α-Mo(W) grains at the gas-metal interface has not been identified. Furthermore, tungsten-rich oxides are also identified on the surface of the NiO scale, Fig. 9.

At temperatures of 900°C or greater, other changes become evident. Whereas at 600-800°C isolated pin-hole porosity was associated with α-Mo(W) particles, for temperatures at or above 900°C the porosity becomes increasingly more related to grain and sub-grain boundaries, Fig. 10. Concomitant with such grain boundary features in the other NiO scale, the surfaces of oxidized specimens exhibit linear features of enhanced oxidation resistance, whose frequency similarly increases with test temperatures, Fig. 11. Examination of specimens oxidized at higher temperatures where such features are further developed shows that these oxidation resistant areas develop because of the localized formation of thin protective alumina-rich scales.

When specimens are exposed at and above 900°C, internal oxidation is observed, Fig. 12. With the outer NiO layer spalled off, the complex $NiMoO_4$, $NiWO_4$ and $NiAl_2O_4$ layer are separated from the underlying internally oxidized metal by a layer of $(Mo, W)O_2$ which is in turn randomly perforated by non-interconnected internally oxidized alumina particles, Figs. 12 and 13. Microprobe studies indicate the aluminum content in the alloy at the base of the internally oxidized γ'-depleted layer is about two weight percent. No

enrichment of Mo or W is observed in or at the base of the internally oxidized layer. Moreover, at the base of the internally oxidized layer, geometric shaped, internally precipitated particles are observed and were found to be aluminum nitride rather than aluminum oxide, Figs. 13 and 14. Nitride particles at the base of the internally oxidized zone indicate that: 1) the oxygen potential is low, and 2) nitrogen apparently diffuses through the oxide scale. Thusly, the oxidized microstructure for specimens of this alloy developed by exposure at 900°C and above are characterized by:

1) an imperfect NiO layer,

2) a complex $NiMoO_4$, $NiWO_4$, and $NiAl_2O_4$ layer which fragments on thermal cycling,

3) a $(Mo, W)O_2$ layer which is randomly penetrated by segregate internally oxidized Al_2O_3 particles,

4) a γ'-depletion zone with internally oxidized Al_2O_3 particles, and

5) randomly precipitated AlN particles in a γ'-depletion zone.

Experiments conducted in pure oxygen as opposed to air also showed internally precipitated oxides, but no nitrides. However, the weight changes observed after 24 hours exposure to either flowing or stagnant oxygen at 900°C did not significantly differ from that resulting from exposure to air. Hence, it is tentatively concluded that the formation of nitride particles does not markedly influence the oxidation behavior of the alloy. Lastly, no evidence was found for Mo(W) rejection to yield α-Mo(W), nor were any microstructural differences observed for specimens oxidized at 900°C in either flowing or stagnant air.

Gamma prime depletion zones increasingly dominate the characterization of specimens oxidized above 900°C, Figs. 12 and 15. Elevated temperature exposure similarly affects the microstructure of the underlying alloy, causing α-Mo(W) precipitation and grain boundary coarsening effects at temperatures of 1100°C or greater, Fig. 15.

In areas of the specimen, oxidized at 1100°C, which showed oxidation resistant ridges, which are associated with grain and sub-grain boundaries, optical metallography and microprobe studies show the coalescence of internally oxidized alumina particles to yield thin locally continuous alumina scales at the metal oxide interface, Fig. 16. Moreover, as observed at lower temperatures, precipitated AlN particles are present in the γ'-depletion zone, e.g., Fig. 14.

In the case of the γ/γ'-α alloy, for specimens exposed at both 900 and 1050°C, the alloy forms a loosely adhering duplex scale. At the outermost surface a thin NiO layer is formed. Below this layer, a friable oxide zone has developed. The oxides consist primarily of $NiMoO_4$ with small amounts of $NiAl_2O_4$. The phases $NiMoO_4$, $NiAl_2O_4$, MoO_2 as well as gamma nickel are identified when the loosely adhering oxide scale is removed and the oxidized metal surface is examined by x-ray diffraction techniques. Metallographic cross sections reveal the presence of extensive internal oxidation, Figs. 17 and 18. Like the tungsten modified NX-188, the microprobe indicates these particles to contain aluminum and nitrogen and are likely AlN, eg. Fig. 14.

3. Studies in Air with NaCl(g)

Depending upon composition, the response of specimens tested in air with NaCl(g) varied widely.

γ-γ'-α

The rate of oxidation of the nickel base alloy γ/γ'-α containing alpha molybdenum fibers was catastrophically rapid when exposed at 900°C to air containing seven (7) ppm NaCl(g), Fig. 1. The rates reported here are much greater than those reported for B-1900 exposed under similar conditions, Fig. 18 in Ref. 5. Unlike the case for oxidation in air alone, metallographic cross sections of the specimen tested with 7ppm NaCl(g) indicate that oxidation rates are so rapid that a γ' depletion zone does not form, Fig. 19 cf. Fig. 17. Along transverse alloy surfaces, unoxidized α-Mo fibers extend up to the oxidized surface.

On the other hand along longitudinal surfaces, unoxidized α-Mo occasionally extend into the oxide scale, Fig. 20. Thus it appears that under the conditions of this experiment the γ/γ' matrix is preferentially attacked.

NX-188 and Tungsten-Modified NX-188

In the presence of NaCl vapors, both NX-188 and the tungsten-modified NX-188 behaved similar to γ/γ'-α. Thusly, while oxidation in air yielded protective kinetics, cf. Figs. 2 and 6, the addition of NaCl vapors distinctly altered such behavior. At 900°C with 10 ppm NaCl(g) in flowing air, initial oxidation rates were accelerated as compared with those for air alone, Fig. 2, 21. Moreover, in the case of the tungsten-modified alloy, after about 25 to 35 hours exposure, isothermal spallation events dominated the thermogravimetric behavior. At 1050°C, the affect of 100 ppm NaCl(g) was to markedly increase the rate of oxidation of the alloy although isothermal scale spallation events were not observed, Fig. 22. Due to the rapid and excessive weight gain, long term exposures were not practical because the weight change exceeded the capabilities of the balance. Other experiments at 900°C involving exposure of a Ni-10 w/o Mo alloy to air containing NaCl vapors also resulted in accelerated oxidation rates, Fig. 23. However, the magnitude of

the effect is not as dramatic as that observed for the superalloys. Nevertheless, it appears that the presence of aluminum in the Ni-Mo-W-Al alloy is not a prerequisite for the rapid oxidation rates observed with NaCl(g).

Although it has been reported that the oxidation behavior of molybdenum-rich alloys is affected by flowing or stagnant environments, no effects were noted herein. In order to study the effect of NaCl(g) on the behavior of alloys with preformed oxide scales, an experiment was designed in which the tungsten-modified NX-188 alloy was oxidized at 900°C in stagnant air for 120 hours, after which a crucible containing NaCl was inserted into the system. The salt-filled crucible was maintained at a temperature which should produce 10 ppm NaCl(g) under flowing air conditions. The crucible was held in place for approximately 70 hours.

As shown in Fig. 24, the initial oxidation under stagnant air conditions conforms well with that observed earlier, Fig. 6. With the insertion of the salt crucible into the quartz tube, an incubation period lasting several hours is followed by accelerated oxidation kinetics. Removal of the salt crucible is followed after a few hours by a return to oxidation kinetics similar to that shown by specimens oxidized in air alone.

Unlike tungsten-modified NX-188 specimens oxidized in air alone, the corrosion morphology associated with NaCl vapors exhibits a pitting-like attack, Fig. 25. The previously observed refractory metal zones seen in the absence of NaCl(g) were not observed. Moreover, in areas away from the oxidation pits, internally oxidized regions are more pronounced than was the case for exposure to air alone, with internally oxidized particles extending virtually throughout the affected alloy layer to the substrate below, Fig. 26. No distinct band of AlN particles is visible at the base of the internally oxidized regions. For specimens oxidized in air, the particles are coarsened and a well-defined γ'-depletion zone separates such oxide particles from the metal below, particularly at 1050°C. At the base of oxidation pits common for such exposure, the thickness of the $(Mo, W)O_2$ layer and adjacent internally oxidized zone is markedly thinner than elsewhere, Fig. 26b, cf. Fig. 26a. If the imperfect $(Mo, W)O_2$ layer is in part responsible for the oxidation resistance of the alloy, then the thinning of this layer by interaction with NaCl would be expected to yield accelerated oxidation kinetics. Significantly, the reported activation energy for the oxidation of molybdenum, i.e., 36.5 kcal, is very close to that reported for Ni, i.e., 34-35 kcal (Refs. 18, 19, 20).

The existence of a gaseous molybdenum oxide-NaCl (and/or NaOH)-bearing vapor species would support such a possibility. Indeed, Fryburg, et al. have reported gaseous species resulting from the oxidation of Mo in air with NaCl(g), namely $(NaCl)_{1,2}(MoO_3)_3$, $(NaOH)(MoO_3)_3$ as well as $(MoO_3)_4$ and $MoO_2(OH)_2$ (Ref. 11). The thinning of an MoO_2 layer was observed for Ni-10 w/o Mo similarly exposed at 900°C to air with NaCl vapors. Hence, the presence of a protective alumina scale is not necessary for accelerated attack by NaCl. However, if alumina scales covered local areas to effect enhanced oxidation resistance, then, based on prior work, such areas would also be subject to attack by NaCl vapors (Refs. 5, 6).

MAR-M509 and Hastelloy

The chromium rich-aluminum free alloys, MAR-M509 and Hastelloy X, did not undergo catastropic oxidation when exposed at 900°C to air containing 7 parts per million NaCl(g). The alloy MAR-M509 behaved very similar to that previously reported for Ni-Cr alloys (Ref. 1). The Ni-Cr alloy family when exposed at elevated temperatures to air containing gaseous NaCl exhibited characteristic "S"-shaped curves, (Ref. 5, 6). The apparent rate of oxidation at the end of the experiment, after breakaway kinetics occurred, appears similar to that for the specimen oxidized in air alone at 25 hours, cf. Fig. 3.

The "S"-shaped oxidation behavior observed for the Ni-Cr alloys as well as MAR-M509 was not noted when Hastelloy X was exposed at 900°C to flowing air containing 7ppm NaCl(g). Nevertheless, for Hastelloy X compared with oxidation in air alone, markedly increased oxidation rates occur, Fig. 4. If breakaway oxidation kinetics similar to that observed for MAR-M509 occur here, such kinetics ensued shortly after the initiation of the experiment. Additionally, at the termination of the experiment, kinetic rates are similar to those observed in the absence of NaCl, cf. Fig. 4.

Metallographic cross sections of tested Hastelloy X reflect differences of exposure based on the presence or absence of NaCl(g). In the absence of NaCl(g) a very thin protective oxide layer forms, Fig. 27. On the other hand, with NaCl vapors present a much thicker scale develops.

IN792

The oxidation behavior of IN-792 in the absence or presence of NaCl(g) is shown in Fig. 5. In many previous tests, although the initial rate of oxidation of the complex alloys was not affected by the NaCl(g), after long term tests, either the rates of oxidation increased or, as a result of metallographic studies, it was possible to demonstrate that an effect has occurred. However based upon weight change data, the oxidation rate

for IN-792, even after extended time periods, did not appreciably differ from that resulting from exposure to air alone.

In cross section, specimens tested in either air alone or air with NaCl vapor showed the formation of thin protective scales and internal oxidation effects which are at least partially related to the original superalloy carbide network, Fig. 28. Incorporated within such oxidation affected alloy zones, tiny precipitates occur, Fig. 28. Specimens exposed to NaCl vapor show many such particles. However, they are certainly not absent in specimens tested in air alone. Although probe studies clearly show titanium enrichments in such particles the presence of other elements in these particles could not be determined. Thus their nature is unknown.

Although no differences in weight gain or metallography were noted for IN-792 specimens exposed to air and air containing NaCl(g), topographical differences were noted.

The external scale morphologies depended on whether or not NaCl(g) was present in the oxidizing atmosphere. In air alone, the dense adherent scale was principally comprised of small crystallites enriched in chromium but with appreciable titanium, Fig. 29. Occasionally more regularly shaped Ti-rich prisms protruded from the scale, Fig. 29.

On the other hand, convoluted oxide layers were found on specimens tested in air with NaCl vapor present, Fig. 30. Additionally, large numbers of well-formed titanium-rich oxide needles decorated the scale surface, Fig. 30. No evidence of aluminum enrichments or alumina whiskers were observed on the external scales of specimens tested with or without NaCl(g) present.

In this program, the oxidation behavior of the alloys in Table 1 was examined. It has been shown that the presence of even minor concentration of NaCl(g) can adversely affect oxidation performance. The presence of molybdenum or tungsten in solid solution in aluminum-free alloys may lead to accelerated (or breakaway oxidation) kinetics. With a relatively high chromium level (12.4 wt%) and a low level of aluminum (3.1 wt%), the 1.9 wt% of molybdenum and 3.8 wt% tungsten in IN-792 does not adversely affect oxidation kinetics in NaCl(g)-bearing atmospheres.

On the other hand, nickel base alloys containing high levels of aluminum and molybdenum have undergone catastrophic oxidation.

B. Effect of Silicon Additions

Three elements in the periodic table are commonly considered capable of forming useful protective scales. These elements are aluminum, chromium and silicon. Extensive work has shown that low levels of volatile chlorides can interact with chromia and alumina scales. A paucity of information exists with respect to silica-containing scales. Additionally, interest is increasing to add silicon to protective coating formulations for possibly enhanced oxidation/hot corrosion resistance. Thus experiments were performed to determine the effect of low levels of NaCl(g) on model silicon-containing alloys.

Tests involved three sets of model alloys:

a. alloys which tend to form primarily silicon-containing protective scales, Ni-5Si and Ni-11.5Si;

b. alloys which tend to form chromia scales and silica-containing scales, Ni-40Cr-5Si and Ni-40Cr-11.5Si;

c. alloys which tend to form alumina and silica-containing scales, CoCrAlY-5Si and CoCrAlY-12.5Si.

The base line oxidation studies of the alloys are shown in Figs. 31-38. In general the addition of more than 5% silicon improved the oxidation behavior of nickel. The alloys Ni-40Cr and CoCrAlY gain weight very slowly in the temperature range of interest and the addition of silicon to one alloy did not strongly alter oxidation kinectics.

The addition of up to 10 ppm NaCl(g) to the environment did not significantly alter the oxidation kinetics of unalloyed or silicon-modified nickel. However the silicon addition strongly influenced the performance of the Ni-40Cr alloy. It had been previously shown tnat the addition of gaseous NaCl results in "S" shaped curves. The initial rapid change in weight associated with scale - NaCl(g) interaction either weakens or cause premature scale breakup. This effect is shown in Fig. 34. The addition of 5% silicon to the Ni-40Cr alloy completely eliminated the breakaway phenomenon, Fig. 34. Thus the addition of a small quantity of silicon to this alloy is quite beneficial with respect to the NaCl(g) oxidation behavior.

The effect of yttrium and silicon on the oxidation behavior of the alloy CoCrAl is shown in Figs. 36 through 38, respectively. In general, the low levels of NaCl(g) for the durations examined did not adversely affect the oxidation behavior of the alloys. As will be discussed, yttrium can exert a beneficial effect and hence the addition of silicon is not readily determined.

C. Influence of Reactive Element Additions

Additions of lanthanide elements such as yttrium (Refs. 21, 22, 23) and elements such as hafnium have been shown to improve the oxidation resistance of coatings; however, the mechanism(s) by which improvement occurs is not fully understood. The

principle mechanisms thought to be responsible for the improved scale adhesion are (a) pegging and (b) vacancy sink formation which minimizes pore formation (Ref. 23). In both mechanisms the atmosphere is not considered except insofar as oxygen is supplied to form the protective scale.

However, gas turbine atmospheres, as noted earlier, contain trace levels of NaCl(g) as well as NaOH(g) and HCl(g). It has already been demonstrated that NaCl(g) can dramatically and deleteriously affect the nature of the protective alumina and chromia oxide scales.

The deleterious effect of NaCl could be attenuated by either or both of two processes. In the first place, the NaCl(g) can conceivably react with the additive oxide to form species such as $(NaCl)_xY_2O_3$ or $(NaCl)_xHfO_2$ which are similar to those observed in the NaCl-Cr_2O_3 system. Alternatively, the rare earths and hafnium have been reported to form oxyhalide species (Refs. 24, 25, 26). In the case of forming either an NaCl-yttria or -hafnia complex or an oxyhalide species, if the chloride moiety is sufficiently stable, protection of the alumina or chromia scale will be effected by such "scavanging" processes.

Secondly, if the additive element, e.g., Y or Hf, were to obstruct diffusion paths of either NaCl(g) into the alumina scale or the "NaCl-Al" moiety back out through it, then the integrity of the protective alumina scale would be enhanced.

Thusly, in addition to mechanical pegging or serving as vacancy sinks, effects either resulting from chemical scavanging or blocking of diffusion paths would provide an alternative mechanism whereby low level additions of elements such as yttrium and hafnium beneficially affect coating behavior.

In the work reported herein as well as in previous studies (Refs. 1, 2), the presence of alumina whiskers on simple alumina formers oxidized in quartz tubes have been associated with the low concentrations of gaseous corrodents, e.g., NaCl, NaOH, HCl. In the presence of low levels of these gaseous corrodents, Al_2O_3 whiskers, blades or platelets are produced, and protective scale rupturing is evidenced. In their absence a dense, compact, adherent alumina oxide scale is formed, and no whiskers are observed.

In order to examine the role of hafnium and yttrium in the oxidation behavior of CoCrAl alloys, the following four alloys (CoCrAl, CoCrAl-0.5Y, CoCrAl-1.3Y, and CoCrAl-0.5Hf) were simultaneously exposed side by side to 10ppm NaCl vapors in flowing air at 900°C for 72 hours. The CoCrAl specimen exhibited a multilayered alumina scale, Fig. 39. The outermost alumina layer consists of a porous layer of thickened alumina whiskers similar to that reported previously for NiAl oxidized in air with 100ppm NaCl(g), Fig. 40, cf. Fig. 10 in Ref. 5.

The CoCrAl-0.5Y specimen similarly evidences coarsened alumina whiskers on the external surface in agreement with behavior previously reported, cf. Fig. 13 in Ref. 1. However, the CoCrAl containing 1.3Y or 0.5Hf exhibited no evidence of either convoluted scales or alumina whiskers.

Concurrent with the above experiment NiAl, CoCrAl, CoCrAl + 0.5Y, CoCrAl + 1.3Y and CoCrAl + 0.5Hf were placed side by side into a box furnace at 1050°C for 94 hours. The furnace had been previously used for hot corrosion studies, and it is assumed that low (ppm) uncontrolled and unmonitored background levels of gaseous corrodents, such as NaCl, were present in the ambient furnace atmosphere during this experiment. The oxidized surfaces were examined by scanning electron microscopy techniques.

The NiAl exhibited the Al_2O_3 whiskers and a highly convoluted oxide surface, similar to that previously reported in Refs. 5, 6.

The surface of the CoCrAl specimen exhibits similar convolutions and the alumina whiskers, Fig. 41. In areas where the scale is removed from the surface, the alumina scale is wrinkled, and no attachment sites are evidenced, i.e., the metal surface is flat, Fig. 42. In areas where attachment of the scale to the metal surface is evident, attachment points of the scale to the metal surface are evident. In areas where attachment is both present and absent, no differences in the morphology of the alumina scale are apparent, Fig. 42.

In the case of the CoCrAlY specimen containing 0.5%Y, exposure in the furnace atmosphere at 1050°C produced an irregular alumina surface with random "blooms" containing yttria, Fig. 43. However, neither a convoluted alumina scale nor alumina whiskers were observed. And, indeed, for the CoCrAl alloys containing 1.3Y and 0.5Hf, similar structures were evidenced-namely, a flat, dense, compact alumina scale and random oxide blooms containing Y or Hf.

Thus based upon the experimental results, the addition of yttrium or hafnium to CoCrAl compositions can inhibit the deleterious effects of NaCl vapors. The means by which this beneficial affect is achieved--that is by scavanging volatile chloride vapors and/or blocking diffusion paths--is unclear.

In order to better understand how yttrium and hafnium mechanistically benefit the scaling behavior of the CoCrAl composition, it is necessary to have a knowledge of whisker morphology.

Thusly, whiskers formed on the oxide scale of an NiAl specimen exposed at 1050°C for 100 hours have been examined by scanning electron microscopy techniques. As shown in Fig. 44, the whiskers grow from "dimple-like" eruptions on the dense scale surface. Near the scale-gas interface, the whisker growths generally are highly segmented and heavily branched and do not possess well-developed, highly geometric surfaces, Fig. 45. Physically they look like tubes. A high degree of segmentation suggests that growth occurs in spurts rather than as the result of a single continuous process. Moreover, an examination of the ends of unbroken whiskers in such areas fails to show any evidence of an open channel to the surface.

Further out from the oxide surface, more regularly shaped crystals form at the ends of the less geometric tubes and/or "dimple-like" eruptions,

Fig. 46. As was the case with the tube-like growths, no evidence of holes protruding through the ends of these crystallites was detected.

To determine the possibility of hollow channels extending through the inside of these whisker growths, the whisker-covered oxide surface was lightly abraded and then re-examined. In the case of the more highly facetted, better geometrically shaped crystals, no evidence of any channels was found. However, for the tube-like features, hollow channels were found, Fig. 47.

The approximately 200 Å diameter channel shown in Fig. 47 closely approaches the ultimate resolving capabilities set by design parameters of the scanning electron microscope. Hence, smaller channels may exist but are below the resolving power of this instrument.

The existence of hollow channels in alumina whiskers as determined here by scanning electron microscopy techniques are also supported by early results of transmission electron microscopy studies conducted by Smialek (Ref. 27) on ion-thinned whiskers.

The presence of hollow channels in such whiskers thus qualitatively supports the growth mechanism earlier proposed (Refs. 5, 6).

Task II. Gaseous Environments Related to Low Power Corrosion

It is generally believed that with respect to sulfidation corrosion, the magnitude of the effect increases with increasing temperature. However, at very high temperature, sulfidation corrosion may not be a problem because the fused salt necessary for corrosion either does not condense or if present as a result of lower temperature operations, evaporates before significant damage occurs. Recently however, in marine environments, an inverse relationship was reported wherein it was observed that within the temperature range of about 1200° to 1400°F, the rate of corrosion associated with deposited alkali salt was greater than that observed at higher temperature (Ref. 9).

At present, many investigators studying hot corrosion are examining the relationship between accelerated oxidation and the formation and deposition of alkali pyrosulfates. These salts melt at relatively low temperatures and have been shown in the boiler industry to play an important role in the accelerated corrosion of boiler hardware.

The relationship between low temperature corrosion, salt, and partial pressure of SO_3 (pyrosulfate formation) is based upon metallographic observations. When sodium sulfate-coated turbine components are exposed in SO_3

environments, the corrosion produced is characteristically similar to that observed on turbine components removed from marine gas turbines which operated at reduced power. This corrosion microstructure is noted primarily on the concave surfaces and at the leading edge (Ref. 9). Moreover, it has been shown that liquid sodium pyrosulfate and SO_3-rich sodium sulfate melts will readily flux alumina scales (Ref. 7). In laboratory tests, additions of SO_3 (SO_2/O_2) required for such effects depends on the particular sulfate salt used and the test temperature. In these experiments, whenever a susceptible substrate such as CoCrAlY is coated with a salt such as sodium sulfate and exposed to the appropriate atmosphere and temperature condition, very rapid attack follows (Ref. 7).

However, an inconsistency associated with the description of the formation of the accelerated corrosion in terms of Na_2SO_4 deposits and SO_3 (SO_2/O_2) additions to test atmospheres is the observation that, although corrosion associated with this microstructure occurs primarily on concave (or pressure) airfoil surfaces, salt deposits are noted on all surfaces (Ref. 9). Moreover, it is reported that within the duty cycle the engine briefly drops to idle (Ref. 28), and as reported by Bessen and Fryxell, the concentration of unburnt hydrocarbons and carbon monoxide can be as high as 0.1 percent. Also, particulate char formation occurs (Ref. 28). Moreover, the corrosion is associated primarily with the surface exposed to line of sight effects and because carbonaceous deposits are reported to be present on the turbine surfaces (Refs. 9, 12, 28), the simultaneous presence of these deposits and the formation of SO_3-rich compounds is thermodynamically not favored. Lastly, it has been reported that similar coatings have performed exceptionally well in the temperature range of 704°C (1300°F) with fuels containing almost 3 percent sulfur (3 percent H_2S), even though based upon chemical analysis, sodium sulfate was found on the airfoil surfaces (Ref. 29).

The observations that the corrosion can be related to (a) impaction phenomena, and (b) the presence of carbonaceous deposits requires re-examination of the role of sulfur and carbon in hot corrosion. In the experiments reported herein, a burner rig was modified by the insertion of a duct between the burner and test specimens. Sulfidation corrosion is induced by the addition of 30 ppm (in terms of the combusted gases) synthetic sea salt solution into the burner. The sulfur content of the fuel is increased to a nominal 1 w/o by the addition of SO_2 to the combustion air, and the average metal temperature of the CoCrAlY specimens is 1350°F. Within 25 test hours the specimens generally exhibit the darkened discolorations associated with low power corrosion, and metallographic examination of the specimens verify that accelerated corrosion has occurred, Fig. 48.

In one series of test a combustion shield was placed between the burner and the rotating specimens. The combustion shield prevents particles from impacting the surface but does not affect gas composition. At the end of 50 test hours, no corrosion was noted, however salt deposits were visually observed on test specimen surfaces, Fig. 49.

In another series of tests, CoCrAlY specimens were honed in order to sensitize the alloy, Fig. 50. Honing apparently increases the sensitivity of the coating to corrosion.

In the tests the specimens revolve at about 1750 rpm or travel into the flame at about 1600 ft/min. The calculated gas velocity at the specimen is 1370 ft/min. Thus, with respect to the CoCrAlY specimen, only the face entering the flame would be subjected to any particles that are generated within the burner. In the nonducted burner the exit gas velocity is close to Mach 0.3, and thus for all practical purposes, both faces of the erosion bar are subjected to particle impaction.

The experimental results are as follows. Hot corrosion occurred primarily on one face of the erosion bar. As shown in Fig. 51, corrosion occurred primarily on the face which enters into the flame. In order to determine the rate of salt deposition, the amount of sodium sulfate present on each face was quantitatively chemically determined. It was found that for all practical purposes the rate of deposition of sodium sulfate on each face was identical, 0.07 $mg/cm^2/hr$, on the face entering the flame and 0.08 $mg/cm^2/hr$ on the face away from the flame.

No significant corrosion was noted on the face that leaves the flame, Fig. 50. Metallographic examination revealed only the presence of thin oxide scales on the trailing surfaces of the salt-coated specimens.

Moreover, metallographic examination of CoCrAlY coatings, tested in ducted burner rigs at 1350°F with sea salt and 1% SO_2 additions, indicates that discontinuous precipitation effects can occur in the coating adjacent to hot corrosion pits, Fig. 52. Here microprobe studies indicate that the β-CoAl phase is locally dissolving in the α-Co (Cr,Al) matrix immediately adjacent to such pits. On reprecipitating, fine lamellae of β-CoAl are distributed in the α-Co matrix all the way to the oxide pit itself. The precipitates shown here have not subsequently coarsened. Of course one way to dissolve and precipitate the β phase could involve brief, intense, highly localized heating effects. No such fine β-precipitates occur in the coating away from such corrosion pits. Thus they are truly a surface related phenomena.

Additionally modified CoCrAlY compositions exposed to the same test conditions show surface carburization affects but only in advance of hot corrosion pits, which only occur on leading edge surfaces, Fig. 53. No carbides occur on trailing surfaces nor anywhere in the bulk of the specimen.

These observations indicate that impaction can alter the surface stability by processes that locally produce very fine grained microstructures or corrosion prone phases (i.e., carbides) at the scale-metal interface. By such effects then impaction plays a role in accelerating corrosion processes.

The fuel is the source of the carbon. The concentration of carbon within the burner depends upon the combustion characteristics of the burner. The combustors currently employed are not very sophisticated, and, in general, are quite similar to the burners used for oil-fired home heating systems. Sulfur is reported to have an effect on the formation of carbon in oil burners. It is reported (e.g., Ref. 30), that the additions of the oxide of sulfur into the combustion flame markedly affects the formation of soot (carbon) within the flame. Thus, the addition of SO_2 to the burner can increase the concentration of carbon in the burner exhaust. Thus, the ducted burner could continually produce soot particles capable of impacting test specimens. The experimental laboratory procedure in which salt-coated specimens together with fuel are inserted into hot furnaces for brief durations and then aged at lower temperatures in part is designed to simulate situations which could occur during ignition or when kinetic conditions are not sufficiently rapid to completely oxidize fuel (or char particles) by the time such atmospheres reach the high pressure turbine section of the gas turbine.

V. SUMMARY AND CONCLUDING REMARKS

Low levels of NaCl(g) have been shown previously to react with normally protective oxide scales that form on NiAl, Ni-Cr alloys and the nickel-base superalloy B-1900 (Ref. 5, 6). Continuing these studies, the results reported here show that, for a variety of complex superalloys, even small levels of NaCl(g) adversely affect oxidation performance. The degree of such adversity depends upon alloy composition.

For aluminum-free alloys, i.e., MAR-M509 and Hastelloy X, molybdenum or tungsten present in solid solution can lead to accelerated (or breakaway oxidation) kinetics similar to that observed for Ni-Cr alloys (Refs. 5, 6). For IN-792, an alloy relatively high in chromium and low in aluminum, molybdenum and tungsten present in solid solution do not adversely affect oxidation kinetics in the presence of NaCl(g). However surface oxide structures are altered. On the other hand, nickel-base alloys containing high levels of aluminum and molybdenum, i.e., γ/γ'-α, NX-188, W-modified NX-188 and B-1900 (Ref. 5), are catastrophically attacked by NaCl(g)-bearing atmospheres.

Isothermal cracking of protective scales and refractory metal enrichments are undoubtedly contributing factors for accelerated oxidation of the high aluminum-molybdenum nickel base alloys. However accelerated oxidation also occurred for the aluminum-free Ni-10 w/o Mo in NaCl(g)-bearing atmospheres. Hence the rupturing of protective alumina-rich scales may be sufficient but not necessary to cause accelerated kinetics. Also for experiments conducted in stagnant, NaCl(g)-free atmospheres, no accelerated kinetics were observed for any of the alloys tested here.

For the γ/γ'-α, NX-188, and W-modified NX-188 compositions, oxidation in air alone produced complex oxide layers with well-defined γ'-depletion zones and internally precipitated AlN particles. In NaCl(g)-bearing atmospheres, kinetics were so rapid that γ'-depletion zones could not form. In fact for the alloy γ/γ'-α oxidized at 900°C in air with NaCl(g), α-Mo fibers can be seen protruding relatively unattacked into the oxide scale.

Silicon additions were, in general, observed to slightly improve oxidation resistance of Ni, Ni-40Cr and CoCrAlY compositions in NaCl(g)-bearing atmospheres.

To the extent that processes responsible for Al_2O_3 whisker formation deleteriously affect the adherence of protective scales, the addition of yttrium or hafnium to CoCrAl composition can inhibit such whisker growth.

Examination of Al_2O_3 whisker formed on NiAl show complex morphologies. Near the scale-gas interface, such growths are segmented, heavily branched and do not possess well-developed highly geometric surfaces. Physically such growths look like tubes. Further removed from the surface at the ends of the less-geometric tubes, more regularly shaped crystals form. Using a scanning electron microscope, hollow channels approximately 200Å in diameter were observed in the irregular tubes. No hollow channels were observed in the regular highly facetted, strongly geometric crystallites. However they could exist but were below the resolving power of the scanning electron microscope used here.

In laboratory studies using a ducted burner rig, CoCrAlY specimens were exposed at 1350°F to sulfidation conditions produced by the addition of 30 ppm synthetic sea salt and by increasing the sulfur content of the fuel to a nominal 1% by SO_2 addition to the combustion air. It was shown that the pitting corrosion observed with features consistent with that reported to result from low power Naval turbine operation was a result of impaction processes. The impaction events at the coating surface cause altered coating microstructure here and locally produce corrosion susceptible carbide particles. The impacting particles include carbonaceous chars whose ultimate source is the fuel and whose presence and formation depend upon combustor characteristics of the burner. It is reported that addition of the oxide of sulfur into the combustion flame markedly affects the formation of char particles (soot) in the flame. Hence, the addition of SO_2 into burners can increase the carbon concentrations in the exhaust gases. Thusly, these results affirm previously reported laboratory tests (Ref. 5) in which salt-coated specimens together with fuel were briefly inserted into hot furnaces for brief durations and aged at lower temperatures to effect pitting microstructures.

VI. ACKNOWLEDGEMENT

The authors gratefully acknowledge helpful discussions with Mr. C. A. Stearns, Dr. F. J. Kohl, and Dr. J. Smialek of NASA-Lewis Research Center, Cleveland, Ohio, and with Drs. M. A. Decrescente, R. A. Pike, and G. K. Layden of the United Technologies Research Center, East Hartford, Connecticut. The efforts of Ms. J. Whitehead, Ms. C. Clark, Mr. R. Brown, and Mr. L. Jackman for assistance in conducting the experiments presented herein are also acknowledged.

VII. REFERENCES

1. Ode, W. H.: Coal Analysis and Mineral Matter, Chapter 5, pp. 202-231, in Chemistry of Coal Utilization, Supplementary Volume, ed. by H. H. Lowrey, John Wiley and Sons, Inc., New York (1963).

2. Fryxell, R. E. and I. I. Bessen: Coating Life Assessment in Gas Turbines Operated for Ship Propulsion. In Proceedings of 1974 Gas Turbine Materials in the Marine Environment, held in Castine, Maine, pp. 259-276, ed. by J. W. Fairbanks and I. I. Machlin, MCIC-75-27, publ. by Metals and Ceramics Information Center, Bettelle Laboratories, Columbus, Ohio, July 1974.

3. Stearns, C. A., R. A. Miller, F. J. Kohl and G. C. Fryburg: Gaseous Sodium Sulfate Formation in Flames and Flowing Gas Environments. Presented at Symposium on Corrosion Problems Involving Volatile Corrosion Products. Electrochemical Society Meeting, Philadelphia, Pennsylvania, May 1977; also NASA TM X-73600 (1977); also J. Electrochemical Soc. 124, 1145 (1977)

4. Kohl, F. J., C. A. Stearns and G. C. Fryburg: Sodium Sulfate: Vaporization Thermodynamics and Role in Corrosive Flames, published in Metal-Slag-Gas Reactions and Processes, edited by Z. A. Foroulis and W. W. Smeltzer, Electrochem. Soc., Princeton, New Jersey, page 649 (1975), also NASA TM X-71641 (1975).

5. Smeggil, J. G. and N. S. Bornstein: Study of the Effects of Gaseous Environments on the Hot Corrosion of Superalloy Materials. NASA CR-159747, Final Contract Report. Conducted for NASA-Lewis Research Center, Contract No. NAS3-21376, January 1980.

6. Smeggil, J. G. and N. S. Bornstein: Study of the Effects of Gaseous Environments on Sulfidation Attack of Superalloys. NASA CR-135348, Final Contract Report, Conducted for NASA-Lewis Research Center, Contract No. NAS3-20038, November 1977.

7. Jones, R. L.: A Summary and Review of NAVSEA Funded Low Power Hot Corrosion Studies. NRL Memorandum Report 4072. Naval Research Laboratory. September 24, 1979.

8. LM 2500 Stage 1 HP Turbine Blade Corrosion Evaluation, Second Interim Report to Engineering Program Notice HT-05 LM 2500 HP Turbine Stage 1 Blade Life, April 26, 1976. Prepared under Contract N00024-76-C-4047.

REFERENCES (Cont'd)

LM 2500 Component Improvement Program for Naval Ships Engineering Center, Code 6146, General Electric Company, Marine & Industrial Department, Cincinnati, Ohio, 45215.

9. Wortman, D. P., R. E. Fryxell and I. I. Bessen: A Theory for Accelerated Turbine Corrosion at Intermediate Levels. Report No. R76AEG558, General Electric Company, Aircraft Engine Group, Cincinnati, Ohio. November 10, 1976. Also in the Proceedings of the 3rd Conference on Gas Turbine Materials in a Marine Environment, paper 11 in Session V, held at the University of Bath, England, September 20-23, 1976.

10. Stearns, C. A., F. J. Kohl, and G. C. Fryburg: Reactions of Chromium with Gaseous NaCl in an Oxygen Environments. Properties of High Temperature Alloys, ed. by Z. A. Foroulis and F. S. Pettit, Electrochemical Society/AIME, p. 655, (1976); also NASA TM X-73476 (1977).

11. Fryburg, G. C., R. A. Miller, F. J. Kohl, and C. A. Stearns: Volatile Products in the Corrosion of Cr, Mo, Ti and Four Superalloys Exposed to O_2 containing H_2O and Gaseous NaCl. Presented at Symposium on Corrosion Problems involving Volatile Corrosion Products. Electrochemical Society Meeting, Philadelphia, Pennsylvania, May 1977; also NASA TM X-73599 (1977).

12. Jones, R. L.: A Summary and Review of NAVSEA Funded Low Power Hot Corrosion Studies, NRL Memorandum Report 4072, Naval Research Laboratory, September 24, 1979.

13. McKee, D. W., and D. Chatterji: Corrosive Effects of Pyrolytic Carbon in Gas Turbines in Thirteenth Biennial Conference on Carbon, Irvine, California, July 18-22, 1977.

14. McKee, D. W. and G. Romeo: Met. Trans. 5, 1127 (1974).

15. Leslie, W. C. and M. G. Fontana, Trans. Am. Soc. Metals, 41, 1213 (1949).

16. Brenner, S. S.: J. Electrochem. Soc., 102, 7 (1955).

17. Gleiser, M., W. L. Larsen, R. Speiser and J. W. Spietnah: The Properties of Oxidation-Resistant Scales Formed on Molybdenum-Base Alloys at Elevated Temperatures. In Symposium on Metals in High Temperatures Environment, Cincinnati, Ohio, February 1955.

REFERENCES (Cont'd)

18. Moore, W. J. and J. K. Lee: Trans. Faraday Soc. 48, 916 (1952).

19. Kubaschewski, O. and O. von Goldbeck: Z. Metall K. 39, 158 (1948).

20. Gulbransen, E. A. and W. S. Wysong: Trans. AIME, 175, 611, 628 (1948).

21. Giggins, C. S. and F. S. Pettit: Oxide Scale Adherence Mechanisms and the Effects of Yttrium Oxide Particles and Externally Applied Loads on the Oxidation of NiCrAl and CoCrAl Alloys, Final Report Contract No. F33615-72-C-1702, to the Aerospace Research Laboratories, Contract Report No. ARL 75-0234, June 1975, Wright-Patterson Air Force Base, Ohio.

22. Allam, I. M., D. P. Whittle and J. Stringer: Oxid. of Met. 12, 35 (1978).

23. Kuenzly, J. D. and D. L. Douglas: Oxid. of Met. 8, 1939 (1974).

24. Nathansohn, S.: J. Inorg. Nucl. Chem. 30, 3123 (1968).

25. Johnson, Q. C. and D. H. Templeton: J. Chem. Phys. 34, 2004 (1961).

26. Ngia, L. H. and F. E. Stafford: Advances in High Temperature Chemistry, Vol 3, p. 213, ed. by L. Eyring, Academic Press, New York (1971).

27. Smialek, J.: Private Communication (1980).

28. Bessen, I. I. and R. E. Fryxell: Turbine Coatings and Protection in Marine Environments, pp. 73-84. Proceedings of Gas Turbine Materials Conference, Washington, D. C. October 1972.

29. Schilling, W. F., H. M. Fox and A. M. Beltran: Field Testing and Evaluation of Next-Generation Industrial Gas Turbine Coatings. In Proceedings of Conference on Advanced Material for Alternate Fuel Capable Directly Fired Heat Engines. Held at the Marine Maritime Academy, Castine, Maine. July 30-August 3, 1979.

30. Palmer, H. B., Equilibria and Chemical Kinetics in Flames in Combustion Technology--Some Modern Developments, p. 24, ed. by H. B. Palmer and J. M. Beer, Academic Press, New York (1974).

TABLE I

Nominal Chemical Composition (in w/o) of Substrate Alloys

Alloy Designation	Ni	Cr	Co	Mo	W	Ta	Al	Ti	Fe	Mn	Si	C	B	Zr
IN-792	61	12.4	9.0	1.9	3.8	3.9	3.1	4.5	---	---	---	0.12	0.02	0.10
MAR-M509	10	23.5	55.0	---	7.0	3.5	---	0.20	---	---	---	0.60	---	0.50
Hastelloy X	47.3	22.0	1.5	9.0	0.6	---	---	---	18.5	0.5	0.5	0.10	---	---
NX-188	74	---	---	18.0	---	---	8.0	---	---	---	---	---	---	---
W-Modified NX-188	72	---	---	14.0	6.7	---	7.75	---	---	---	---	---	---	---
γ/γ'-α	60.7	---	---	33.8	---	---	5.5	---	---	---	---	---	---	---

Ni
Ni-5Si
Ni-11.5Si
Ni-40Cr
Ni-40Cr-5Si
Ni-40Cr-11.5Si

CoCrAlY (20Cr, 10Al, 0.5Y)
CoCrAlY-5Si
CoCrAlY-11.5Si

CoCrAl
CoCrAl-0.5Y
CoCrAl-1.3Y
CoCrAl-0.5Hf

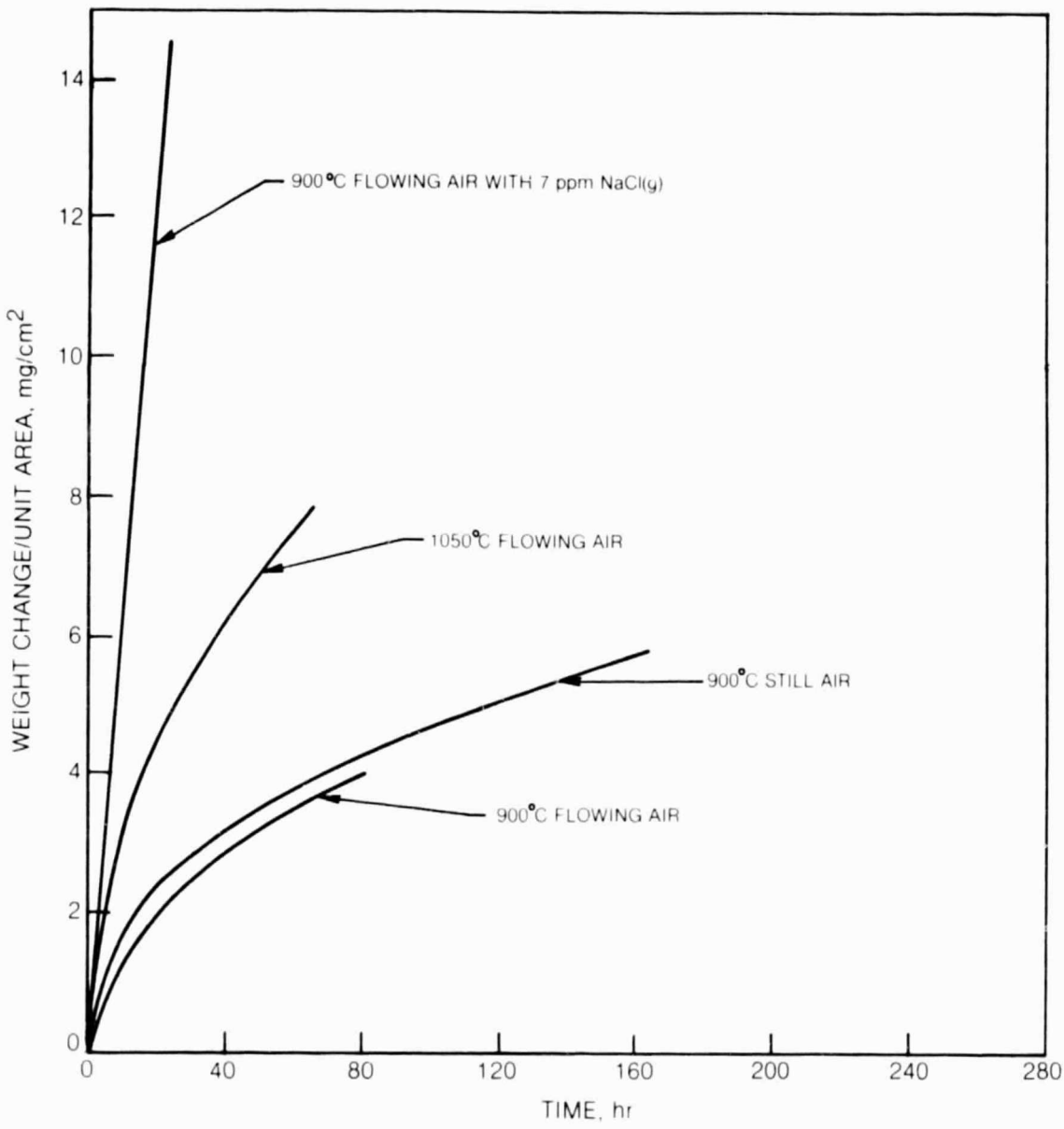

Fig. 1 Oxidation Behavior of γ/γ'-α

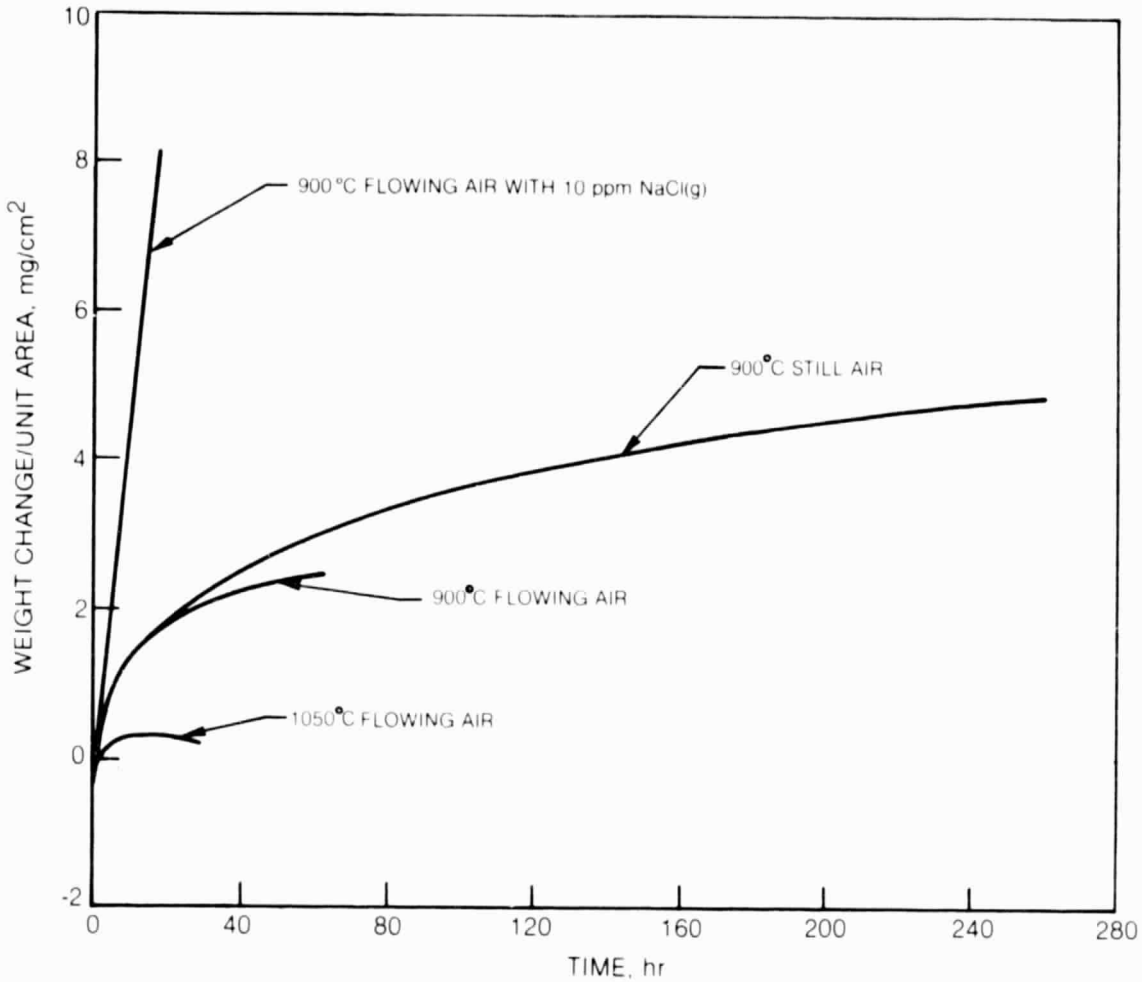

Fig. 2 Oxidation Behavior of NX-188

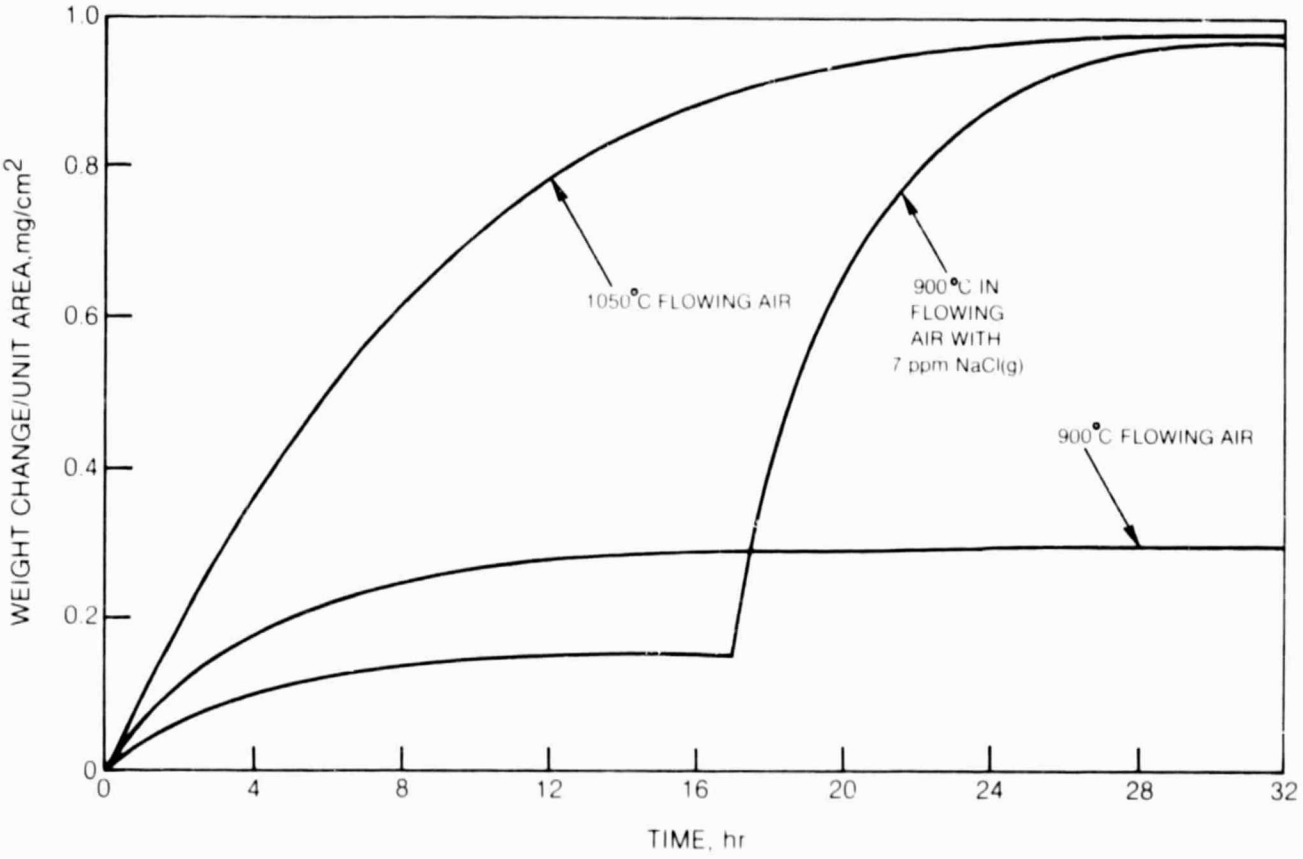

Fig. 3 Oxidation Behavior of MAR-M 509

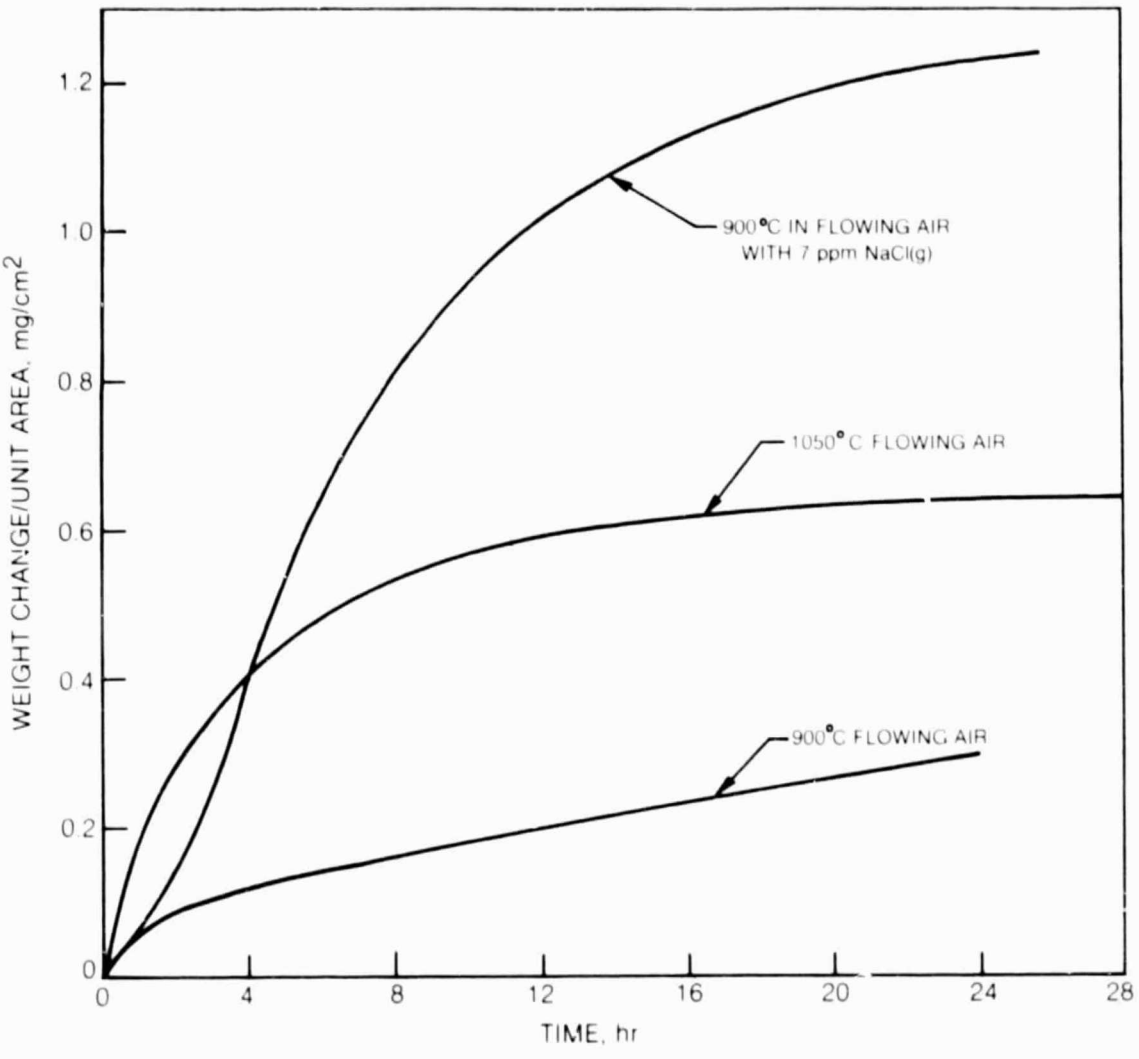

Fig. 4 Oxidation Behavior of Hastelloy X

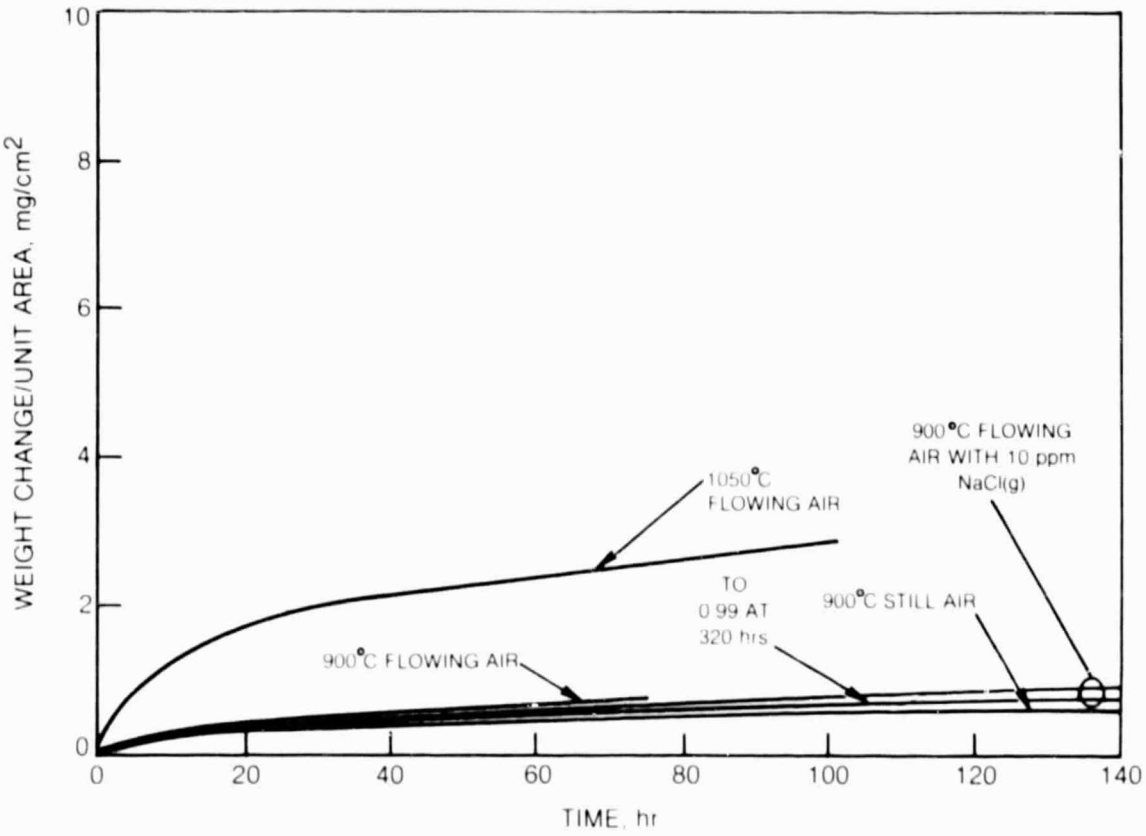

Fig. 5 Oxidation Behavior of IN-792

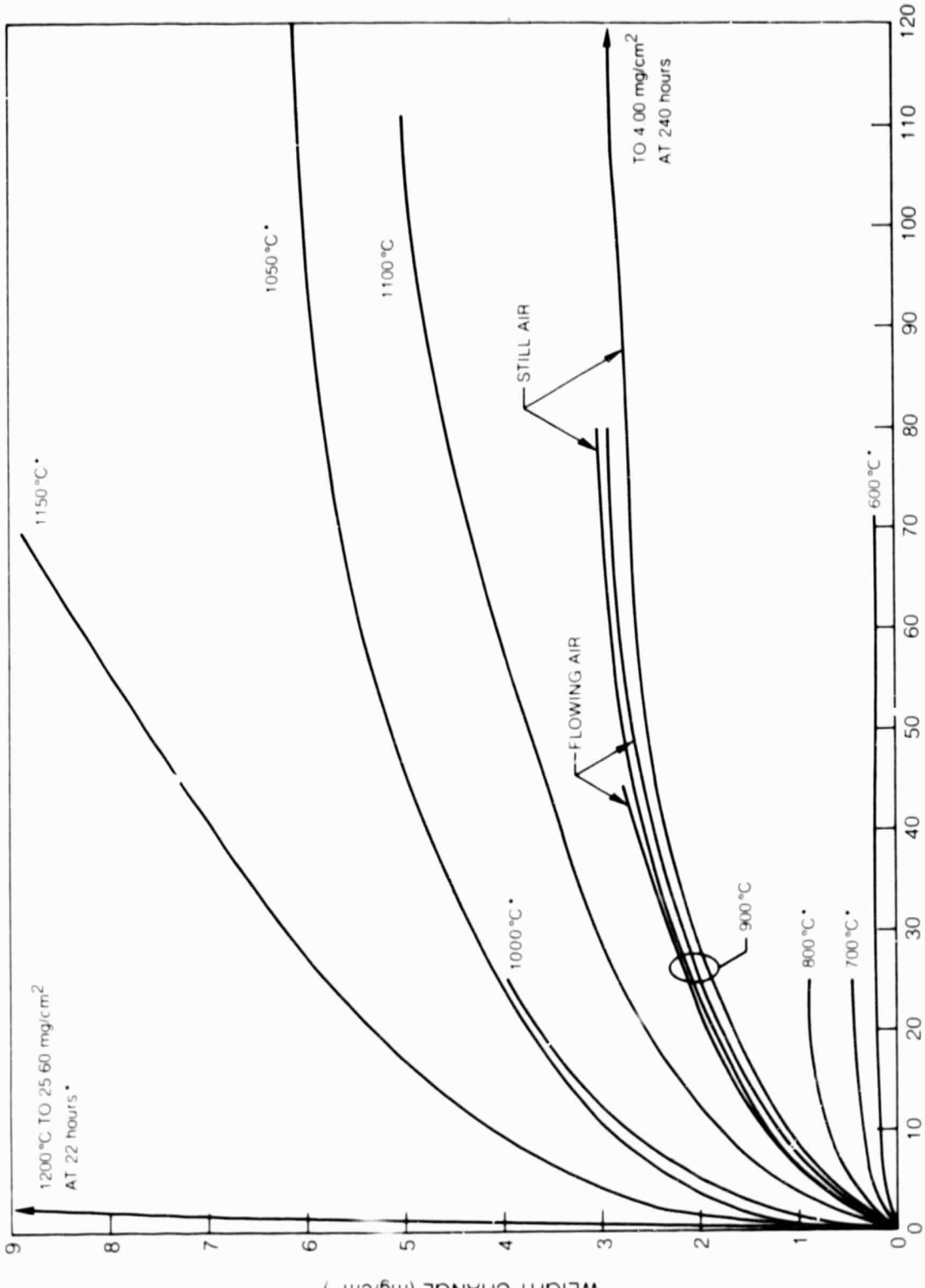

Fig. 6 Oxidation Behavior of Tungsten-Modified NX-188 in Air Alone (* Flowing Air)

Fig. 7 Pin Hole Porosity in NiO Scale on Ni-Mo-W-Al Alloy After 25 hours at 800 °C in Air. External NiO Surface.

a) 600 °C FOR 70 hours

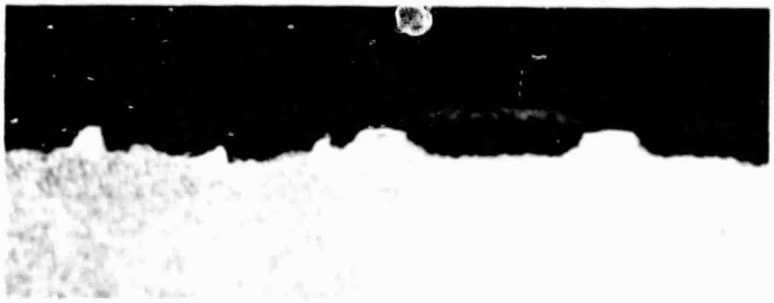

b) 700 °C FOR 24 hours

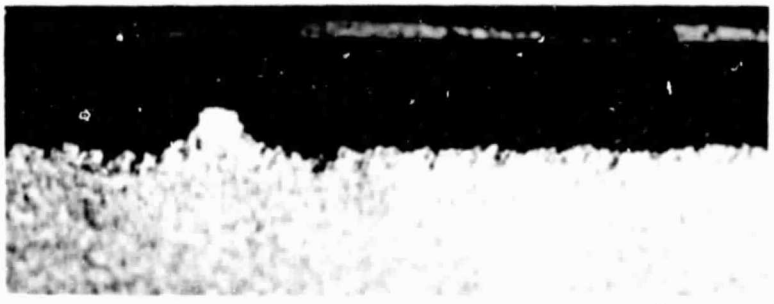

c) 800 °C FOR 24 hours

10 μm

Fig. 8 Failure of NiO Layer to Form Over α-Mo(W) Grains at the Metal-Scale Interface

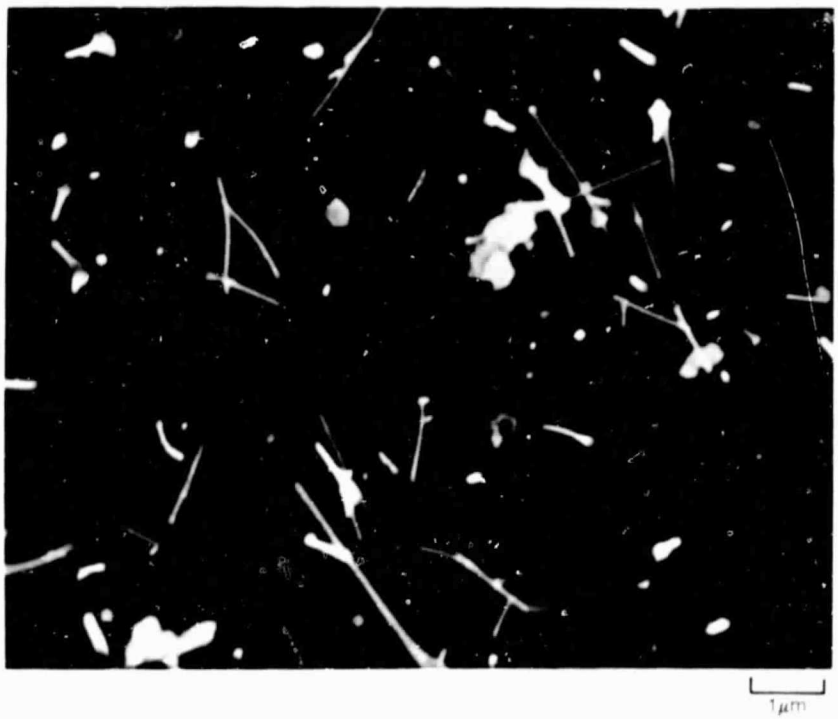

Fig. 9 Tungsten Oxide Crystals on NiO Scale After 25 hours at 700°C

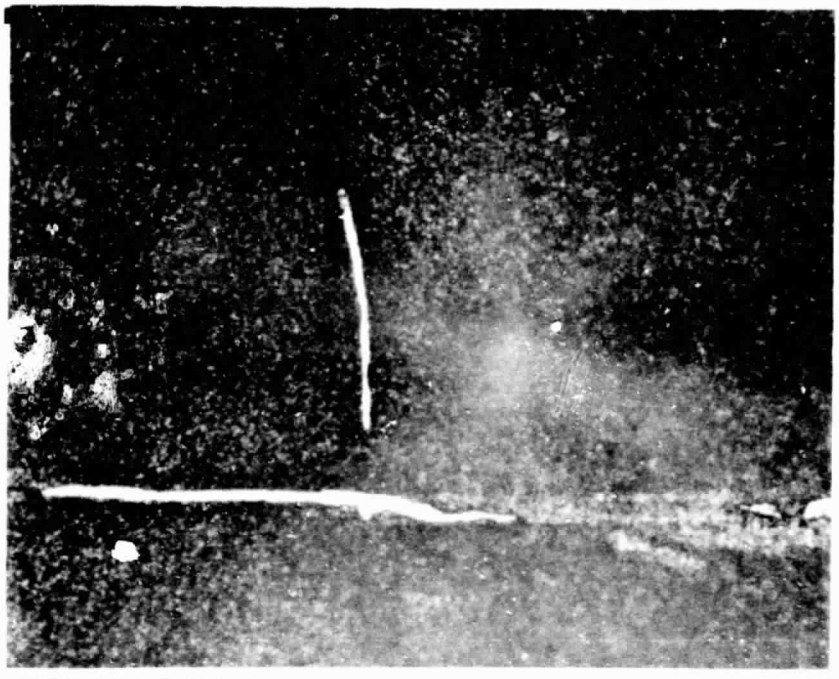

a) TRANSMITTED LIGHT

b) REFLECTED LIGHT

50 μm

Fig. 10 Grain Boundary Porosity in Exfoliated NiO Layer after Oxidation at 900°C for 80 hours

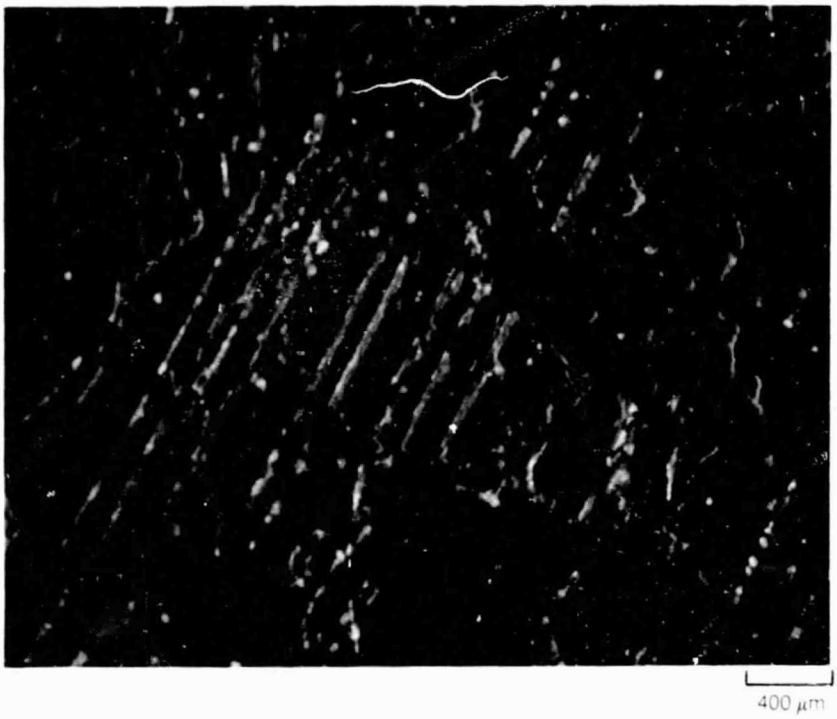

Fig. 11 Oxidation Resistant Metal Ridges at Base of Scale after 110 hours at 1100°C

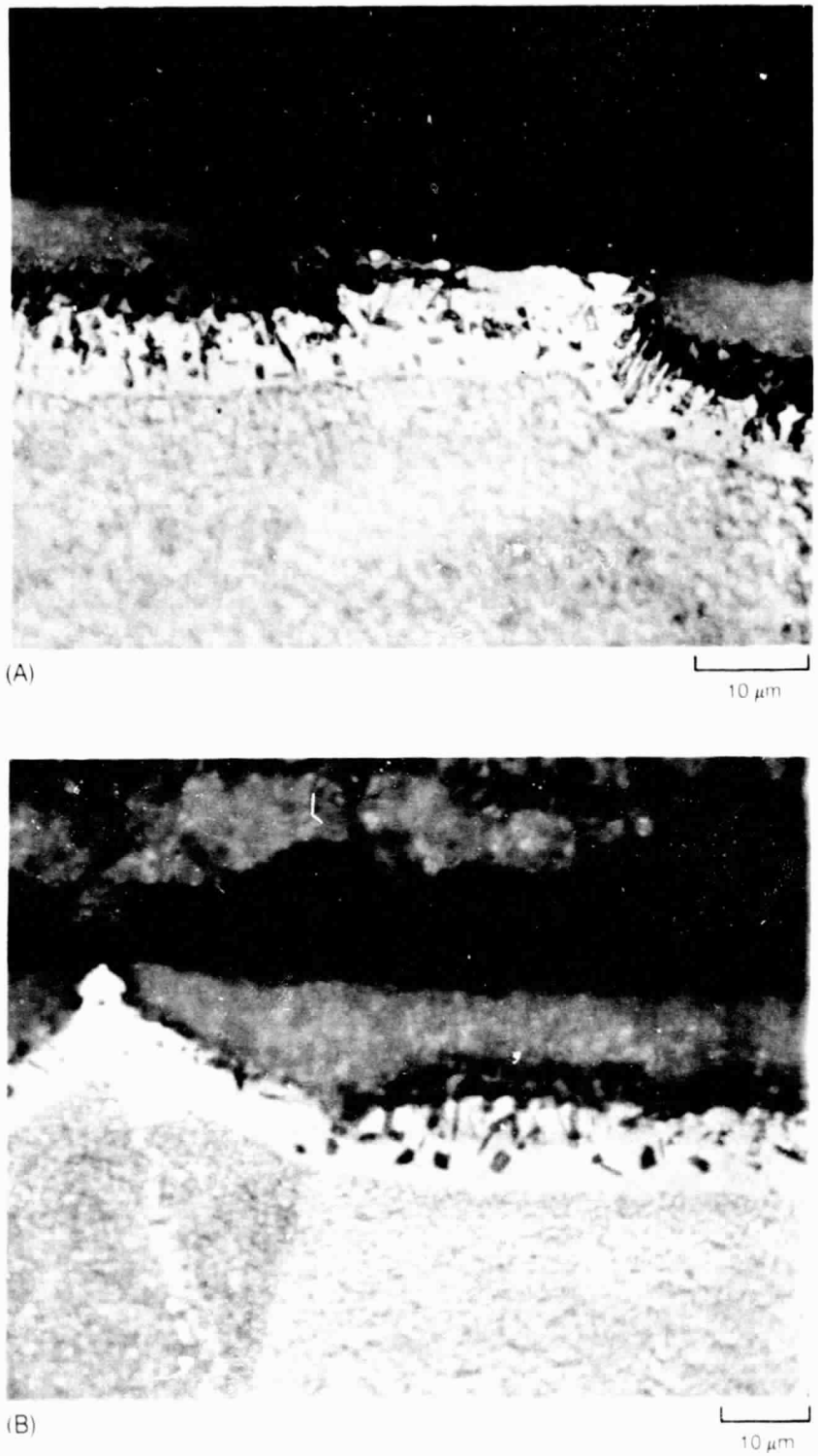

Fig. 12 Oxidation Resistant Metal Ridges after Oxidation at (A) 900°C for 90 hours and (B) 1100°C for 110 hours

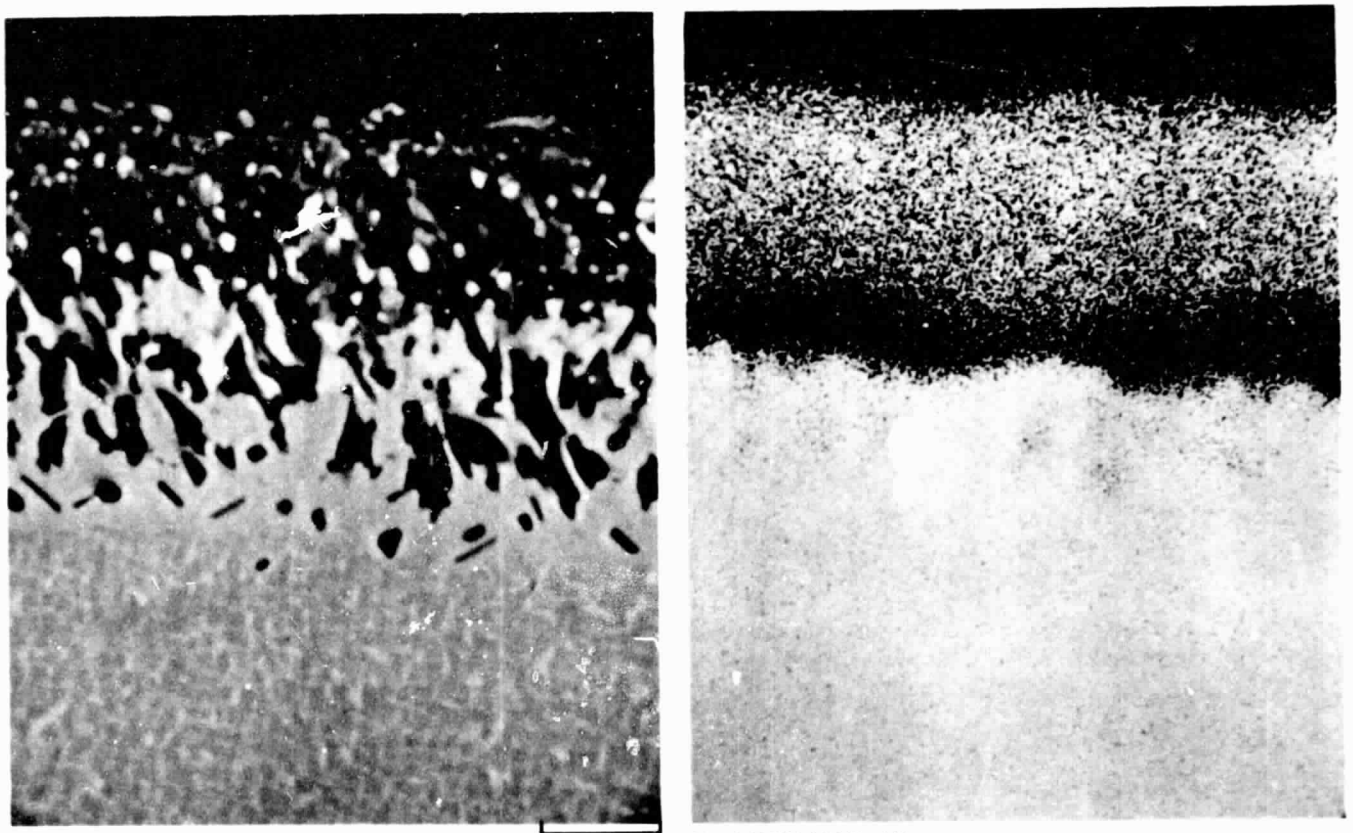

a) SCANNING ELECTRON MICROGRAPH

b) X-RAY MAP: Ni

Fig. 13 Elemental Distribution in Oxide Zone after Exposure at 900 °C for 80 hours

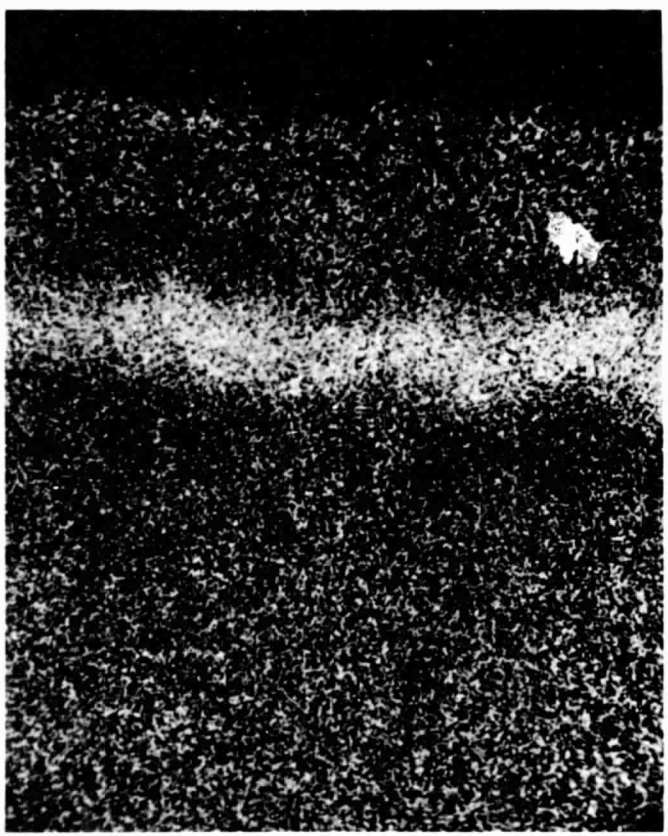

c) X-RAY MAP: Mo

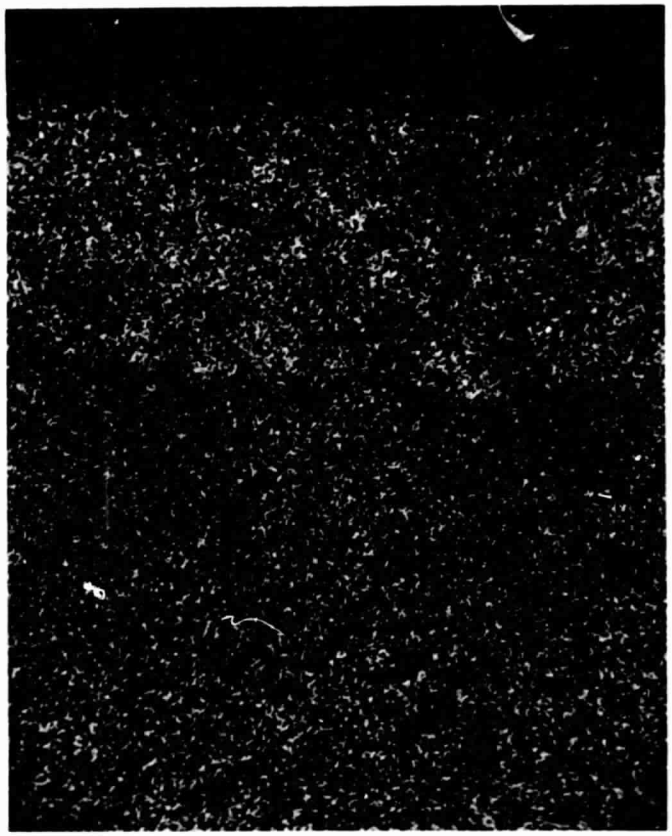

d) X-RAY MAP: W

Fig. 13 Elemental Distribution in Oxide Zone after Exposure at 900 °C for 80 hours (Cont.)

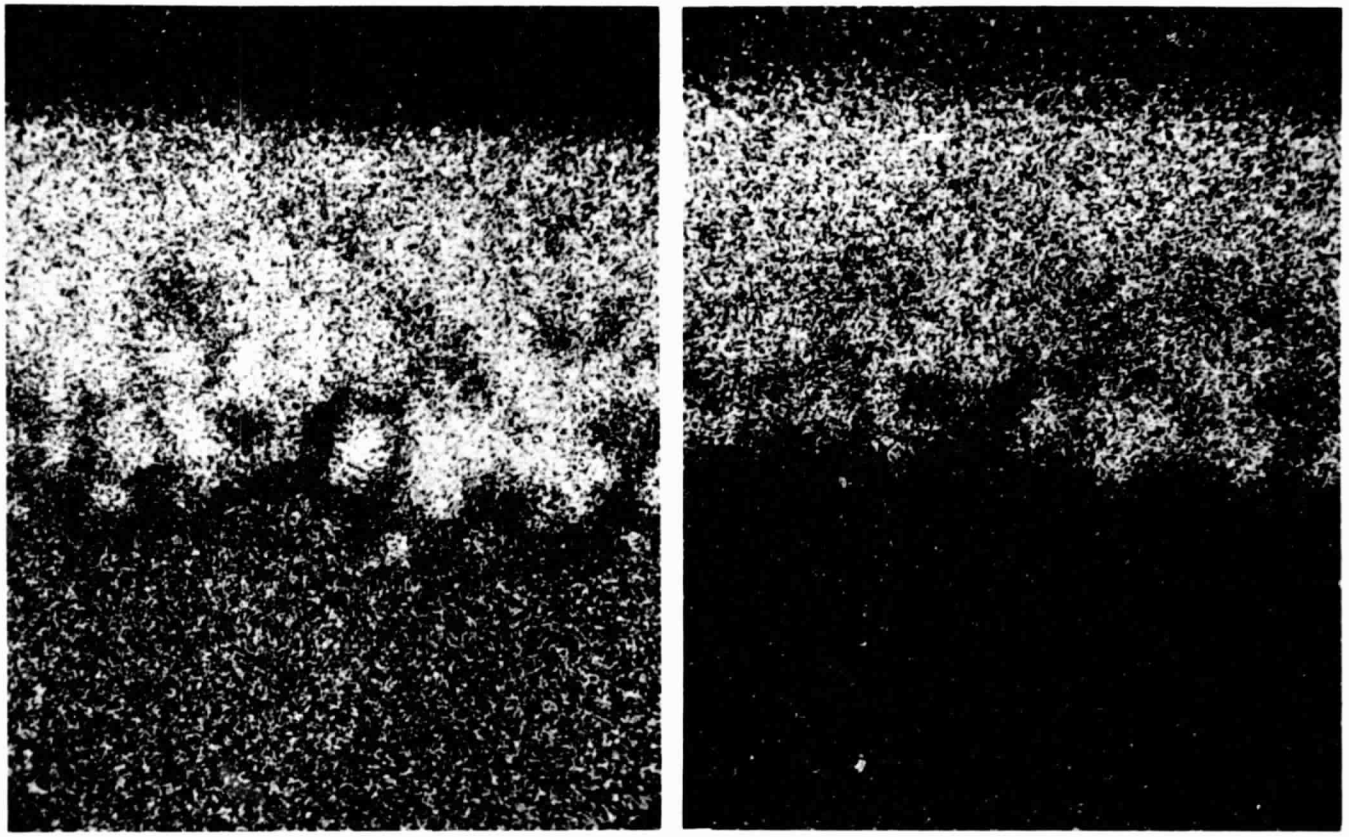

e) X-RAY MAP: Al

f) X-RAY MAP: O

Fig. 13 Elemental Distribution in Oxide Zone after Exposure at 900°C for 80 hours (Cont.)

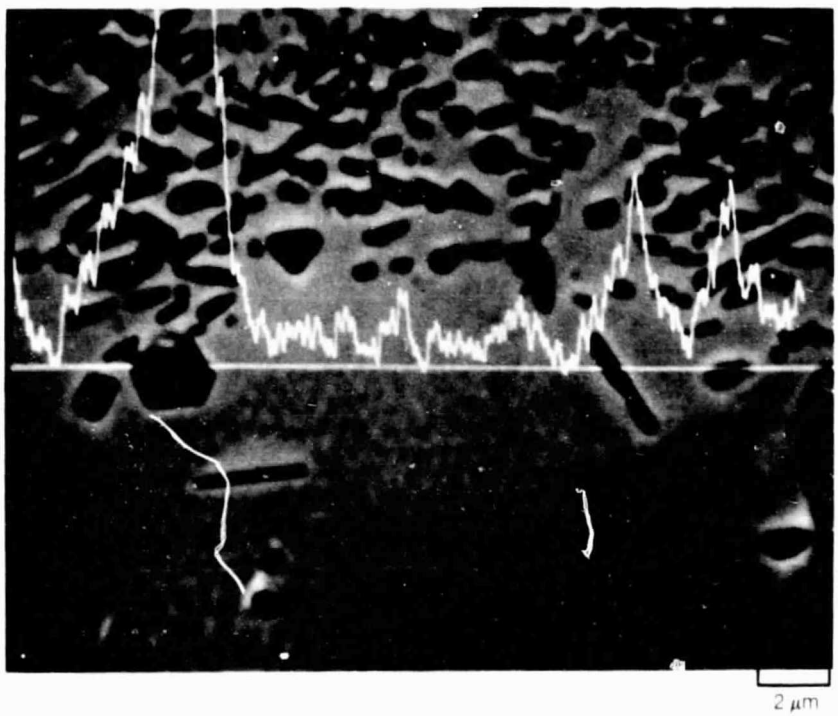

Fig. 14 Nitrogen Trace Showing AlN at Base of Internally Oxidized Layer Exposed at 900°C for 80 hours

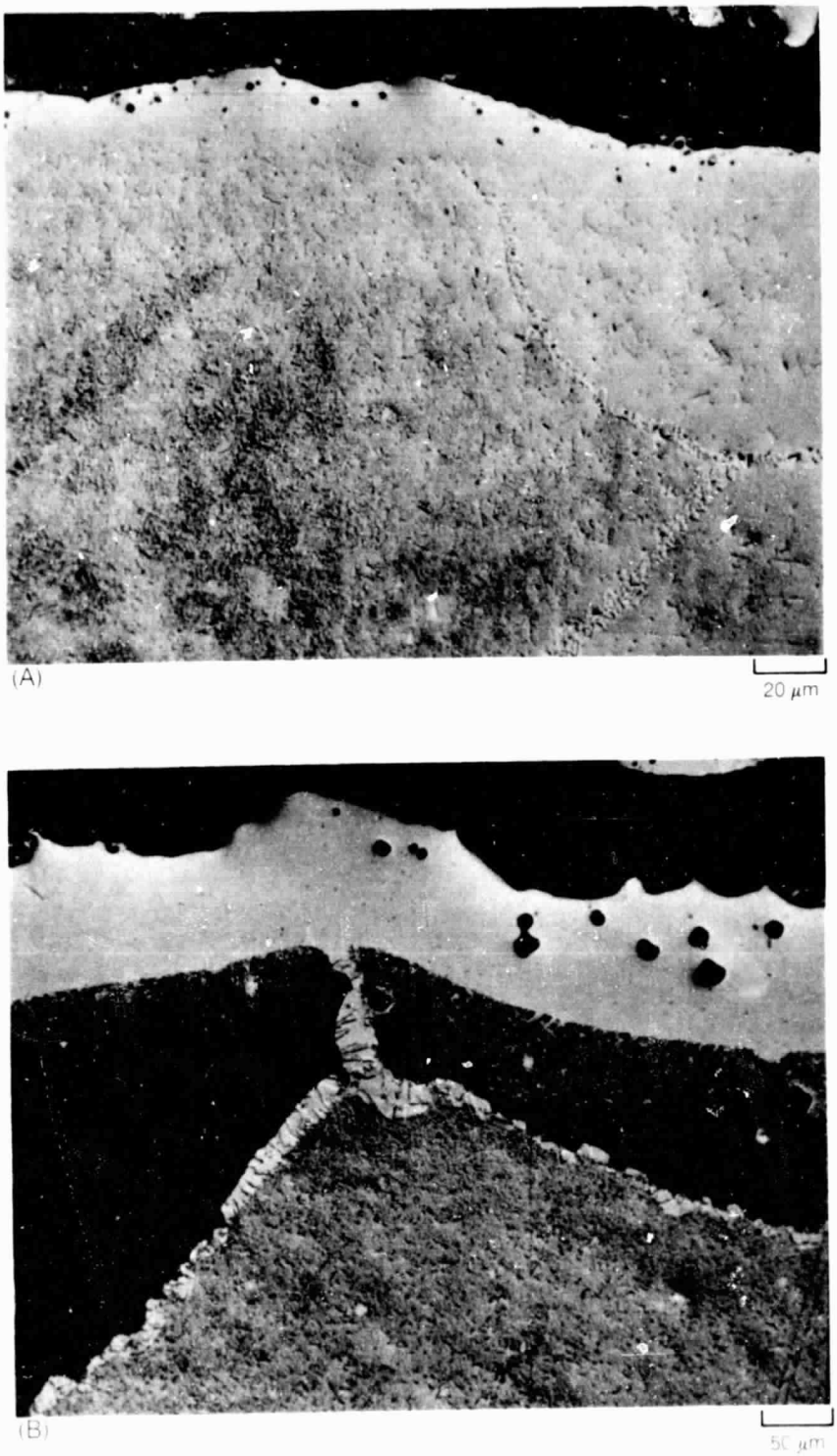

Fig. 15 Kirkendall Porosity, Precipitated α-Mo(W), Grain Boundary Coarsening Effects and AlN Particles in γ′-Depletion Zone for Specimens Oxidized at (A) 1100 and (B) 1150°C

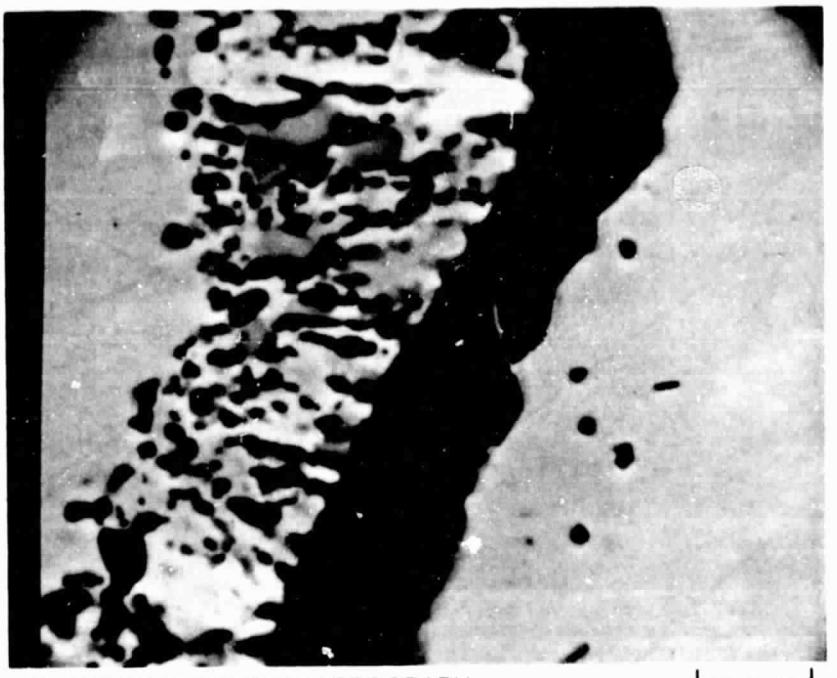

a) SCANNING ELECTRON MICROGRAPH

4 μm

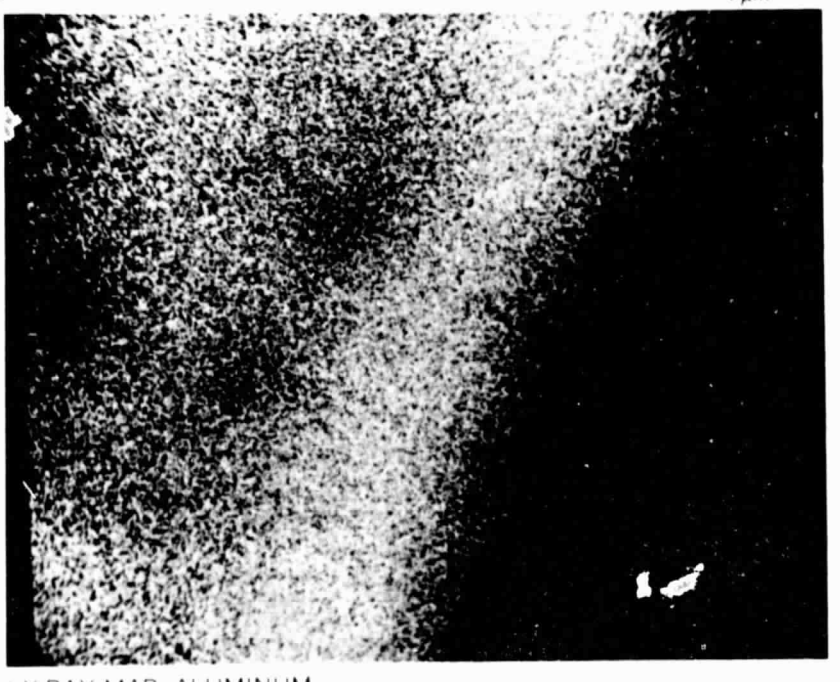

b) X-RAY MAP, ALUMINUM

Fig. 16 Local Formation of Protective Al_2O_3

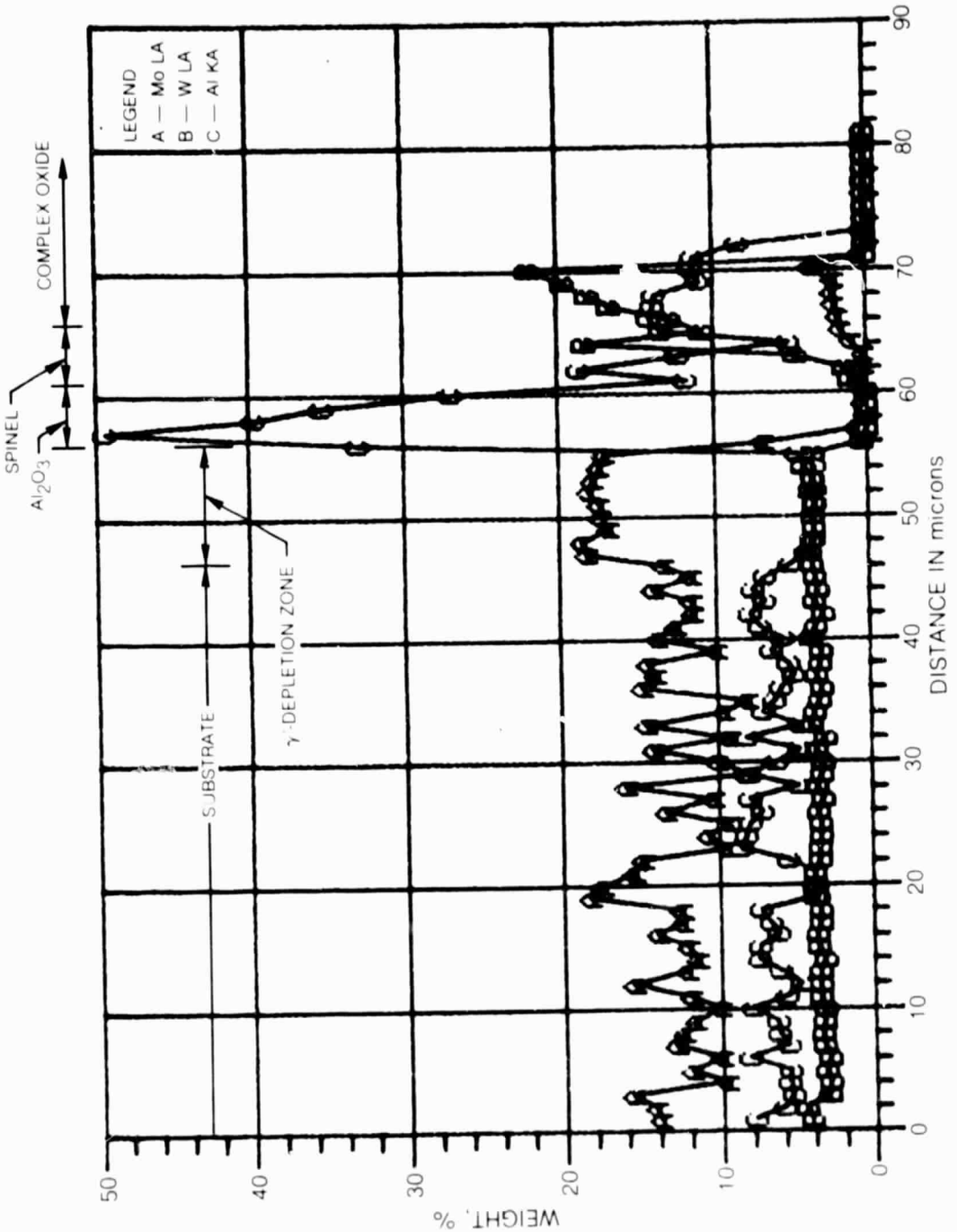

Fig. 16 Local Formation of Protective Al_2O_3 (Cont.)

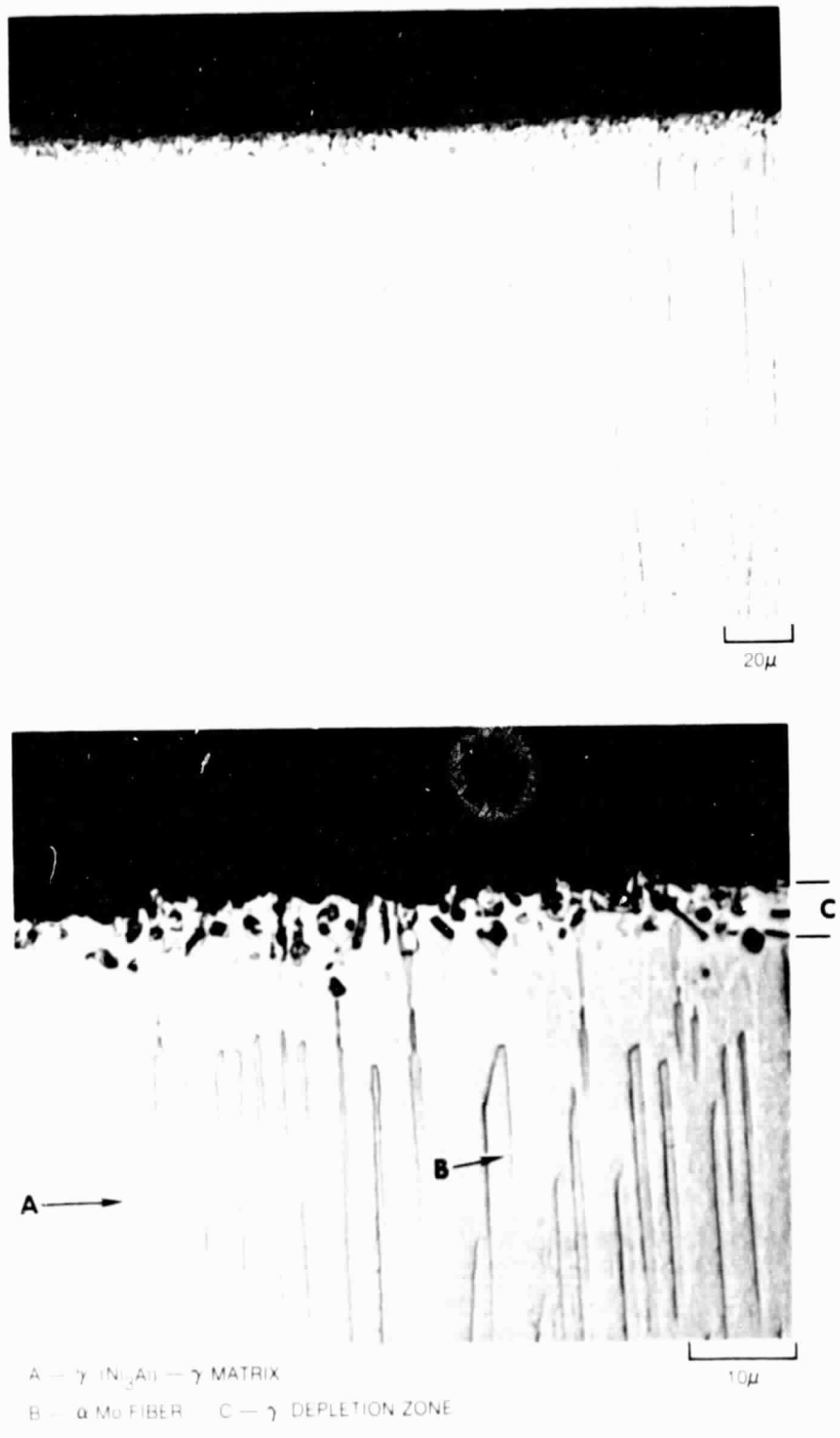

Fig. 17 γ/γ'-α Oxidized at 900°C in Flowing Air for 76 Hr Showing Extensive Internal Oxidation

80-10-67-25

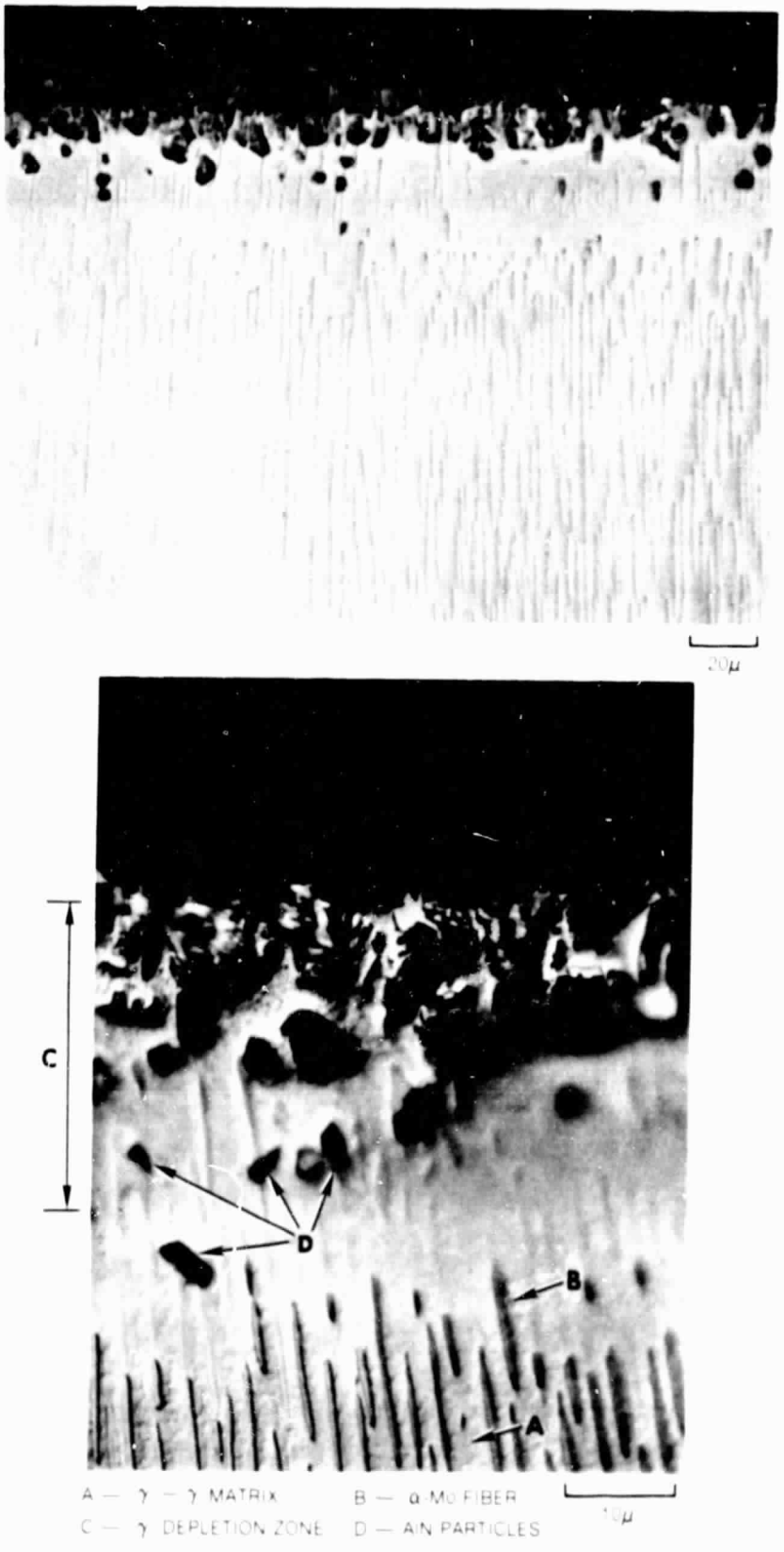

Fig. 18 γ/γ'-α Oxidized in Flowing Air at 1050°C for 64 Hr Showing γ' Depletion Zone and Internal Oxidation

80-10-67-26

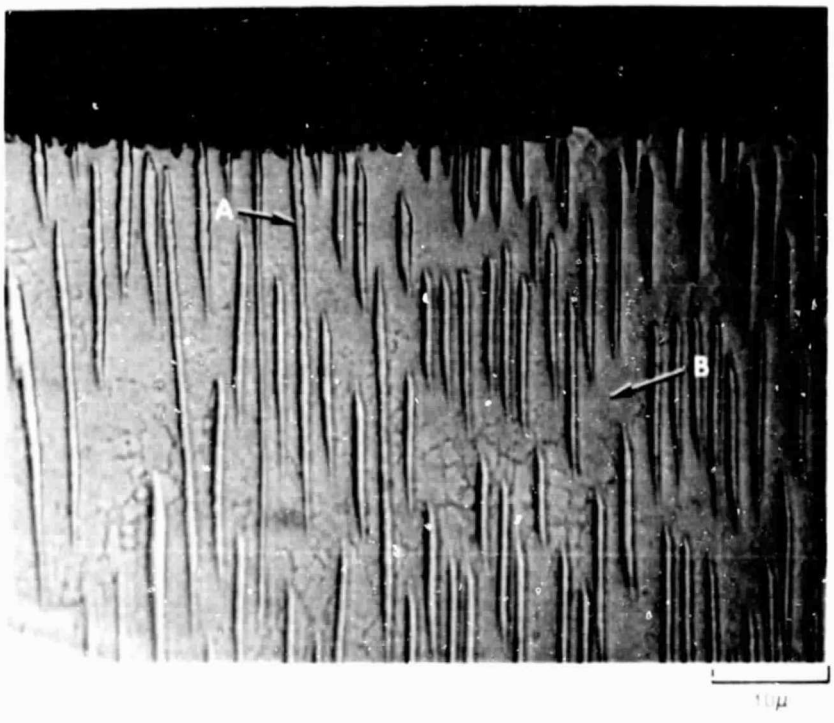

A — α Mo B — γ — γ MATRIX

Fig. 19 γ/γ'-α Oxidized in Flowing Air at 900°C with 7 ppm NaCl(g) for 26 Hr Transverse Surface

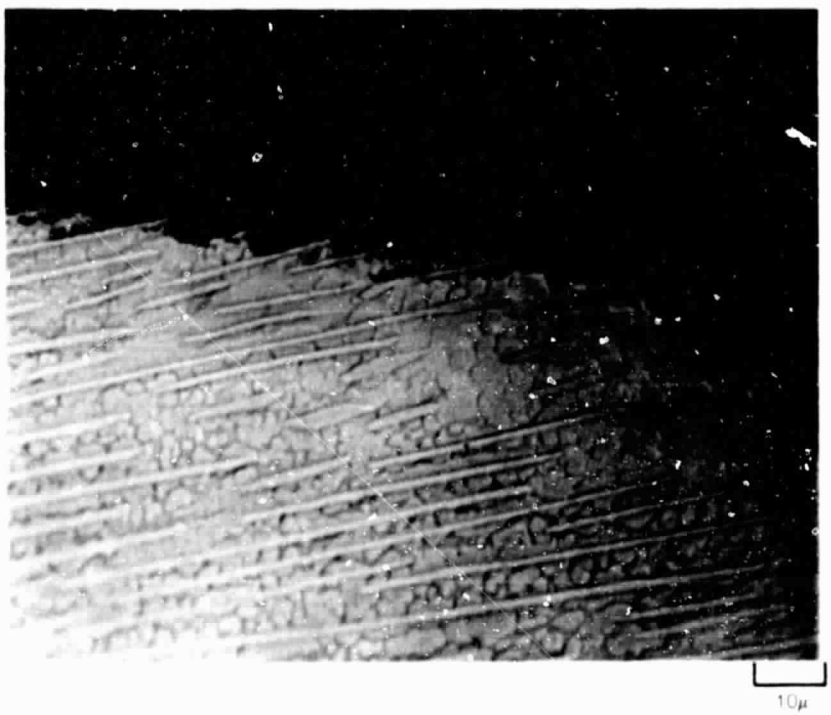

Fig. 20 γ/γ'-α Oxidized in Air at 900°C with 7 ppm NaCl(g) for 26 Hour Longitudinal Surface

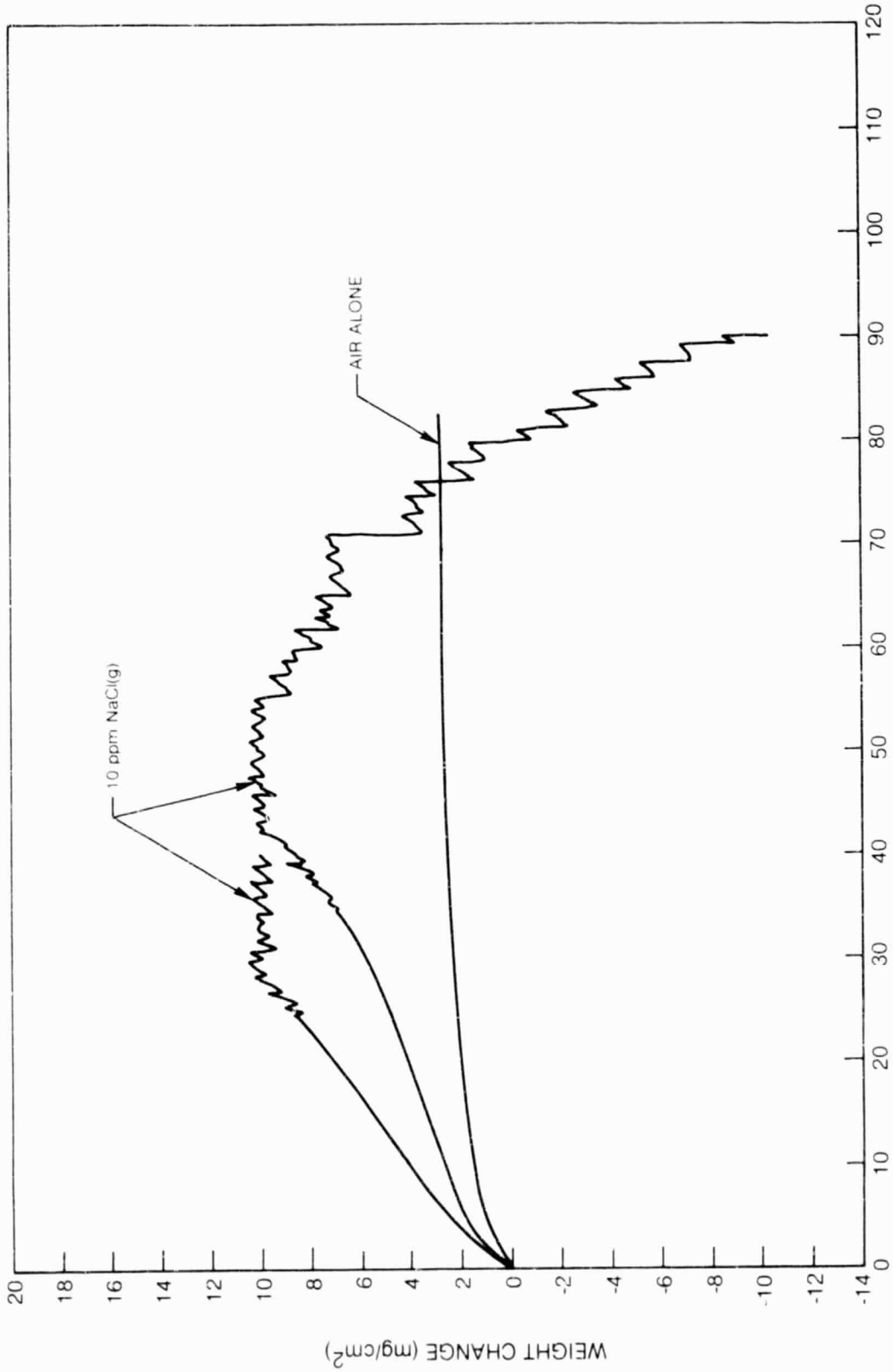

Fig. 21 Effect of NaCl(g) on Oxidation of Tungsten-Modified NX-188 at 900°C in Flowing Air

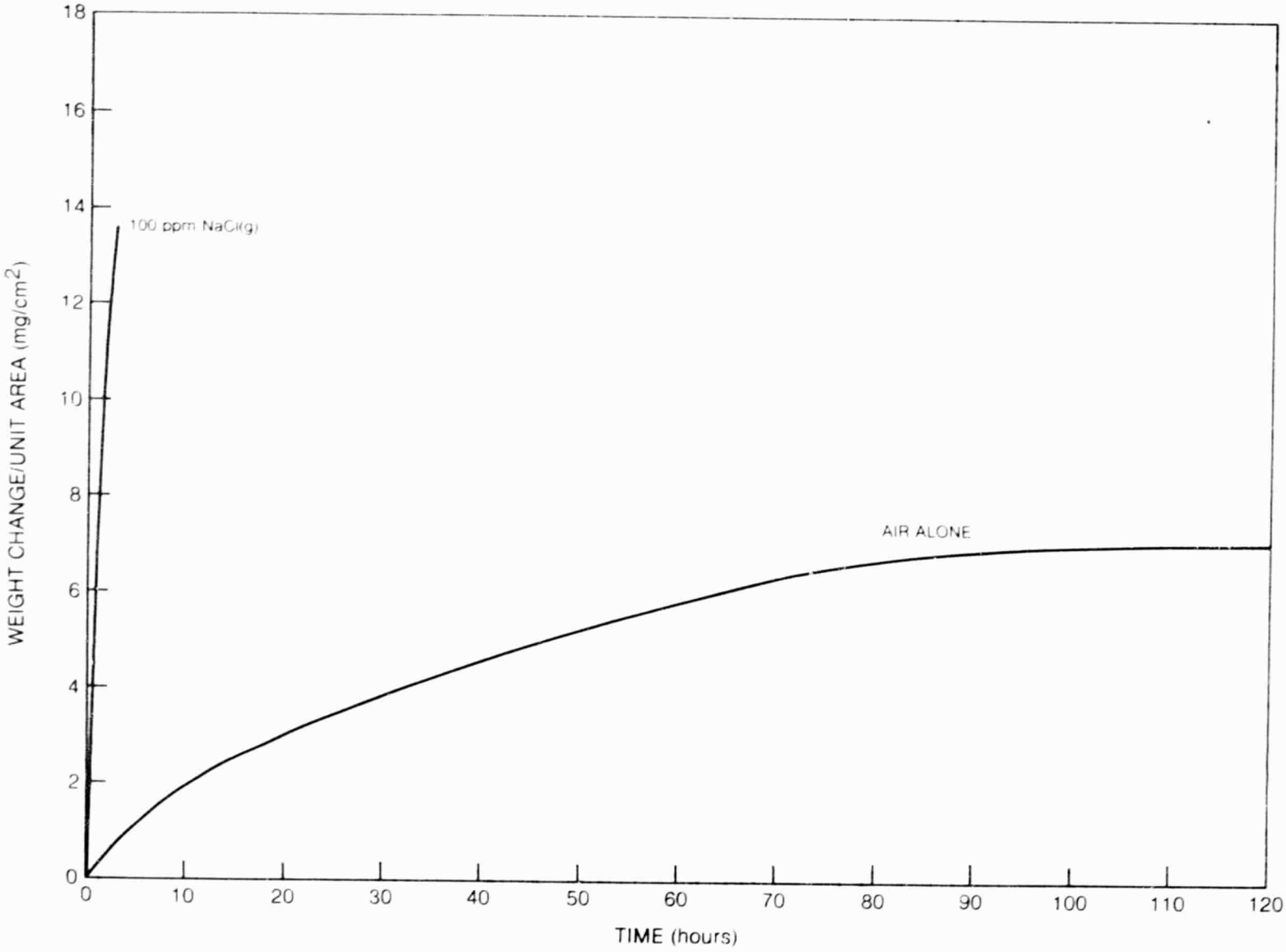

Fig. 22 Effect of NaCl(g) on Oxidation of Tungsten-Modified NX-188 at 1050°C in Flowing Air

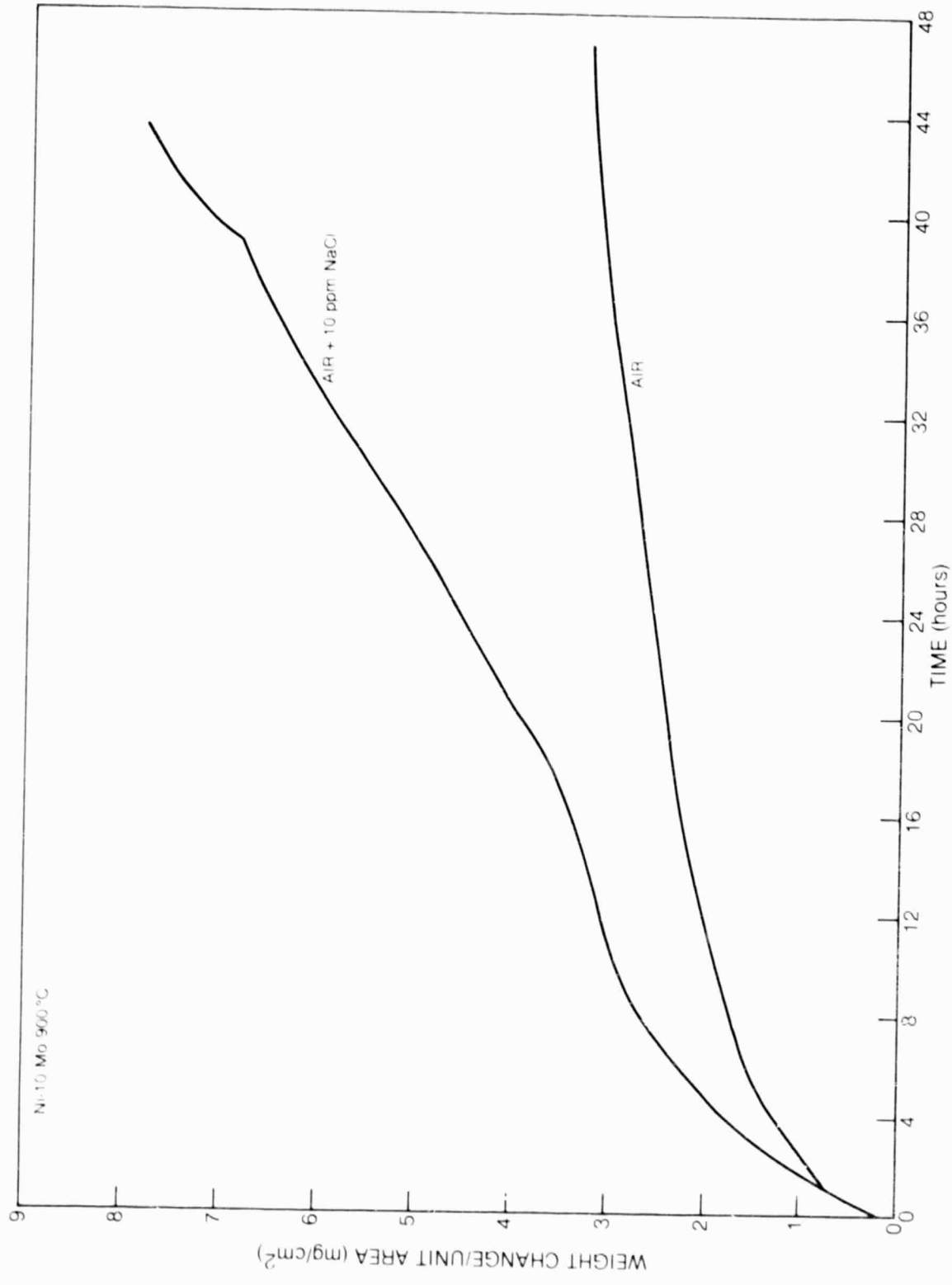

Fig. 23 Effect of NaCl(g) on the 900°C Oxidation Behavior of Ni-10 w/o Mo

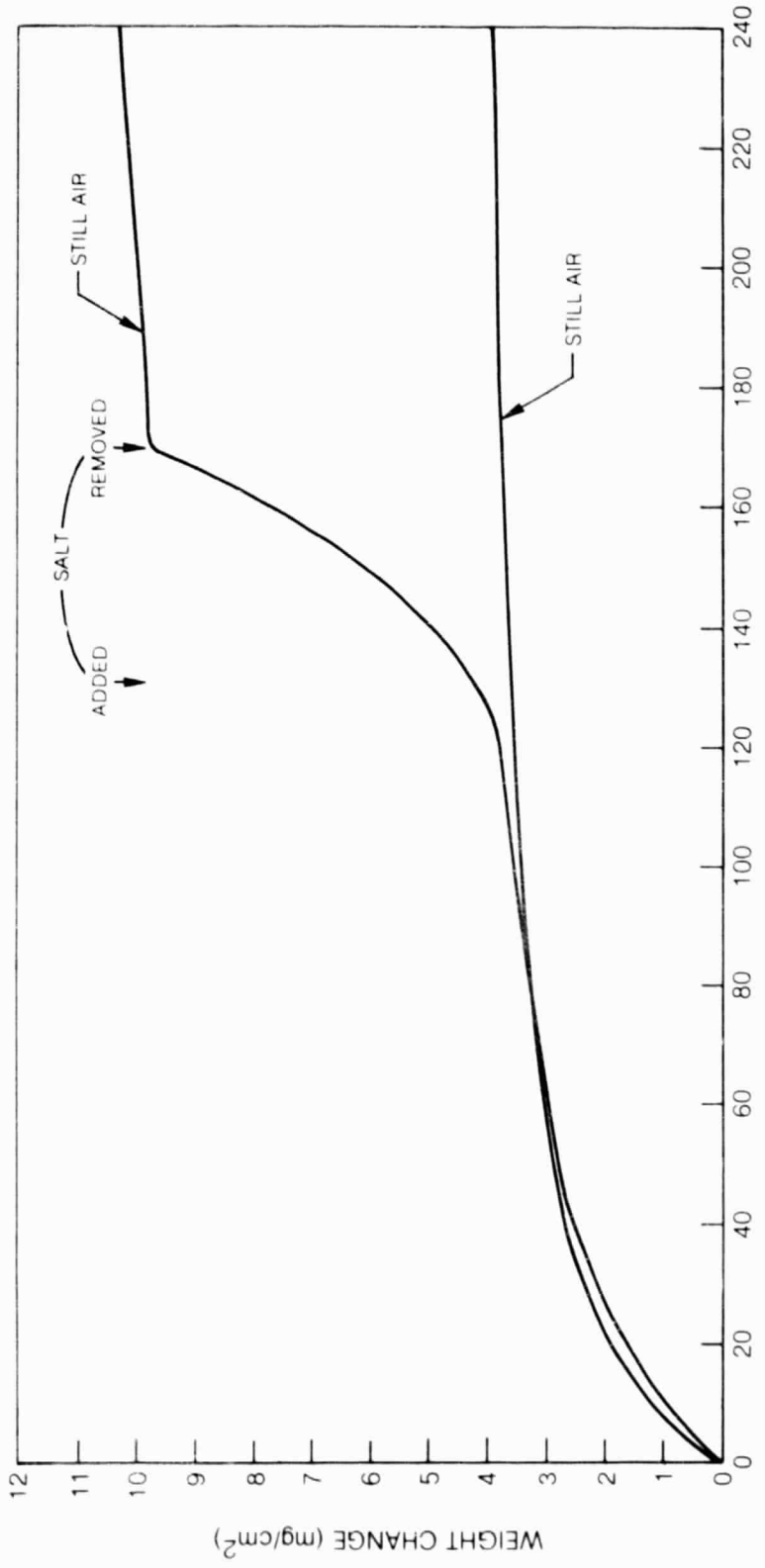

Fig. 24 Effect of NaCl(g) on Oxidation of Tungsten-Modified NX-188 at 900°C in Still Air

81-2-25-4

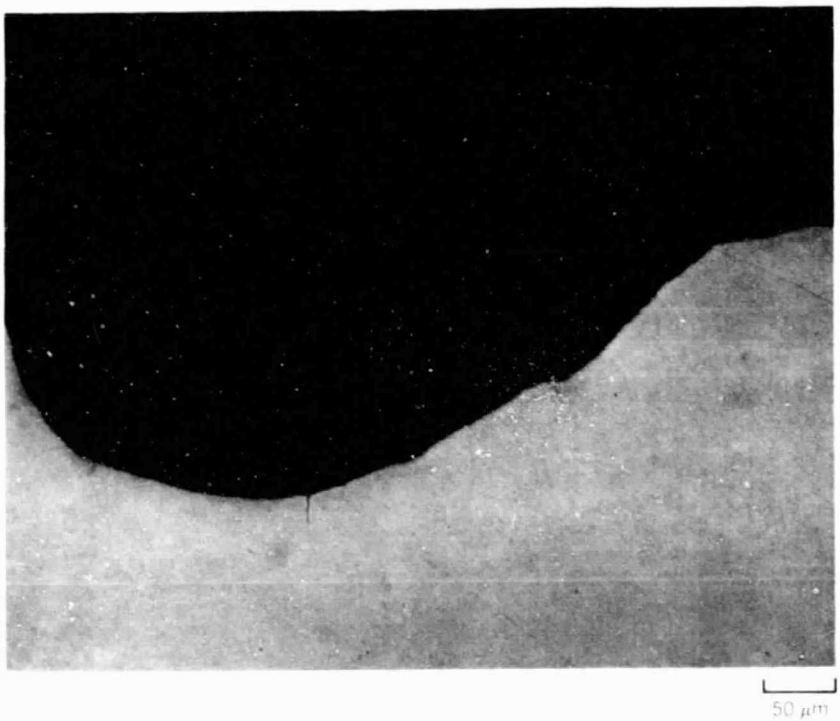

Fig. 25 Pitting Attack Effected by 10 ppm in Air at 900°C for 40 hours Tungsten-Modified NX-188

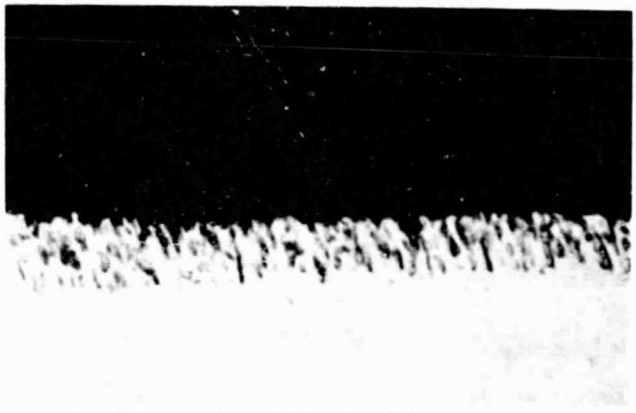

a) AWAY FROM AN OXIDATION PIT

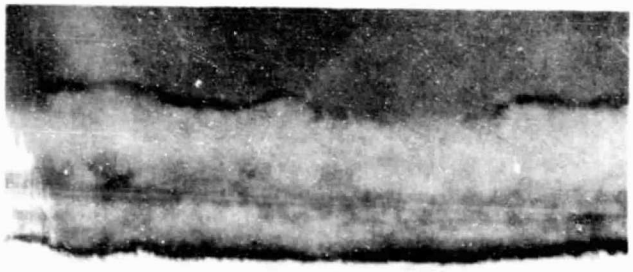

b) AT THE BASE OF AN OXIDATION PIT

10 μm

Fig. 26 Difference in Thickness of Internally Oxidized Region after Oxidation in Air with 10 ppm NaCl(g) Tungsten-Modified NX-188

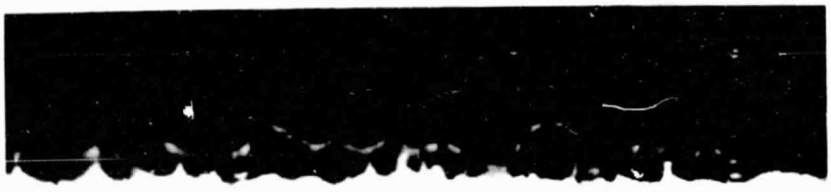

a) FLOWING AIR ALONE

8μ

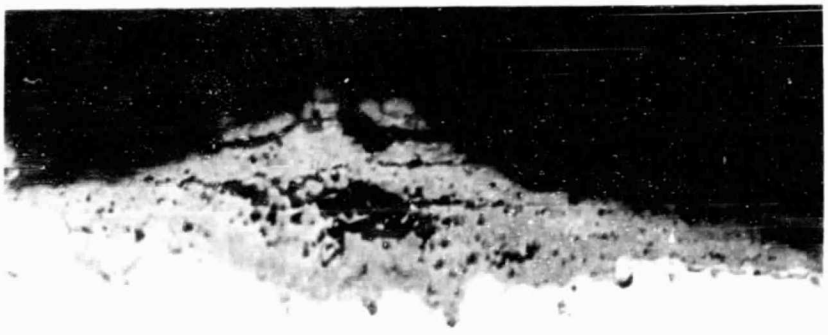

b) FLOWING AIR WITH 10 ppm NaCl(g)

8μ

Fig. 27 **Scales Found on Hastelloy X Oxidized at 900°C**

Fig. 28 Oxide Scales Formed on IN-792 Tested in Air with 10 ppm NaCl(g) at 900°C for 140 Hours

A PROTECTIVE SCALE
B INTERNALLY OXIDIZED PARTICLES
C Ti-RICH PRECIPITATE

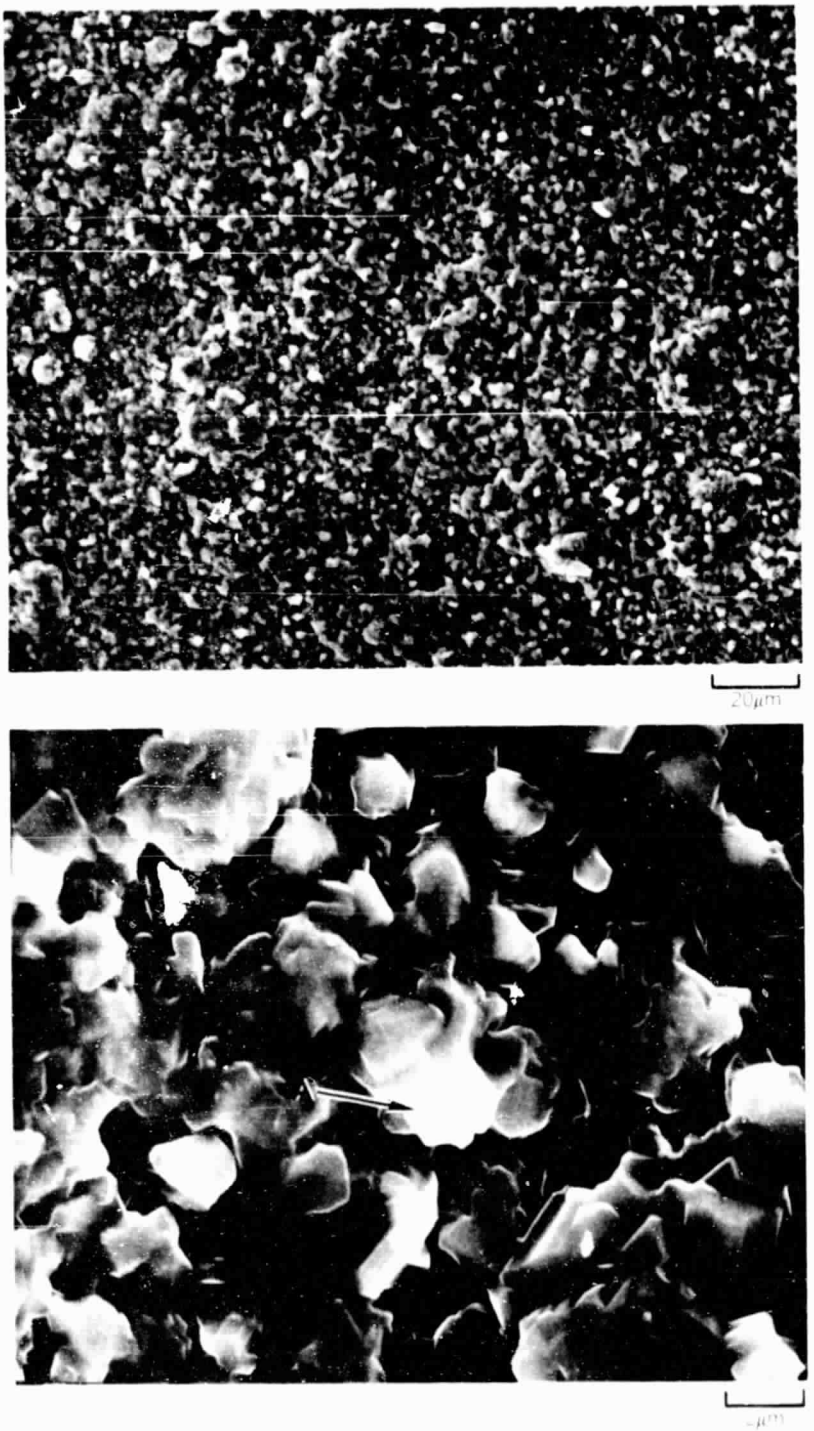

Fig. 29 IN-792 Oxidized in Air at 900°C for 130 Hours

A Ti-ENRICHED CRYSTAL PRISM EMERGING FROM DENSE SCALE

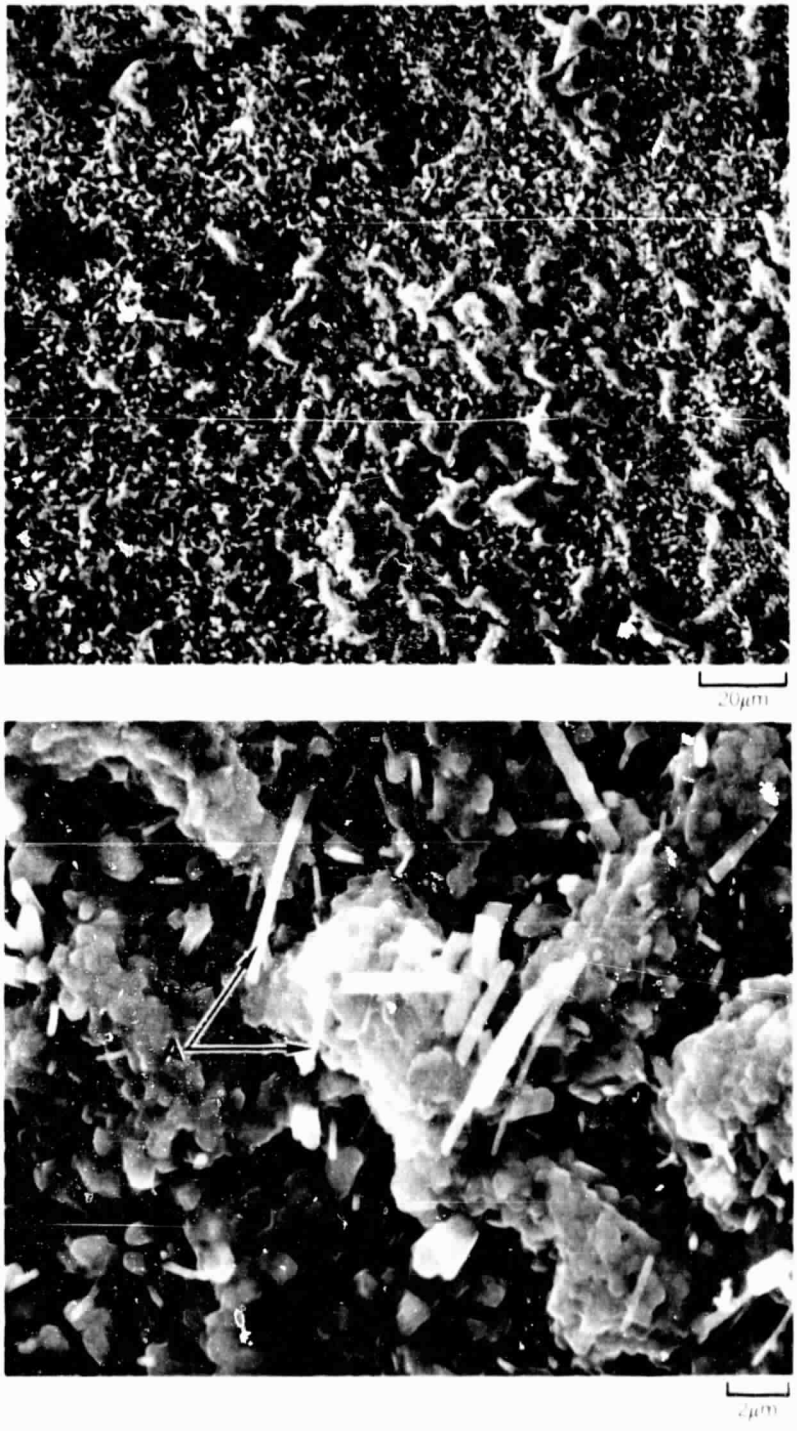

Fig. 30 IN-792 Oxidized in Air with 10 ppm NaCl at 900°C for 140 Hours

A Ti-RICH OXIDE NEEDLES GROWING ON TOP OXIDE SCALE

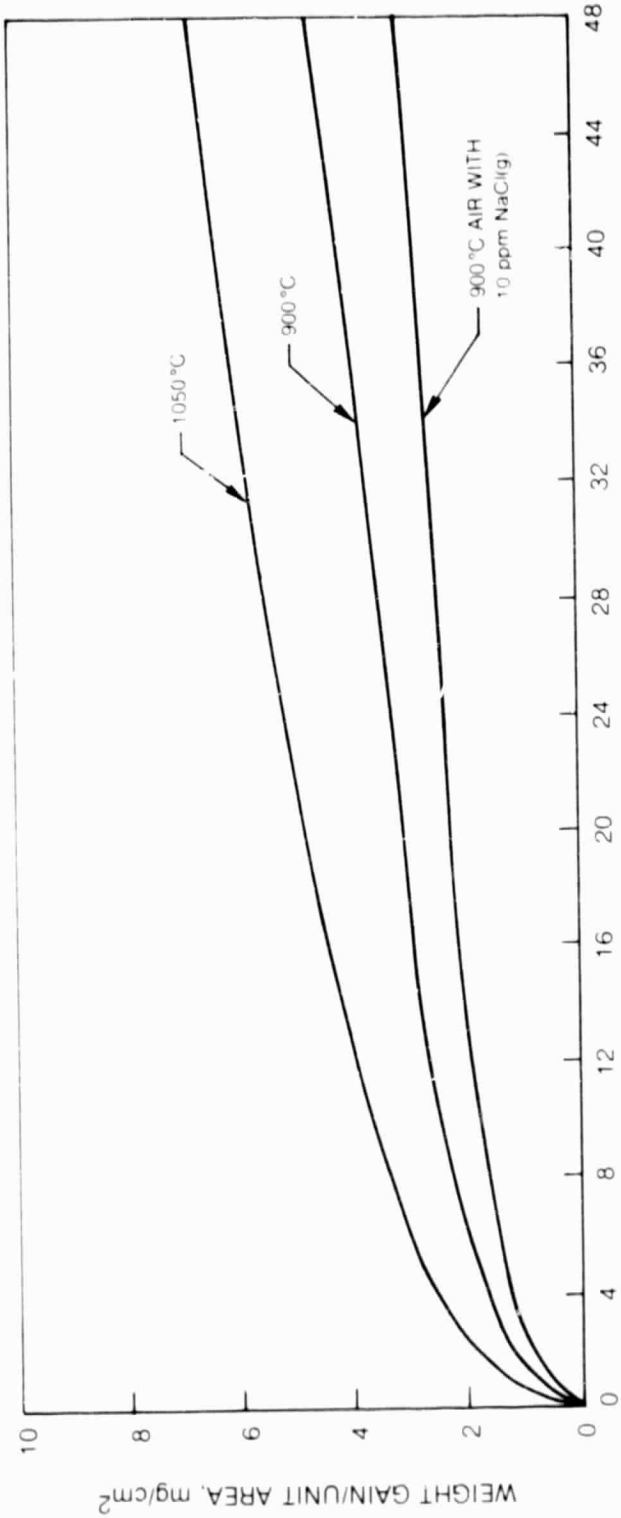

Fig. 31 Oxidation Behavior of Ni

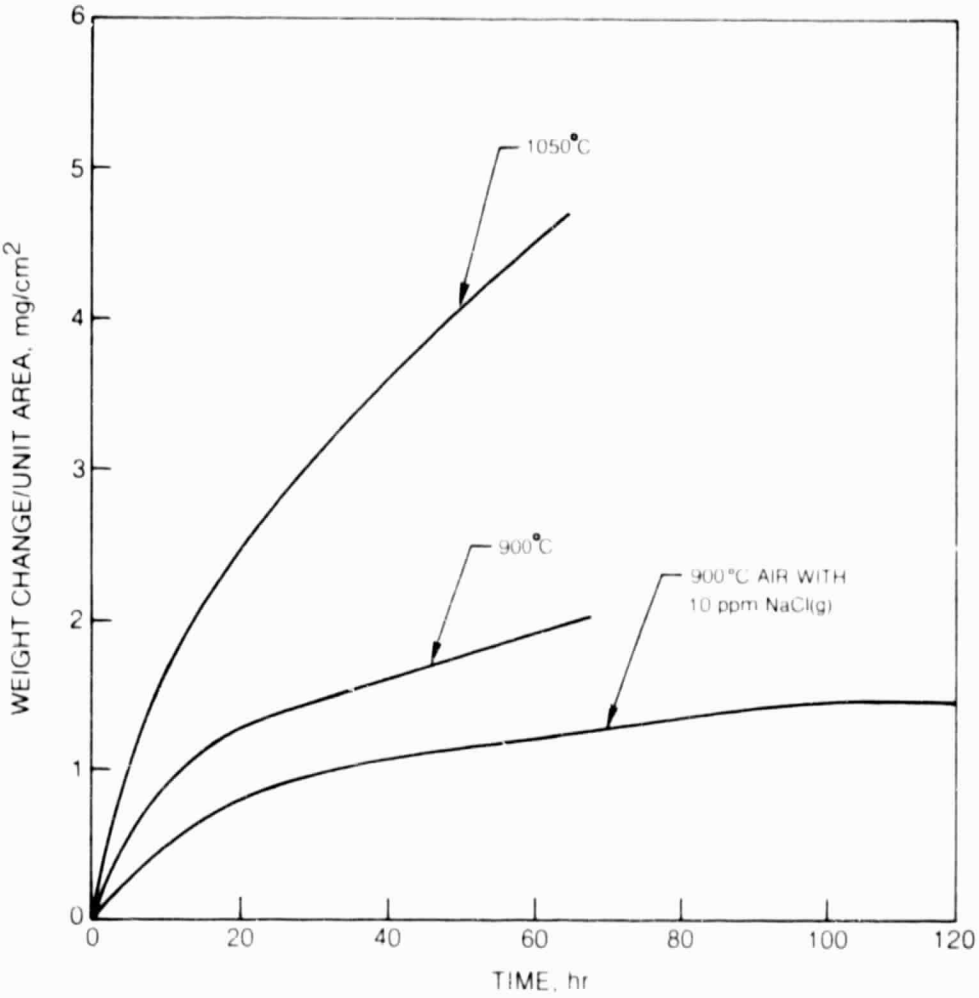

Fig. 32 Oxidation Behavior of Ni-5 Si

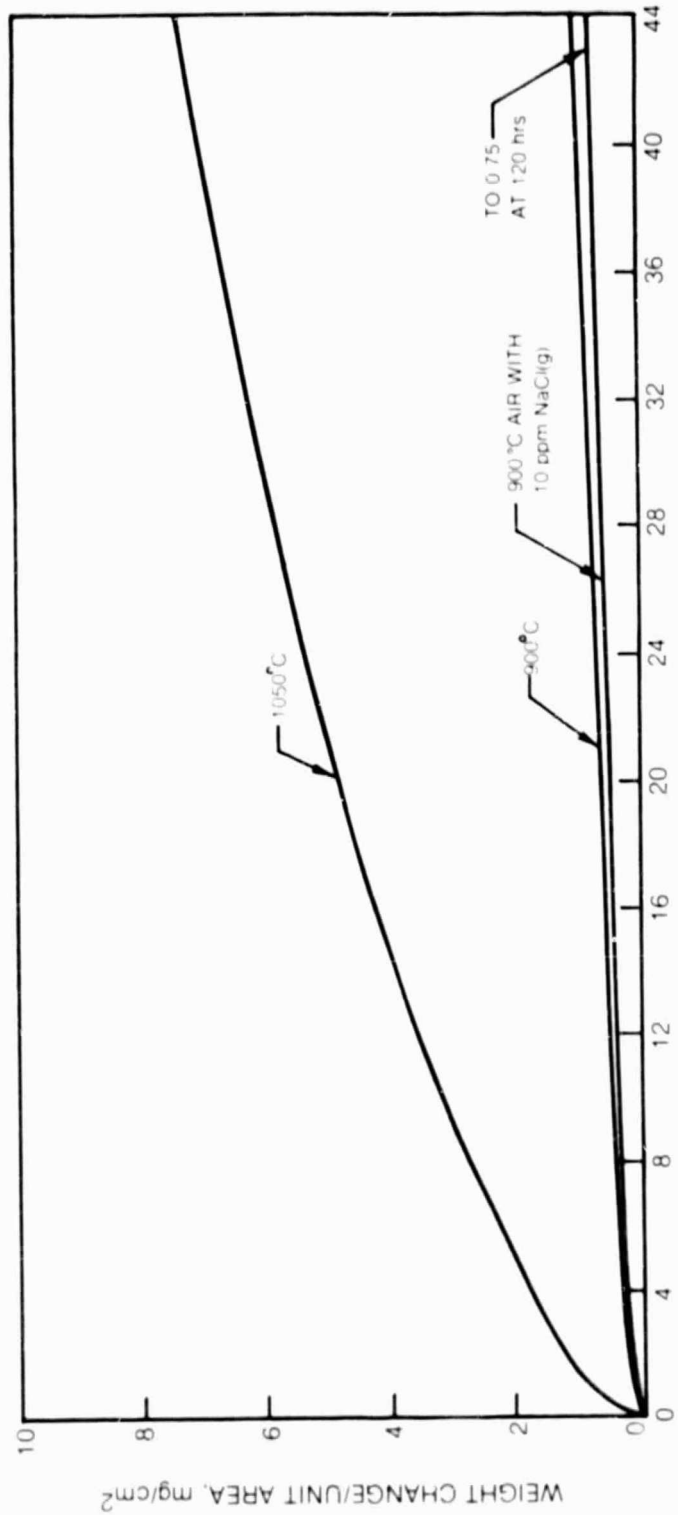

Fig. 33 Oxidation Behavior of Ni-11.5 Si

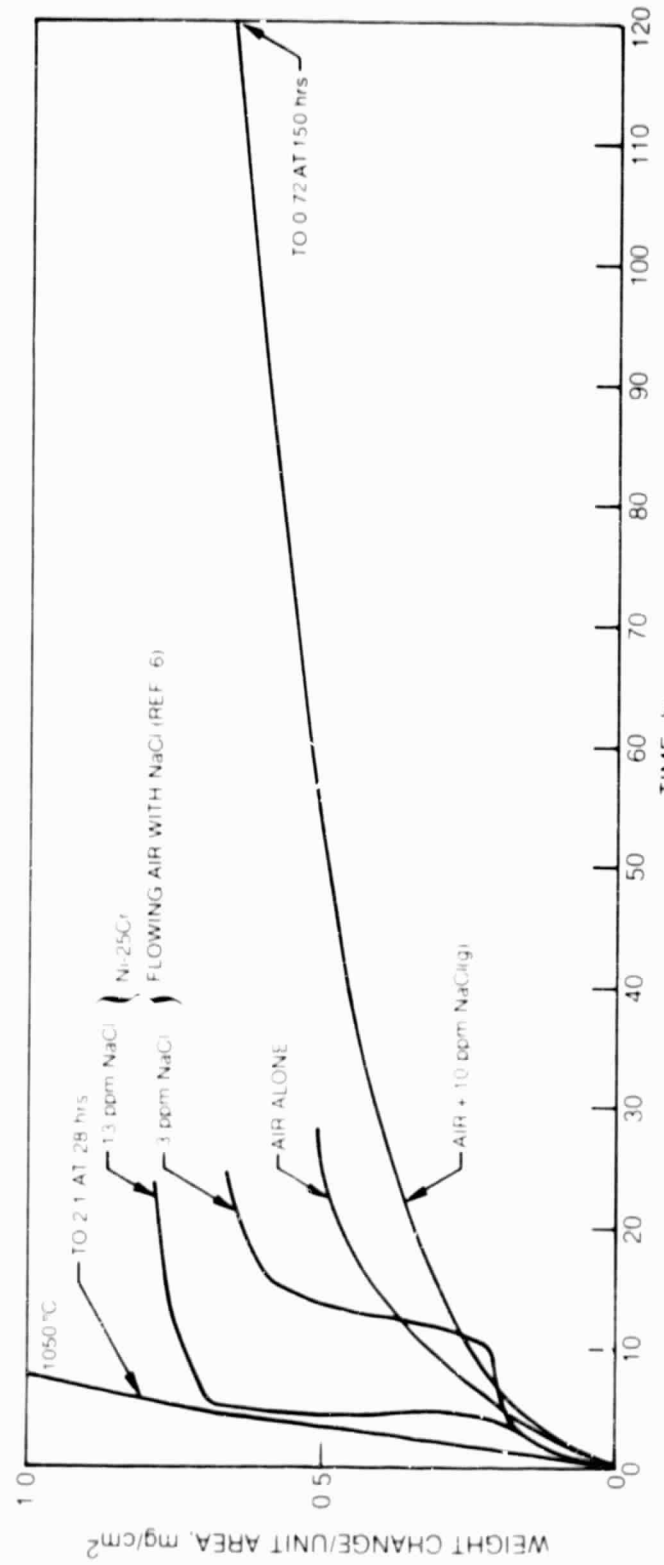

Fig. 34 Effect of NaCl(g) on the Oxidation Behavior of Ni-40 Cr-5 Si Air at 900°

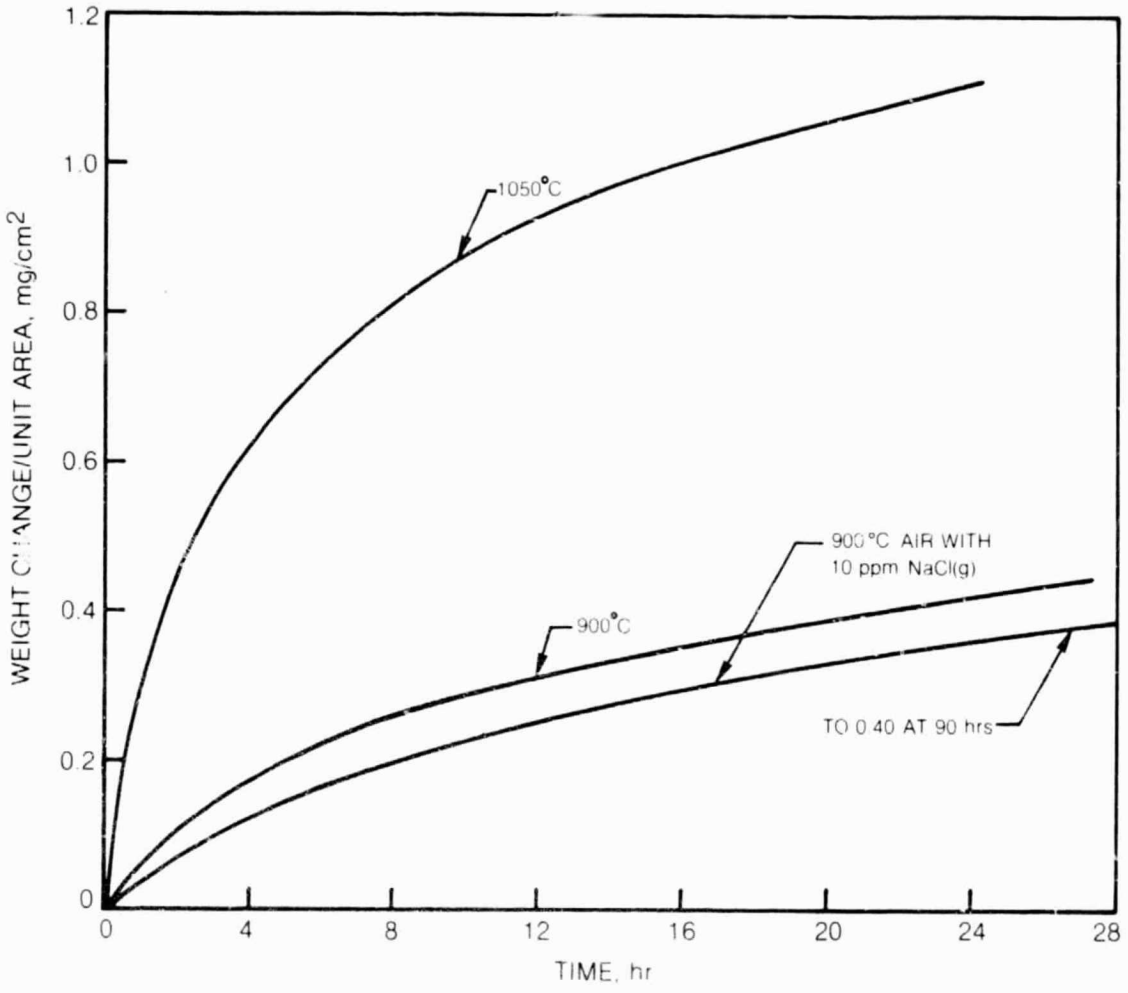

Fig. 35 Oxidation Behavior of Ni-40 Cr-11.5 Si

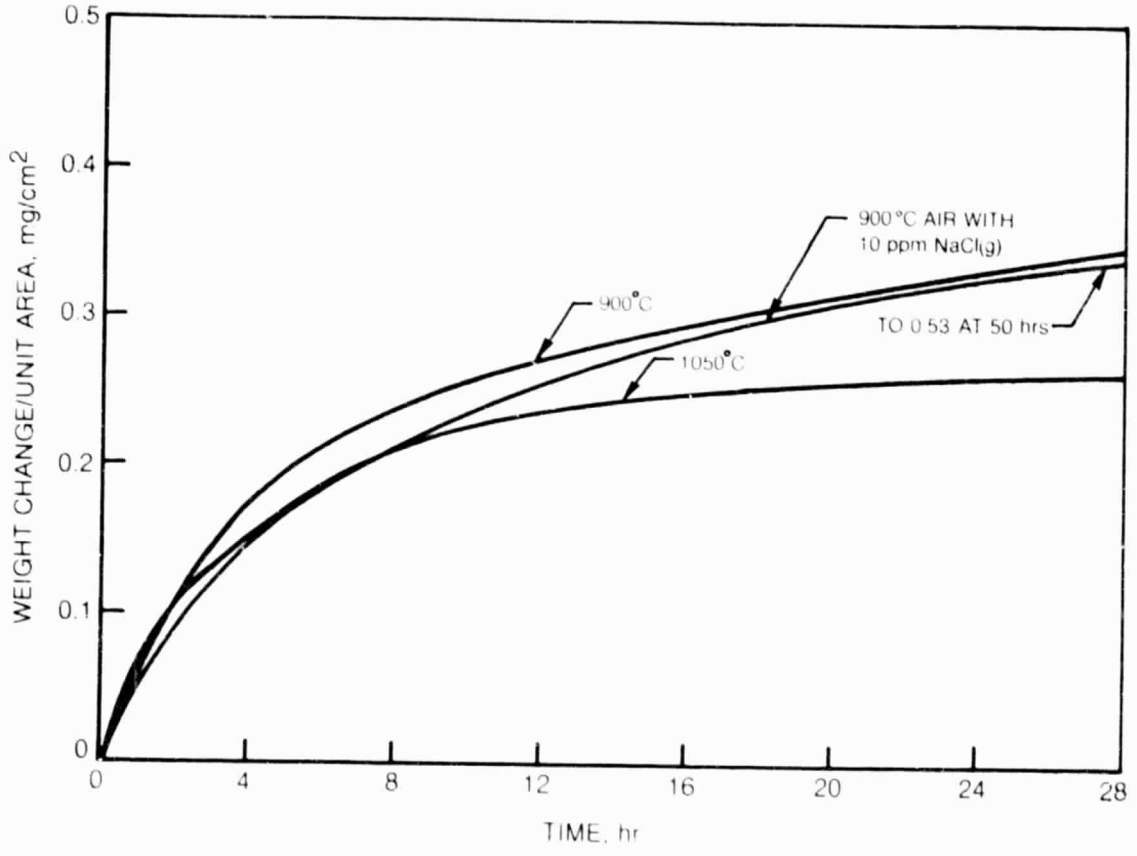

Fig. 36 Oxidation Behavior of CoCrAlY

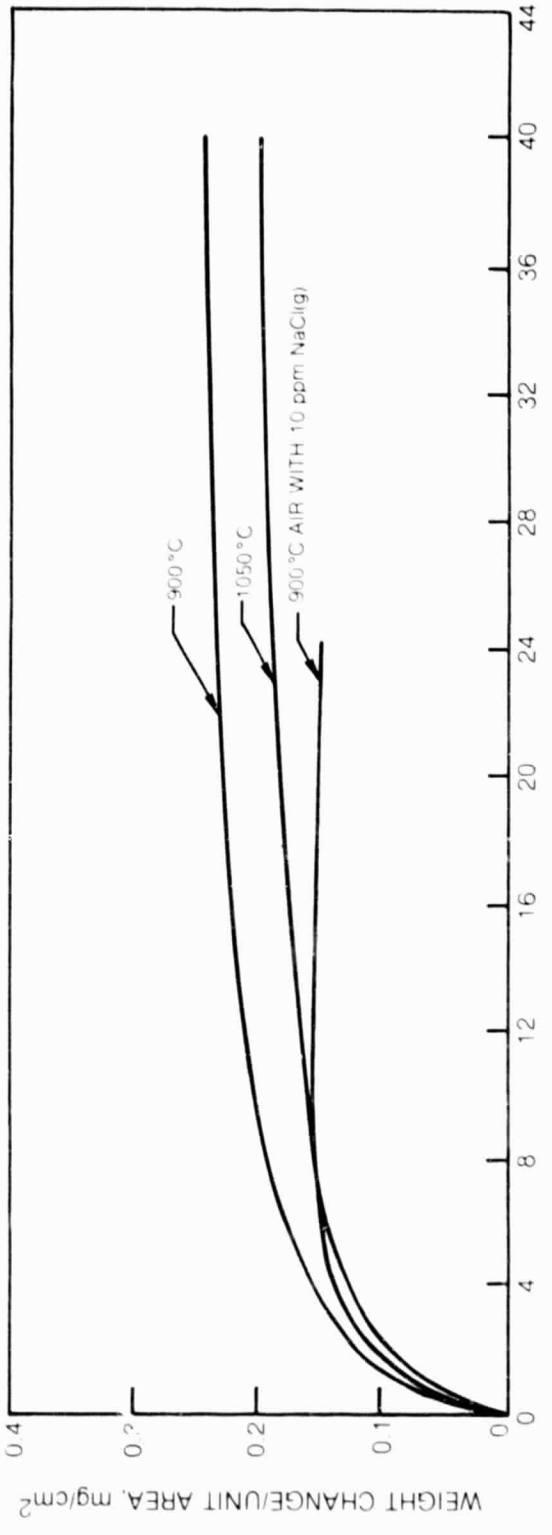

Fig. 37 Oxidation Behavior of CoCrAlY-5 Si

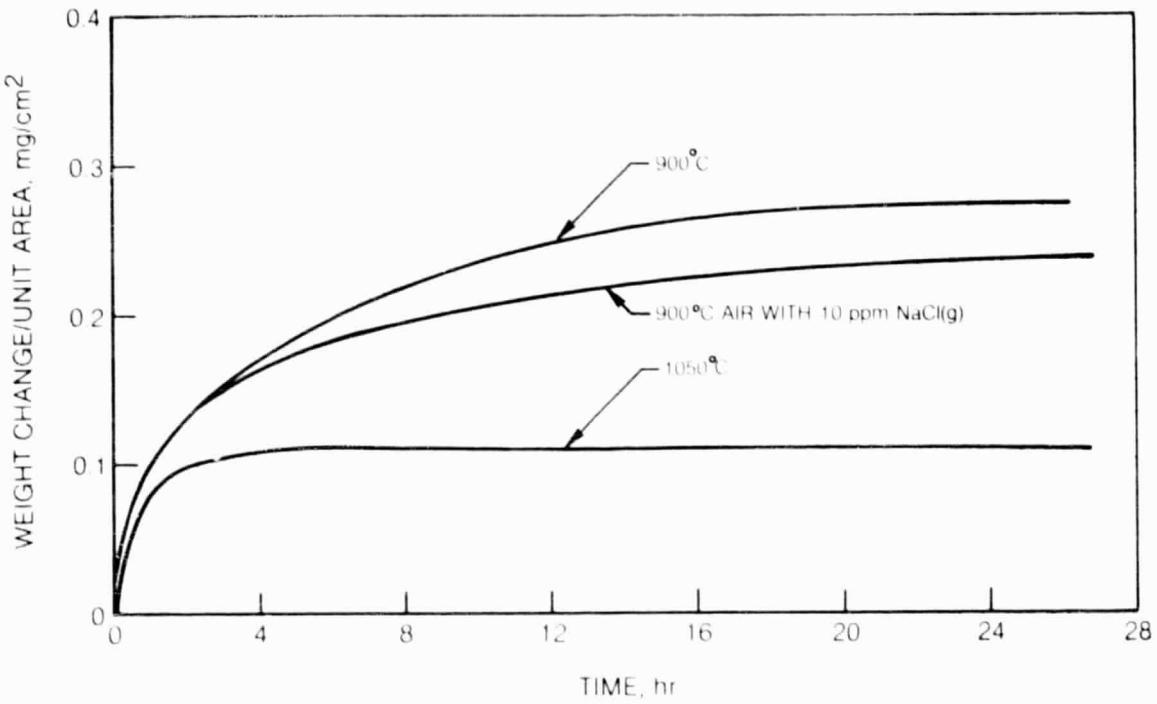

Fig. 38 Oxidation Behavior of CoCrAlY-12.5 Si

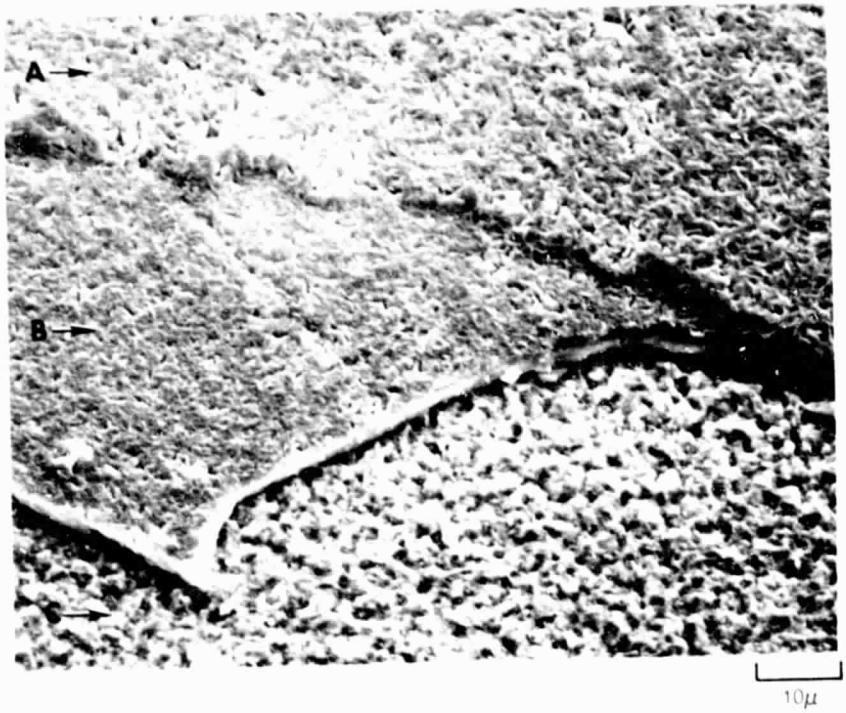

A — OUTERMOST LAYER
B — MIDDLE LAYER
C — INNER LAYER

Fig. 39 CoCrAl Oxidized in Air at 900°C for 72 Hr Showing a Multilayered Oxide

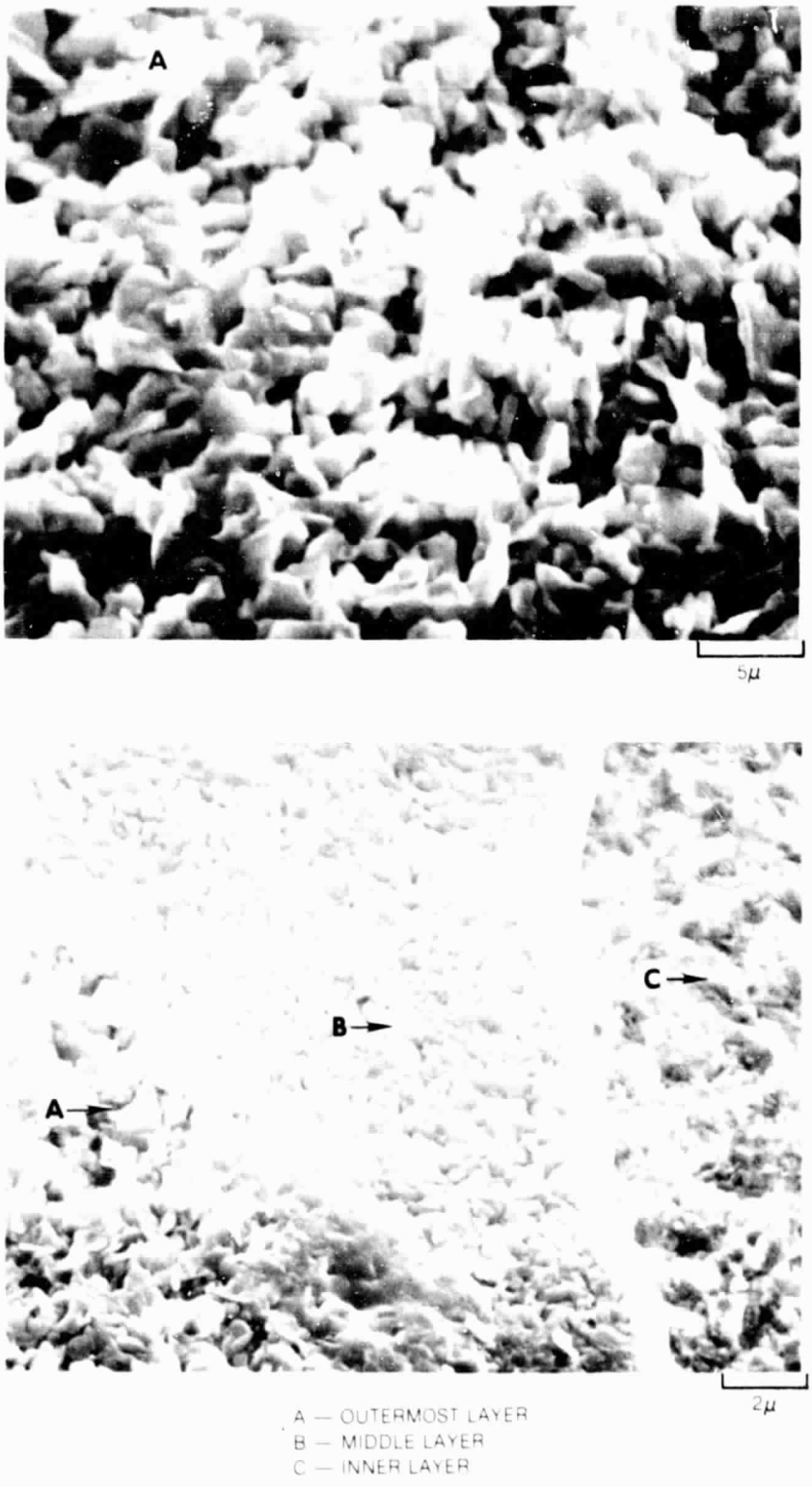

Fig. 40 Coarsened Alumina Whiskers in the Outermost Oxide Layer on CoCrAl Oxidized at 900°C in Air with 10 ppm NaCl(g)

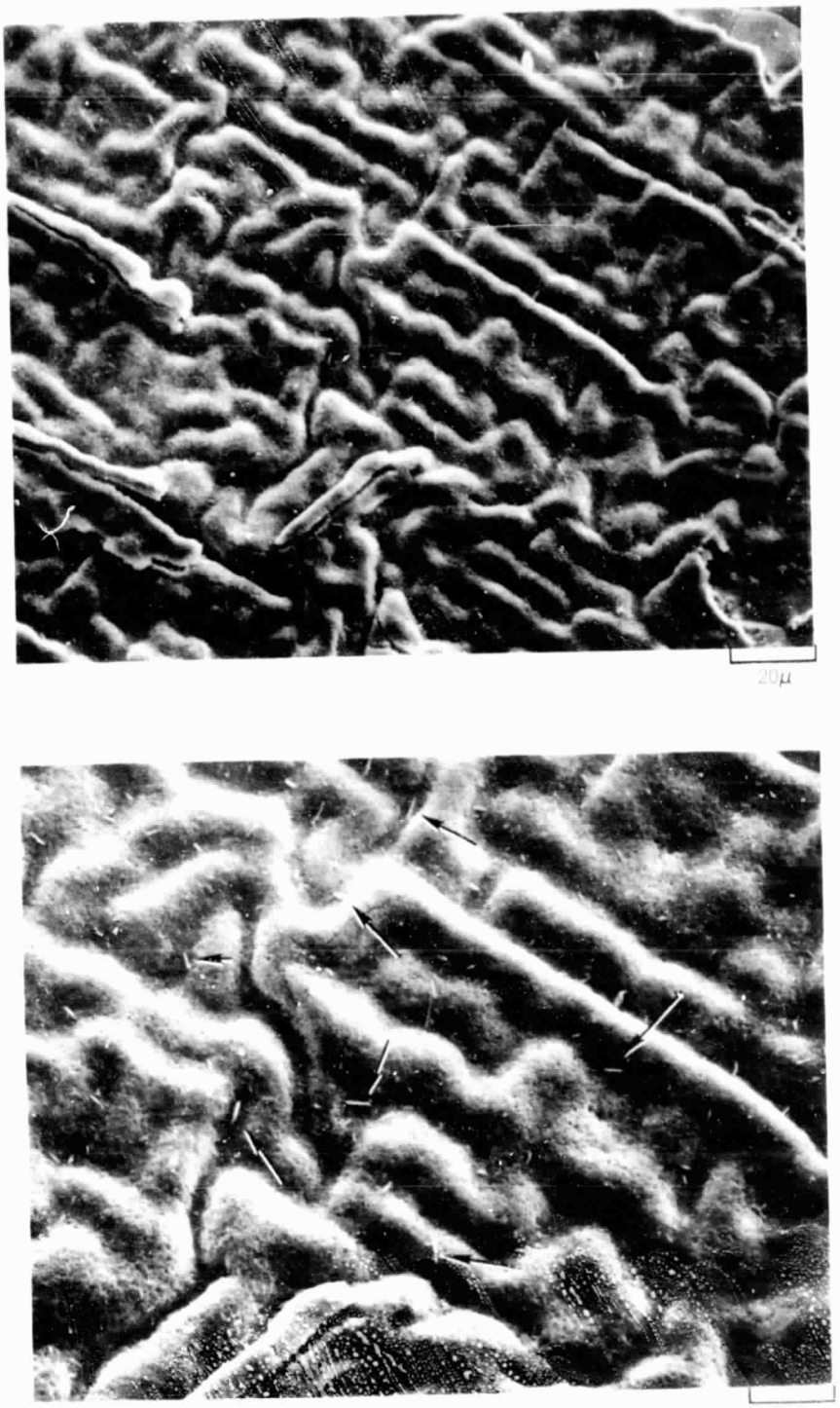

Fig. 41 Highly Convoluted Alumina Scale and Alumina Whiskers (Arrows) on the Oxidized Surface of a CoCrAl Specimen Oxidized at 1050°C for 94 Hr

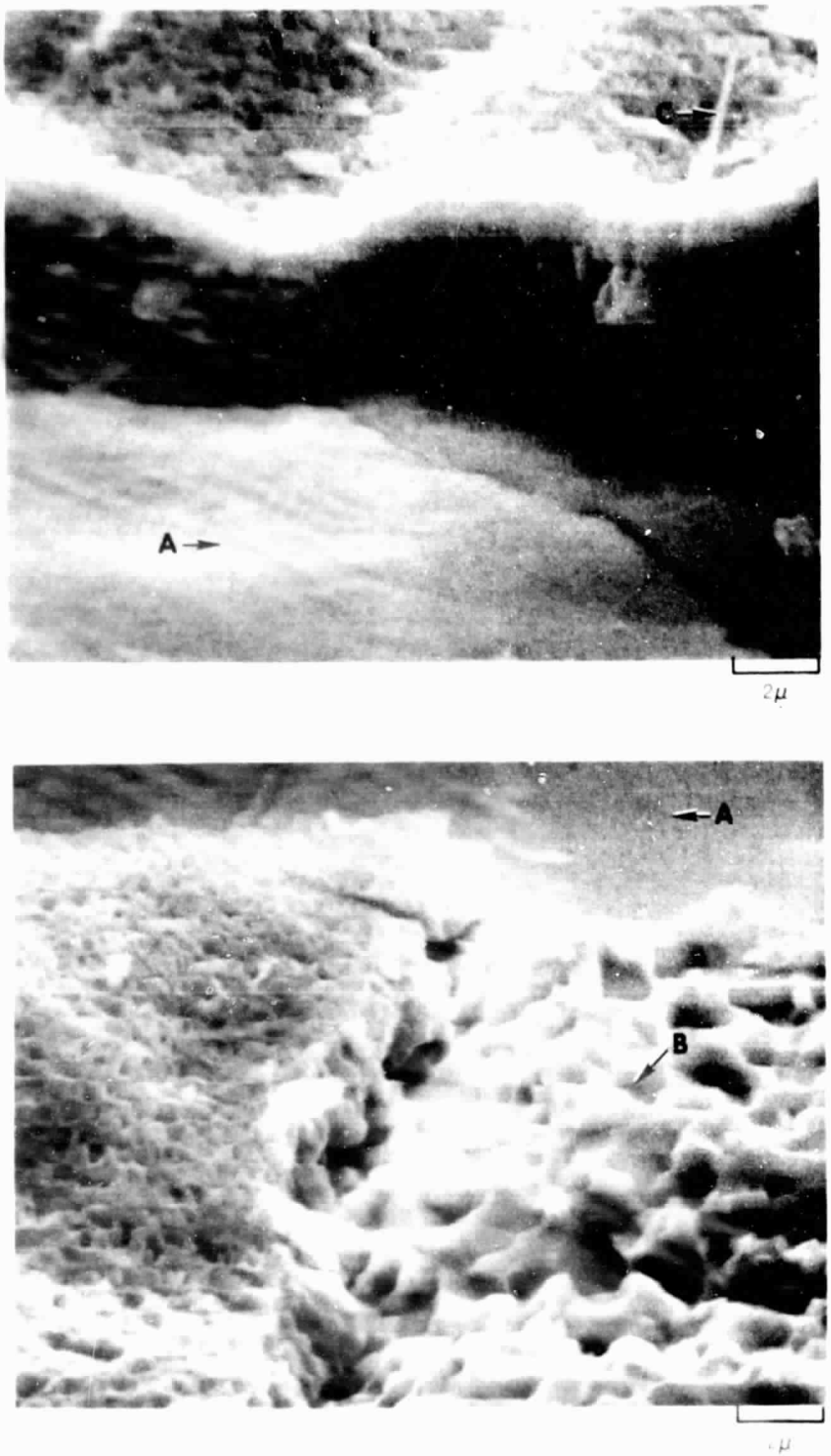

Fig. 42 Lack (A) and Presence (B) of Attachment Sites of Alumina Scale to Substrate, (C) Alumina Whisker

80-10-67-23

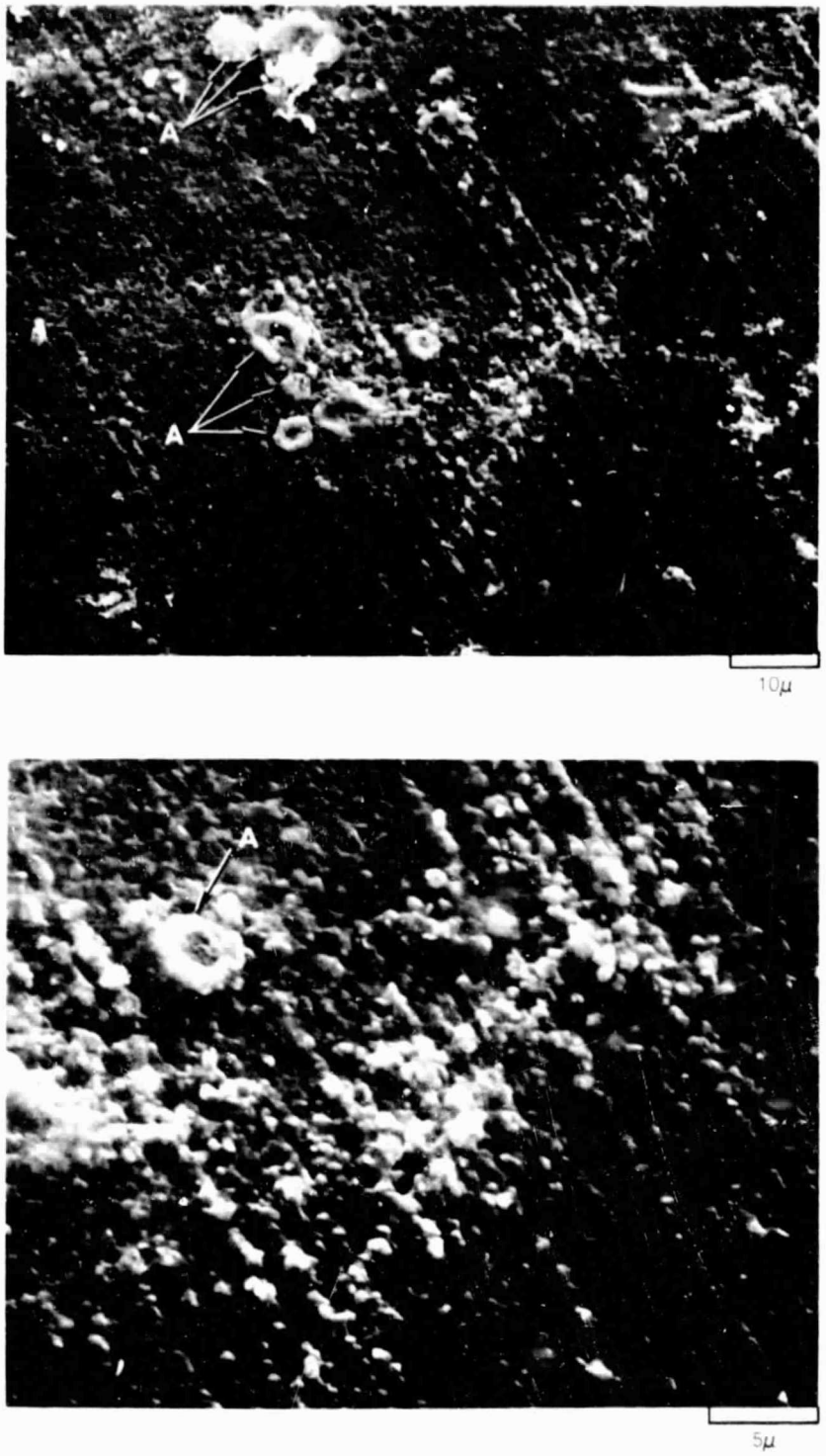

Fig. 43 Absence of Both a Convoluted Alumina Scale and Alumina Whiskers in CoCrAl-0.5Y Oxidized at 1050°C for 94 Hr

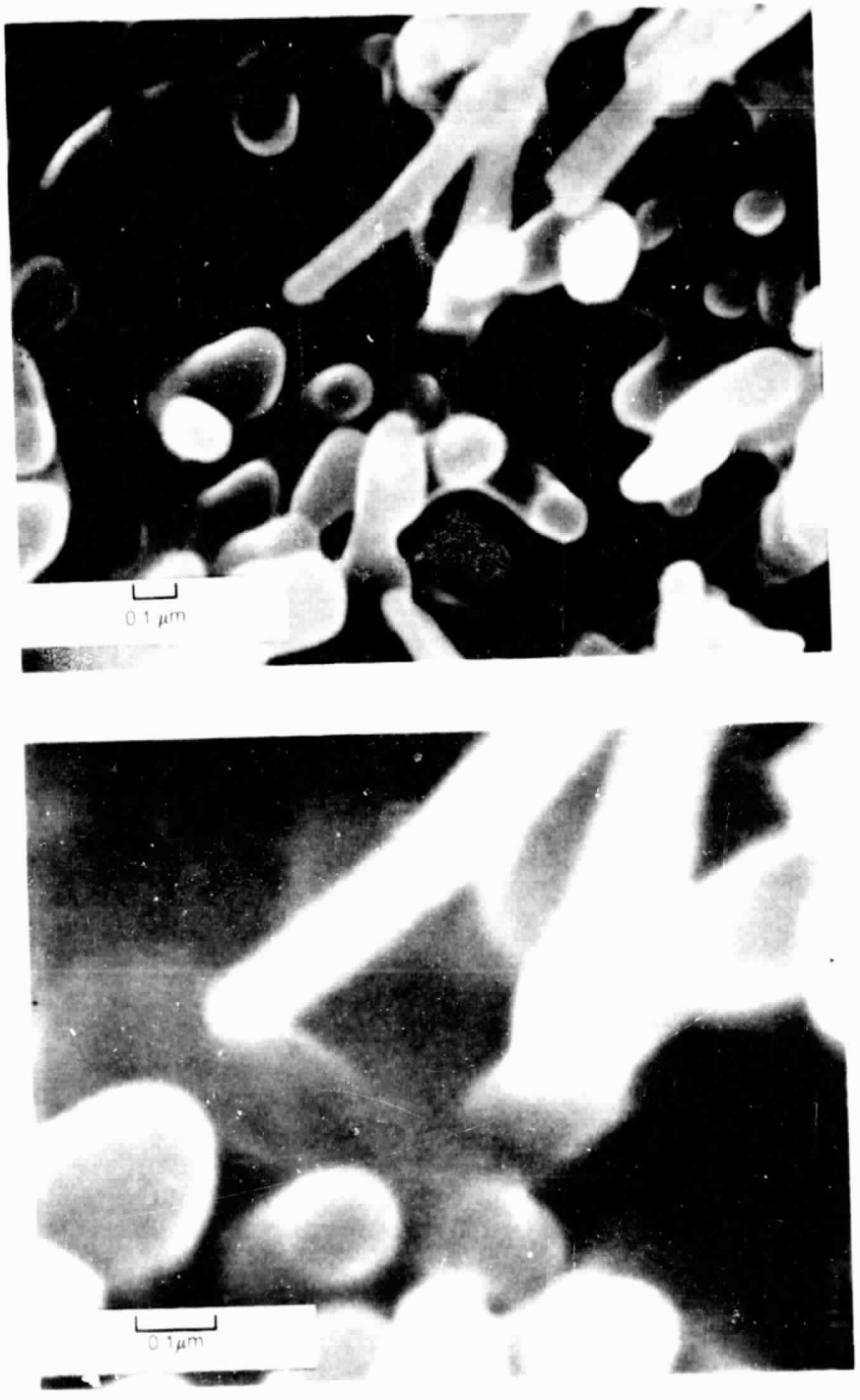

Fig. 44 "Dimple-like" Eruptions at the Base of Alumina Whiskers

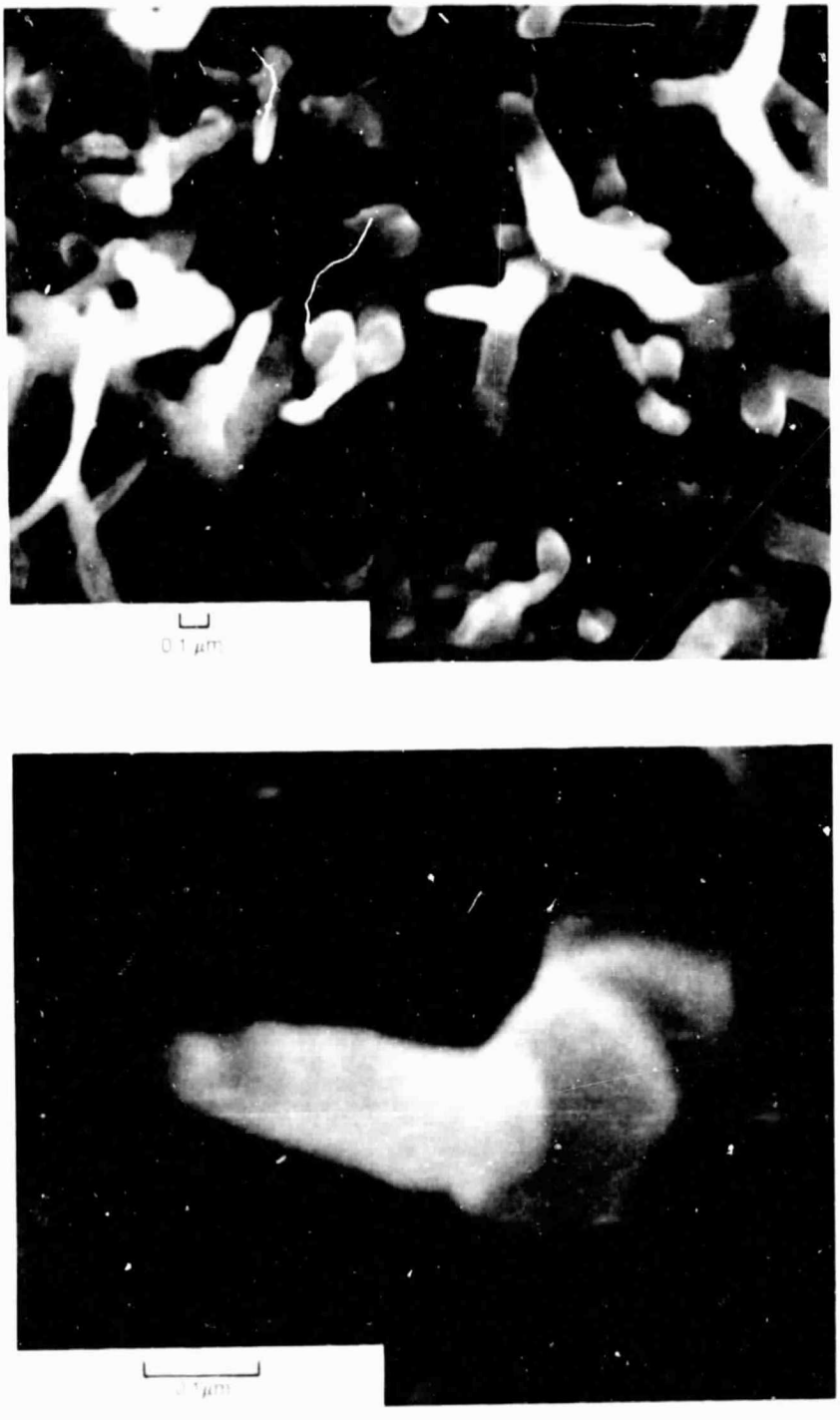

Fig. 45 **High**ly Segmented, Heavily Branched Alumina Whiskers Near the **Surface of the** Alumina Scale

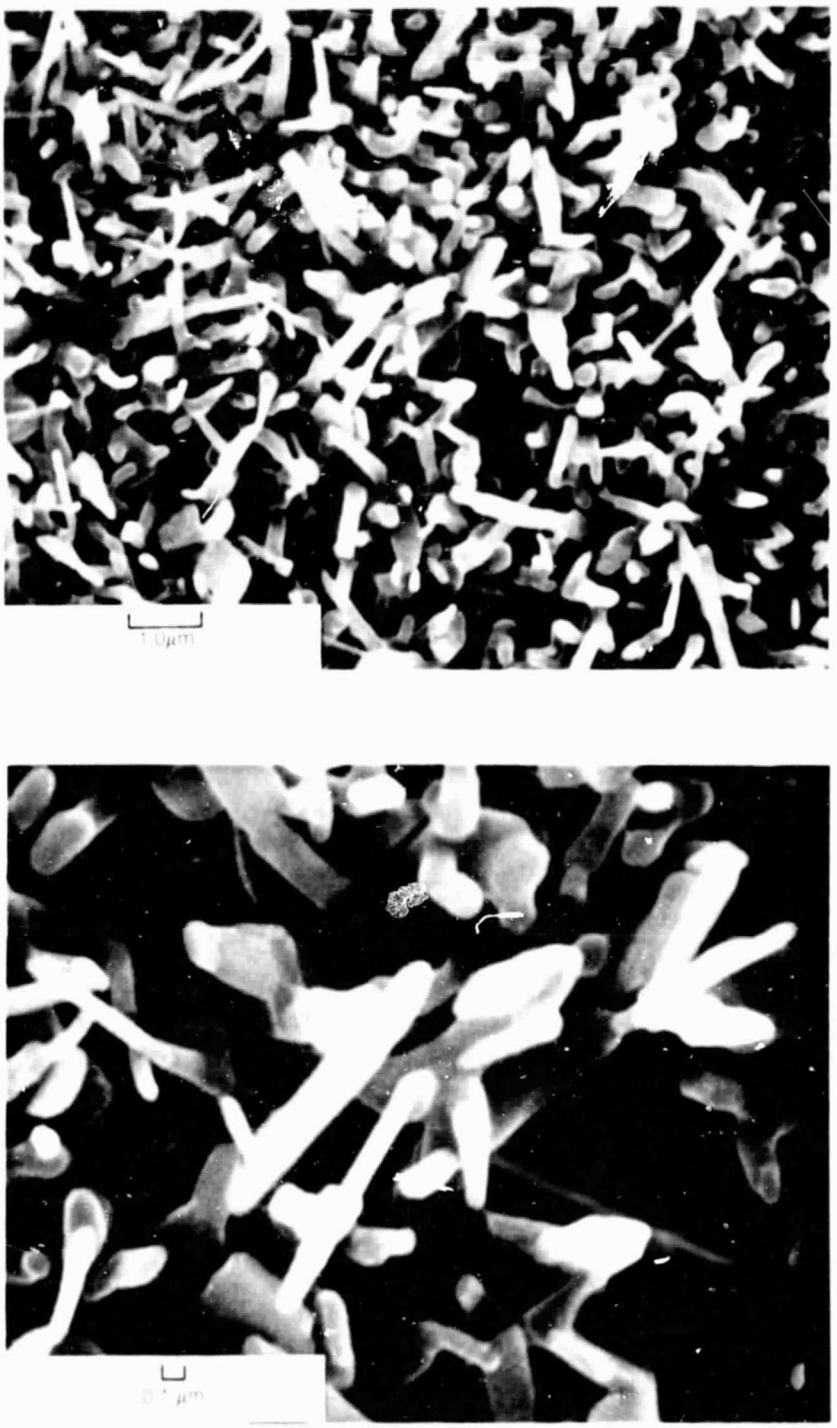

Fig. 46 Better Geometrically Shaped Crystals, Formed in the Ends of Less Geometric Tubes and/or "Dimple-like" Eruptions

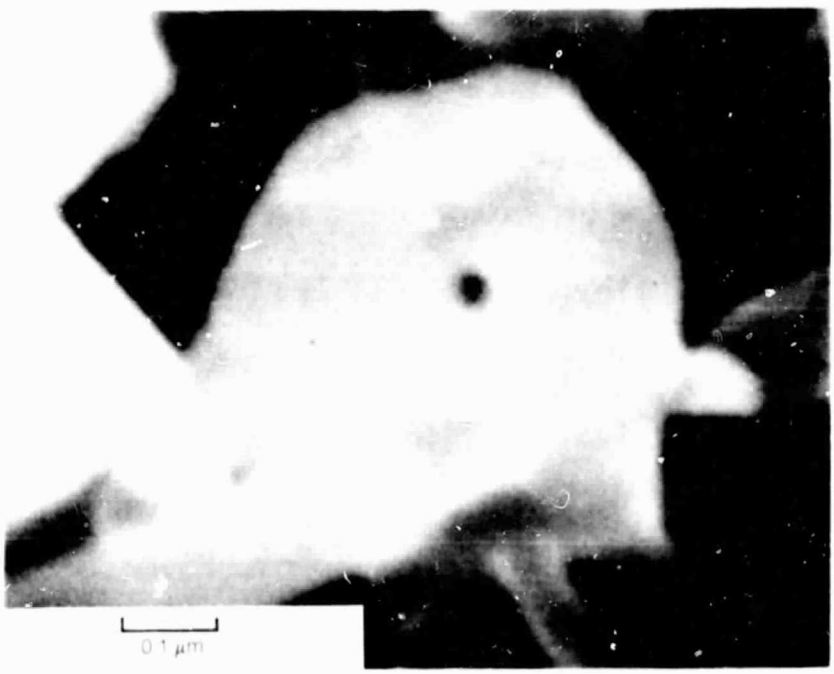

Fig. 47 An Approximately 200 Å Channel Down the Center of an Alumina Whisker

Fig. 48 1350°F Burner Rig Studies

Fig. 49 1350°F Burner Rig Studies

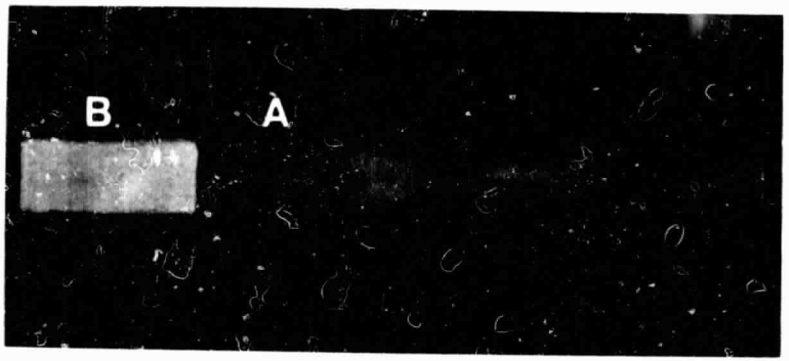

LEADING SURFACE

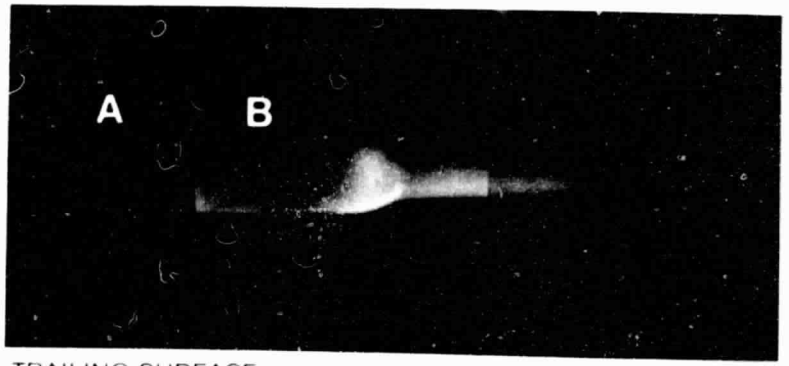

TRAILING SURFACE

A — AS-COATED SURFACE
B — HONED SURFACE

Fig. 50 Honed CoCrAlY Coated Erosion Bar

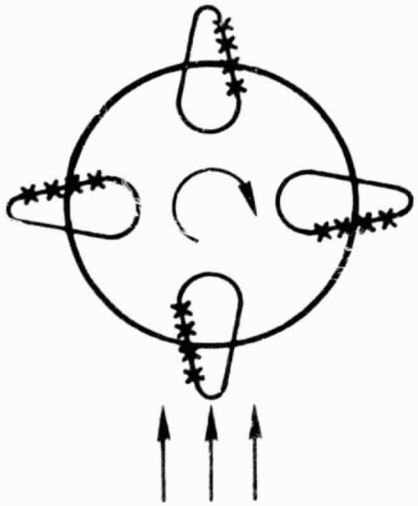

LEADING SURFACE

DEPOSITION RATE
6.8×10^{-2} mg/cm^2 hr

TRAILING SURFACE

DEPOSITION RATE
7.9×10^{-2} mg/cm^2 hr

Fig. 51 Burner Rig Studies

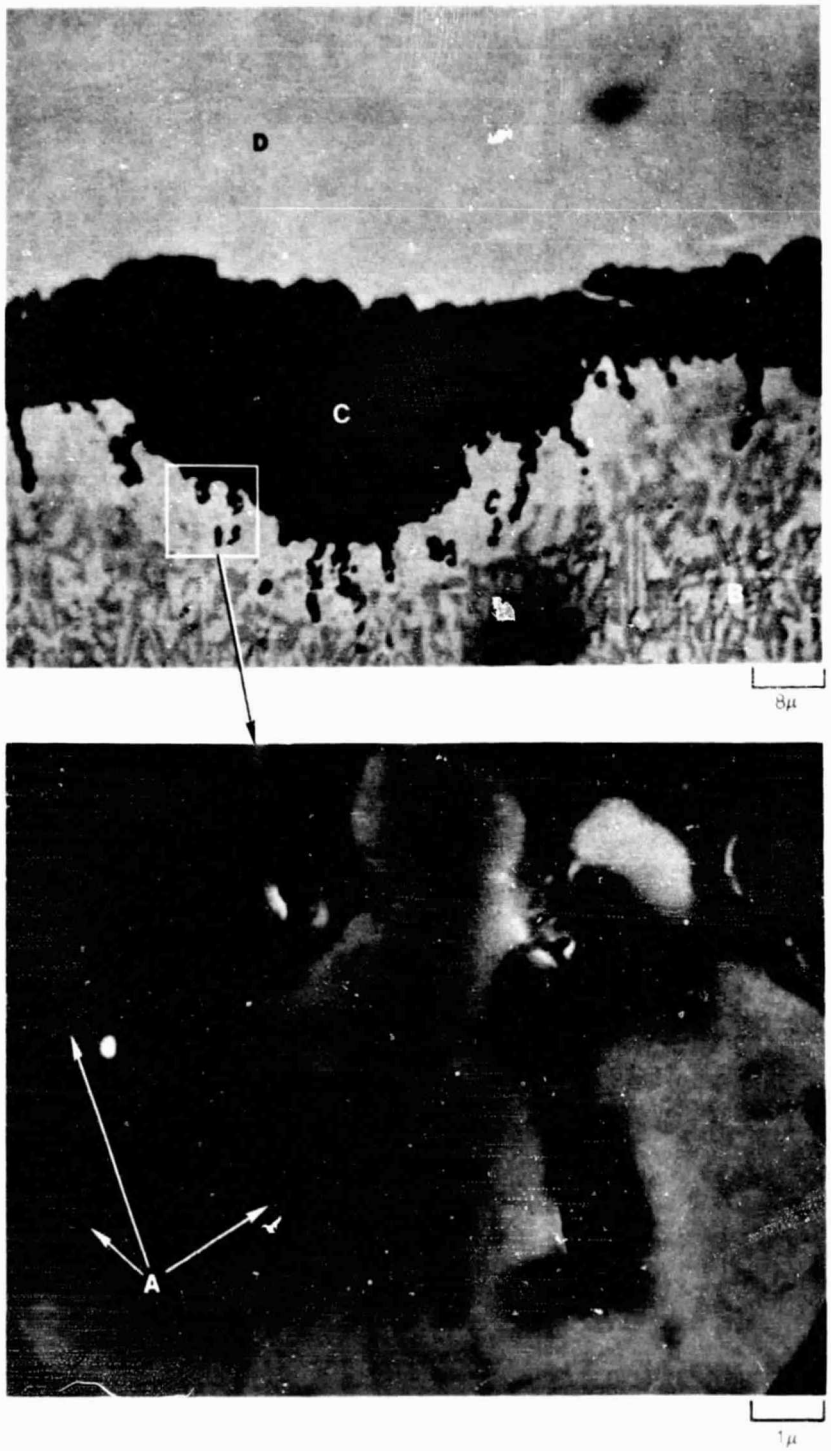

Fig. 52 Discontinuous Precipitation of β-CoAl (A) in α-Co (Cr, Al), CoCrAlY Coating. 1350°F, 30 ppm Synthetic Sea Salt, 1% SO_2 Added to Flame (B).CoCrAlY Coating ,(C) Oxide Pit, (D) Mounting Material

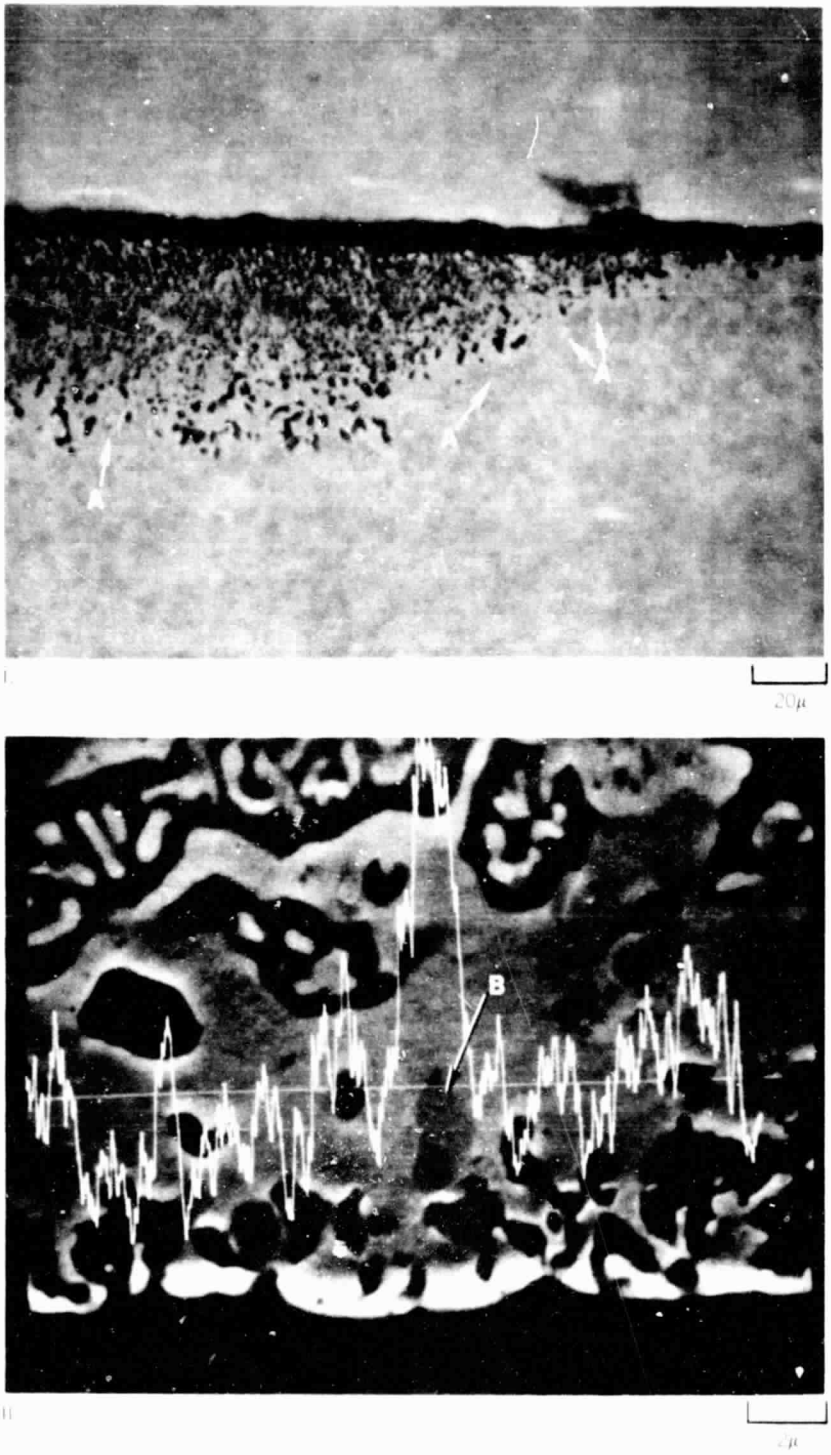

Fig. 53 Carbide Formation (A) in Modified CoCrAlY Immediately in Advance of Corrosion Pit i) Optical Micrograph ii) Carbon Scan Across Carbide Particle (B) 1350°F, 30 ppm Synthetic Sea Salt, 1% SO_2 Added to Flame